This is to certify that the
dissertation entitled

Composite Proton Exchange Membranes for Fuel Cells

presented by

Ping Liu

has been accepted towards fulfillment
of the requirements for the

Ph D degree in Chemistry

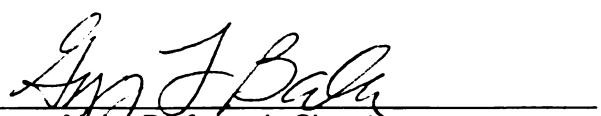

Major Professor's Signature

July 20, 2006

Date

Composite Proton Exchange Membranes for Fuel Cells

By

Ping Liu

A DISSERTATION

Submitted to
Michigan State University
in partial fulfillment of the requirements
for the degree of

DOCTOR OF PHILOSOPHY

Department of Chemistry

2006

ABSTRACT

Composite Proton Exchange Membranes for Fuel Cells

By

Ping Liu

A fuel cell converts the chemical energy of fuels such as H_2 directly into DC electricity. Protons formed at the anode diffuse through a proton exchange membrane (PEM) to the cathode to form water and heat. The requirements for PEM membranes include good chemical and mechanical stability, high conductivity, low permeability to reactant species and for practical applications, low cost. Perfluorinated sulfonic acid membranes (e.g., Nafion®) are the membranes of choice for use in practical fuel cell systems, however Nafion's high cost, poor ionic conductivity at low humidity and/or elevated temperatures, and its high methanol permeation limits its widespread use.

This research explored the design of composite proton exchange membranes as alternatives to single component membranes such as Nafion. The driving hypothesis was that adopting a two component approach simplifies membrane design by decoupling the problems of optimizing the physical and conductive properties of proton exchange membranes. Other advantages of a composite approach include simplification of membrane synthesis, rapid prototyping, and reduced cost. The conductivity of some membranes were comparable to Nafion, and had better high temperature performance.

The composite membranes studied used inorganic particles chemically functionalized to have acid groups on their surface. While this work focused on silica particles, any inert particle, in principal, could be compatible with the two-phase

composite membrane approach. Various sized particles were examined, ranging from macroscopic silica to nanoparticles. The higher surface to volume ratio of nanoparticles allowed higher loadings of acid groups in composite membranes. Another benefit of using nanoparticles was improved water retention at high temperatures, presumably due to more effective capillarity in aggregates of nanoparticles.

The proton conductivity depends on the number of charge carriers (protons) and their mobility (related to electrolyte structure). We found that immobilizing a single layer of acid groups on the surface of A200 fumed silica provided too few carriers to support conductivity. We solved this problem in two ways. First, we increased the concentration of acid groups on the surface by growing polystyrene from initiators anchored to the surface, and then sulfonated the polymers. Tethering acids to the polymers dramatically increases the number of available acid groups (2~3 mmol/g) and membranes prepared by embedding these particles in PVDF had conductivities of ~0.08 S/cm. A second approach was the sol-gel synthesis of nanoparticles containing alkyl thiols as a component of their structure. Oxidizing the thiols provided sulfonic acids tethered to the surface. Composites prepared from these particles also exhibited high conductivities.

The proton mobility in a composite membrane depends on the existence of conductive paths through the membrane. We observed percolation thresholds when measuring the proton conductivity of membranes, with the conductivity increasing several orders of magnitude when the particle content approached 30 wt%. Examination of membranes using TEM and confocal microscopy showed that particles in poorly conductive membranes aggregated in non-continuous domains, but in membranes with high conductivity, the domains were connected.

To My Family

Acknowledgments

I would like to express my deep appreciation to my advisor Dr Gregory L Baker for his guidance, patience and constant encouragement throughout the course of this research. Dr. Baker is a unique educator. One of his requirements for graduate students is to be an independent researcher which I realized how important it is. What I benefited from his guidance would be a great gift in my future work.

I would also like to thank my committee members: Dr. Walker, Dr. Bruening, Dr. Swain and Dr. Jackson for their time and assistance over the years. Many thanks to Dr. Dye for allowing me using the instruments in his lab.

My present and past lab mates made my five years lab work in MSU enjoyable thanks to their assistance and friendship.

Special gratitude goes to my family. My parents and my sister gave me constant encouragements during my graduate studies. My husband Shihua has always been supportive in taking care of our son Bowen who is my source of courage to overcome difficulties in my life.

TABLE OF CONTENTS

LIST OF SCHEMES

LIST OF TABLES

LIST OF FIGURES

LIST OF ABBREVIATIONS

AFC	alkaline fuel cell
AIBN	2,2'-azobisisobutyronitrile
ATRP	atom transfer radical polymerization
BAPFDS	diamine 9,9-bis(4- amionphenyl)fluorine-2,7-disulfonic acid
BDA	4,4'-diamino-2,2'-biphenyl disulfonic acid
CLPE	cross-linked high density polyethylene
DLS	dynamic light scattering
DMF	N,N-dimethylformamide
CTAB	cetyl trimethylammonium bromide
DMFC	direct methanol fuel cell
dNbipy	4,4′-di(5-nonyl)-2,2′-bipyridine
DRIFT	diffuse reflectance infrared Fourier transform
DS	degree of sulfonation
FTIR	Fourier transform infrared
GC	gas chromatography
GPC	gel permeation chromatography
HPA	heteropolyacid
IEC	ion exchange capacity
MCFC	molten carbonate fuel cell
MEA	membrane electrolyte assembly
M_n	number average molecular weight
M_w	weight average molecular weight
NDA	1,4,5,8-tetracarboxylic dianhydride
NMR	nuclear magnetic resonance
ODA	4,4'-oxydianiline
PAFC	phosphoric acid fuel cell
PATBS	poly(acrylamide-*tert*-butylsulfonic acid
PDI	polydispersity index calculated as M_w/M_n
PBI	polybenzimidazole
PEEK	polyetherether ketone
PEMFC	polymer electrolyte membrane fuel cell
PEO	polyethylene oxide
PP	poly-*p*-phenylene
PPO	polypropylene oxide
PS	polystyrene
PTMO	polytetramethylene oxide
PVDF	polyvinylidene fluoride
PWA	12-phosphotungstic acid
RH	relative humidity
SAXS	small-angle X-ray scattering
SDCDPS	disodium 3,3'-disufonate-4,4'-dichlorodiphenylsulfone
SOFC	solid oxide fuel cell

sPEEK	sulfonated polyaryletherketons
TGA	thermal gravimetric analysis
THF	tetrahydrofuran
TEM	transmission electron microscope
TEOS	tetraethyl orthosilicate
TMS-Cl	trimethylchlorosilane
UV/VIS	ultraviolet/visible
VBC	vinylbenzylchloride
X_n	number average degree of polymerization

Chapter 1

Introduction

Fuel cells

A fuel cell converts the chemical energy of fuels directly into DC electricity.[1] As shown in Figure 1 for a polymer electrolyte membrane (PEM) assembly using hydrogen as the fuel,[6] a basic fuel cell assembly consists of two electrodes and an electrolyte sandwiched between the electrodes. Gaseous fuels such as H_2 are fed continuously to the anode and oxidized to produce protons, and electrons that are supplied to the external circuit.[2] The protons diffuse through the electrolyte to the cathode, where oxygen or air

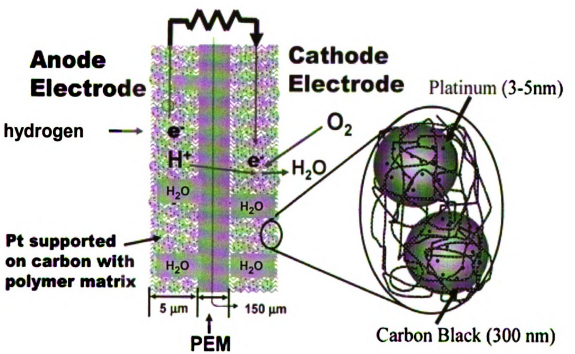

Figure 1.1. Basic membrane electrode assembly (Reprinted with permission from *Chem. Rev.* **2004**, *104*, 4587-4612. Copyright American Chemical Society.)

fed to the cathode combine with protons and electrons from the external circuit to form water and heat.

Fuel cells can be categorized into six major types based on the electrolyte:[3,5] alkaline, phosphoric acid, molten carbonate, solid oxide, PEM, and direct methanol fuel cells. The electrolytes in alkaline fuel cells are aqueous potassium hydroxide solutions retained in a porous matrix. Their normal operating temperature ranges from room temperature to 80 °C, and their advantages are low cost and a long operating life. Alkaline fuel cells require high purity fuel and oxygen. If exposed to air, the potassium hydroxide electrolyte is degraded by reaction with CO_2 in air to form carbonates. AFCs are usually used in spacecraft where reliability is paramount.

Phosphoric acid fuel cells (PAFCs) use phosphoric acid retained in a SiC matrix as the electrolyte. Because of phosphoric acid's low vapor pressure and high boiling point, PAFCs are usually run at 150 °C to 220 °C. They have been commercialized for stationary electricity generation, but a disadvantage of PAFCs is that they require expensive platinum catalysts.

The electrolytes in molten carbonate fuel cells are alkali carbonates retained in a ceramic matrix of $LiAlO_2$ at 600 - 700 °C. As the name suggests, the carbonates are in a molten state and are the mobile ionic species in the electrolyte. The high operating temperatures allow the use of non-precious metals as the catalyst which decreases the cost. But corrosion of cell components remains a problem at high temperatures.

Solid oxide fuel cells (SOFC) use a solid Y_2O_3 stabilized ZrO_2 as the electrolyte. Their high operating temperature (800 - 1000 °C) allows the use of non-precious metal

catalysts and eliminates the need for external fuel reforming. Solid oxide fuel cells are attractive for stationary power sources that can tolerate their slow startup and the need for significant thermal shielding.

Polymer electrolyte membrane (PEM) fuel cells, also termed proton exchange membrane fuel cells, use a thin proton conductive membrane as the electrolyte. Their typical operating temperatures are ~ 60-80 °C, which enables a fast startup. PEM fuel cells also require expensive noble metal catalysts which increase the cell cost.

Direct methanol fuel cells are similar to PEM fuel cells except that the fuel is methanol. Direct methanol fuel cells have yet to be commercialized, but are expected to operate at about 120 °C. Their greatest potential advantages are elimination of the complex fuel reforming process, and compared with hydrogen gas, methanol is a fuel that can be easily obtained and transported.

The development of membranes for PEM fuels cells will be emphasized in this thesis.

Fuel cell performance

A fuel cell's performance is characterized by its current density vs. voltage curve (also called a polarization curve). Drawing current from the cell causes the cell potential to drop from its open circuit potential, and these irreversible losses result in a cell voltage less than its ideal potential. A typical fuel cell polarization curve, shown in Figure 1.2,[4] can be roughly divided into three regions. The voltage drop at low current densities is related to the electrochemical reaction rates on electrode surfaces. At higher current densities, the voltage loss reflects resistance to the flow of ions in the electrolyte and resistance to the flow of electrons in electrodes. In regime II, cell voltage usually is

linearly related to current density. Further increases in the current density results in the sharp voltage decrease in region III. As reactants are consumed on electrode surfaces, a concentration gradient is formed between bulk fluid and electrode surface, and since the rate of the electrochemical reaction is controlled by diffusion of reactants, the cell potential will drop dramatically.

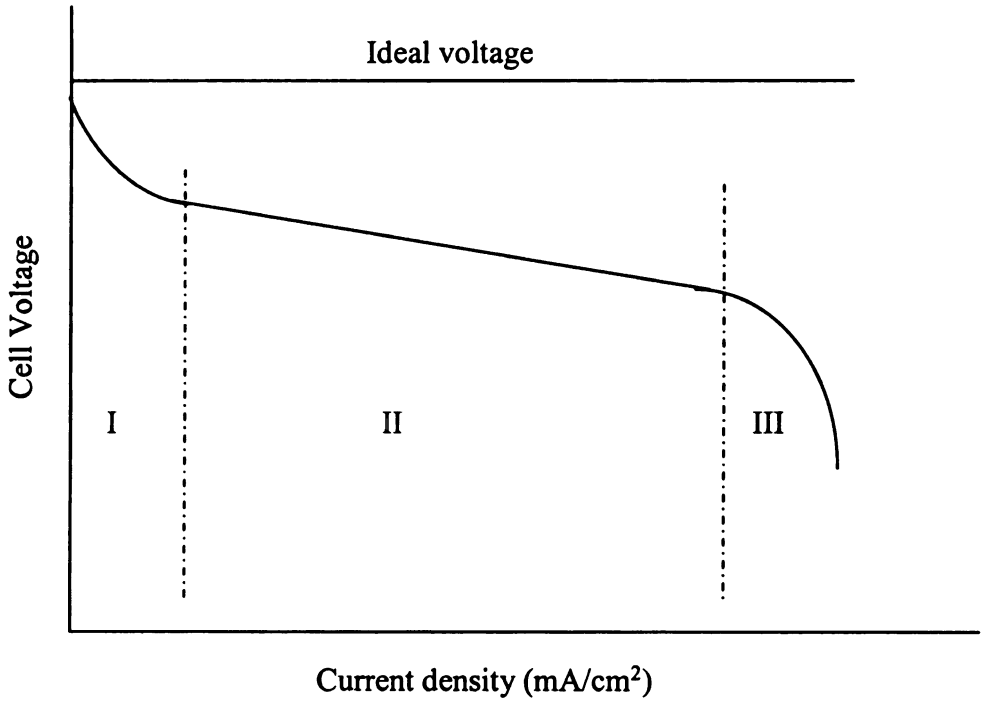

Figure 1.2. Voltage/current density characteristics of ideal and practical fuel cells

PEM fuel cells

Because of their fast start up and favorable power-to-weight ratio, PEM fuel cells are being extensively investigated as energy sources for vehicular transportation and

portable utilities. The membrane electrolyte is one of the most important components in a PEM fuel cell. Usually the membranes are ionomers, polymers that have negatively charged side chains attached to the polymer backbones. The requirements for a high performance PEM include high proton conductivity (~0.1 S/cm),[6] a low permeability to the fuel and oxidant, and good mechanical and chemical stability. Another important issue which relates to their commercial application is the cost of membrane.

Nafion, developed by DuPont in the late 1960's, is the prototype PEM membrane and nearly all commercial available membranes are based on Nafion. **Table 1.1** shows the generic chemical structure of Nafion and lists commercial Nafion materials.[7] The equivalent weight (EW) indicates the dry weight of Nafion per mole of sulfonic acid groups. For Nafion 117, the first two digits 11 indicate a membrane with an EW of 1100 and 7 indicates a membrane thickness of 0.007 inch.

Table 1.1. Commercialized Nafion ionomers

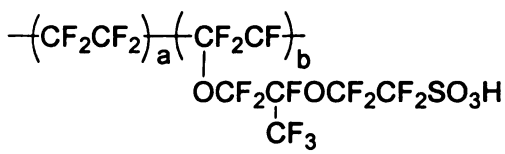

Type	Equivalent weight	Thickness (um)
Nafion 120	1200	260
Nafion 117	1100	175
Nafion 115	1100	125
Nafion 112	1100	80

Nafion's perfluorinated carbon backbone provides membranes with good chemical, oxidative and thermal stability. The semicrystalline morphology of Nafion is important for its mechanical strength. When hydrated, the high mobility of the protons in the SO_3H groups at the end of side chains leads to highly conductive membranes. The disadvantages of these membranes are poor ionic conductivities at elevated temperatures or at low humidity conditions. For example, the conductivity of Nafion is as high 10^{-2} S/cm in its fully hydrated state but the conductivity dramatically decreases at temperature above 100 °C because of the loss of water absorbed in the membrane.[8] The high cost of the perfluorated ionomer membrane is also a major reason limiting its widespread application.

Proton conductivity mechanisms

Proton mobility in water determines the conductivity of water-based proton conductors.[9-11] The conductivity of distilled water is very low due to the small dissociation constant of water, which results in a low concentration of mobile protons. There are several models suggested for proton transport. In the Grotthus mechanism,[12-14] also referred to as a proton hopping mechanism, the translocation of the positive excess charge along the hydrogen bonded network occurs by a structural diffusion process. The excess proton is part of an H_3O^+ ion, in which all three protons are equivalent. The excess proton hops from a H_3O^+ donor site to a neighboring water acceptor molecule, leaving a neutral water molecule behind as shown in **Figure 1.3**.[14]

In Zundel complexes,[14-18] the proton is located approximately halfway between two water molecules with considerably shorter O-O distances than the O-O distance in

bulk water. The excess proton is initially localized in the initial Zundel complex (black). The nearest neighbor water molecule forms a hydrogen bond with oxygen (2), while another proton is now located inside the new Zundel complex (black). Both mechanisms require an adjustment in orientation and deformation of both adjacent and remote water molecules in the original H_3O^+ or $H_5O_2^+$ cluster. IR data show that H_3O^+ is less a stable molecular entity than $H_5O_2^+$ in water.[19]

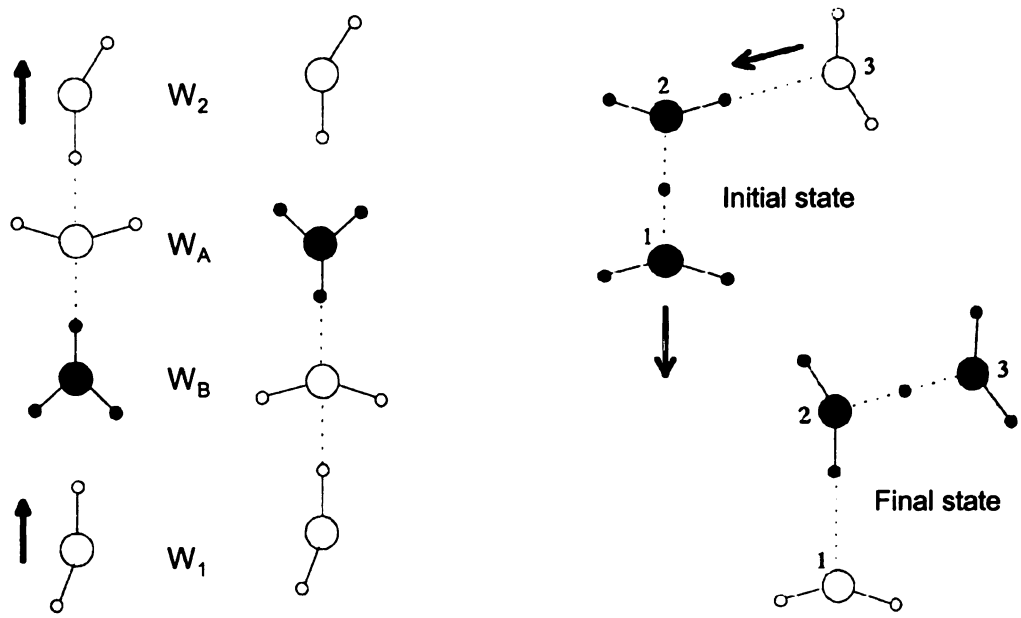

Figure 1.3. Proton transport via the Grotthus (left) and Zundel (right) mechanisms. (Reprinted with permission from *J. Phys. Chem. B.* **2003,** *107*, 3351-3366. Copyright 2003 American Chemical Society.)

The conductivity of 100% H_3PO_4 is about 0.025 S/cm. Its proton conducting mechanism involves self-ionization and self-dehydration,[21] and is thought to follow the Grotthus mechanism. The proton hopping consists of orientation of the solvent molecules followed by a proton transfer between proton donor and acceptor.[23, 24]

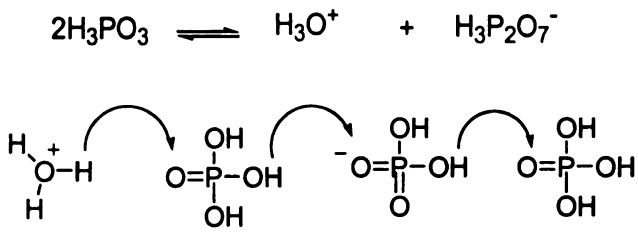

PEM conduction mechanism

Nafion is the prototypical PEM for fuel cell applications. There has been substantial work invested in characterizing Nafion, but many features of its performance are not fully understood. This is probably due to the very inhomogeneous nature of the membranes when hydrated.[25] In an effort to understand ion and water transport properties of Nafion, Gerke et al.[26] suggested a cluster-network model (**Figure 1.4**) to explain proton transport in Nafion. This model proposes inverted micelle structures, ionic clusters of perfluroalkylsulfonates, interconnected by narrow channels. Under fully hydrated conditions, the ionic cluster size is about 4 nm and the inter-cluster distance is about 5 nm. When hydrated, the ionic clusters are interconnected by narrow channels to provide continuous proton conducting pathways. In essence, the cluster-network model divides the ionomer microstructure into bicontinuous domains: a continuous hydrophilic domain embedded in a hydrophobic matrix

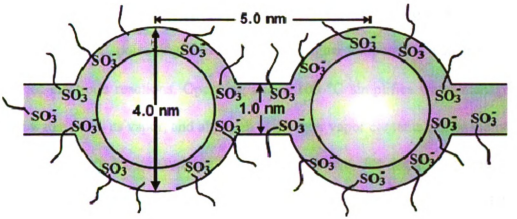

Figure 1.4. The cluster-network model (Reprinted with permission from *Chem. Rev. 2004, 104*, 4535-4585. Copyright 2004 American Chemical Society)

Although experimental investigations indicated that the spherical shape and uniform spacing of clusters in the model were over simplified, the substantial work on Nafion characterization is consistent with a bicontinuous phase nature for Nafion and established the cluster-network model as a reasonable starting point for the design of new membrane materials.

Limitations of Nafion-based PEM membranes[27]

Despite generally favorable properties, significant improvements in Nafion-based PEMs are needed to improve their high temperature performance and reduce their cost. The practical temperature range for Nafion PEMs is limited to 60-80 °C. Above 100 °C, the membranes are not fully hydrated and the membrane conductivity abruptly decreases as a result of water evaporation. However, operating PEM fuel cells above 100 °C would provide important advantages. PEMs use expensive platinum catalysts and CO

contamination in fuel streams can irreversibly adsorb to Pt and poison the catalyst. However, at ~150 °C, poisoning is insignificant.[22] Higher temperature also enhances the kinetics for electrode reactions. Operating above 100 °C simplifies water management since the water exists as vapor, and although high water vapor contents can be maintained at high temperatures by pressurizing the fuel cell system, the complexity and energy consumption of the resulting system could forfeit the benefits of operating at higher temperature.

In general, water management in PEM membranes is a significant problem. **Figure 1.5** shows the water transport modes in PEM fuel cell. As the Nafion's conductivity depends on proton solvation by water, the membrane must remain hydrated to be proton conductive. Water is transported in membranes by two mechanism: electro-osmotic drag and back-diffusion of water.[28,29]

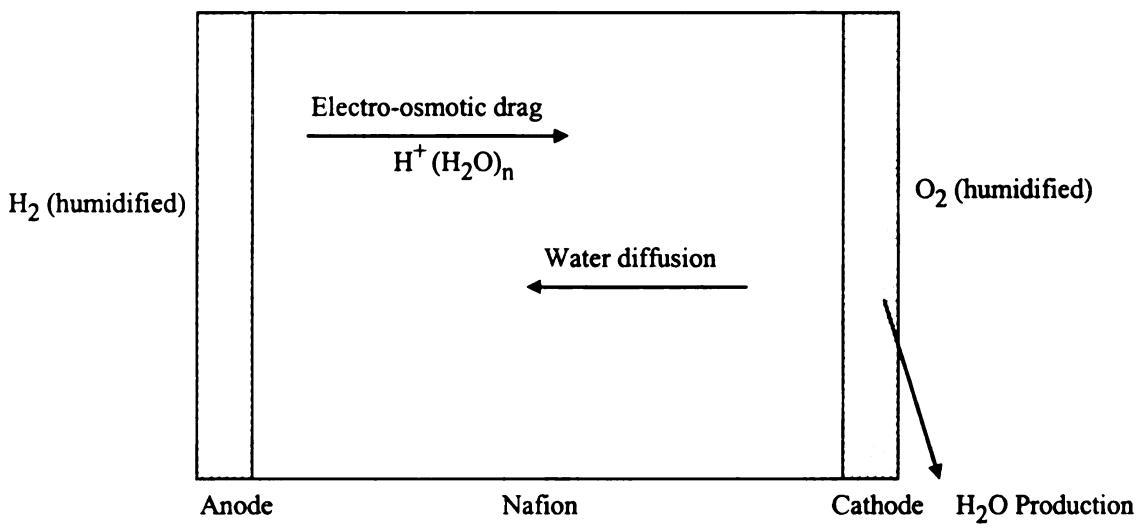

Figure 1.5. Water transport modes in PEM fuel cells

Electro-osmotic drag is the transport of protons with water molecules from the anode to the cathode. At the cathode, reduction of oxygen produces an excess of water which causes water to diffuse opposite to the direction of electro-osmotic drag.[30] The imbalance of water within a membrane can greatly influence cell performance. For example, electrode flooding decreases the contact of fuel with catalyst, and dehydration of membrane will result in decreased conductivity.[31]

Fuel permeation is a problem when Nafion is used in direct methanol fuel cells. Because of the similar physical properties of methanol and water, methanol is also transported by electro-osmotic drag.[32] The permeated methanol oxidizes at the cathode producing water and heat, and decreases the cell voltage and cell efficiency.[33]

Alternative materials for PEM membrane

The high cost of Nafion and its poor performance at high temperatures has stimulated extensive research aimed at developing new PEM materials. Since Nafion is viewed as the prototype PEM material, it is not surprising that the goal of most research is to replicate Nafion's favorable properties in more robust materials. Although the exact morphology of hydrated Nafion is not fully understood, there is general agreement that Nafion is a heterogeneous material comprised of a continuous network of hydrophilic domains that support proton transport. Its favorable mechanical properties and chemical stability are provided by Nafion's perfluorinated carbon backbone.[25] Since Nafion appears to be an example of the bicontinuous cluster-network model suggested earlier, many PEM materials have been designed to be bicontinuous in which hydrophobic phases provide chemical and mechanical stability, and hydrophilic phases support proton

conduction. Given the need for chemical and mechanical stability at high temperatures, it was natural that aromatic polymers were chosen for the hydrophobic phase due to their better oxidative stability compared with aliphatic polymers. The structures of some common commercially available aromatic polymer are shown in **Figure 1.6.**

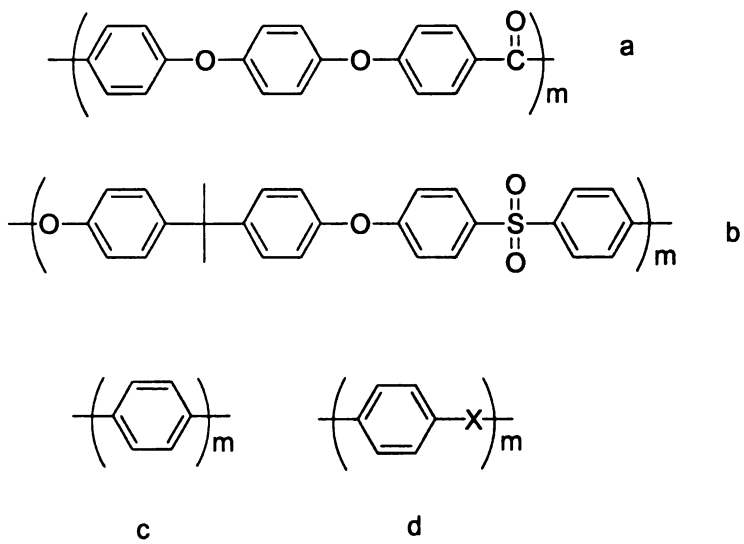

Figure 1.6. Chemical structures of representative aromatic polymers. **a,** polyarylene ether ether ketones; **b,** polysulfone; **c,** poly(*p*-phenylene); **d,** a poly(*p*-phenylene) with flexible links (X) where X is S, O, or other atoms.[34]

However, a significant challenge is to introduce the hydrophilic phase to provide proton conductivity while retaining the favorable mechanical properties of the aromatic polymer. Initially, sulfonic acids were introduced by reacting polymers with different sulfonating reagents such as concentrated sulfuric acid, chlorosulfonic acid or sulfur trioxide.[35] For example, polyarylene ether ether ketone (PEEK) was treated with concentrated sulfuric acid, providing sulfonated PEEK with an IEC of 0.65 mmol/g and a

conductivity of 0.04 S/cm at 100 °C and 100% relative humidity.[36] The major disadvantage of the direct sulfonation approach is the lack of control over the degree and location of sulfonic groups, and possible side reactions such as chain scission and cross-linking. In addition, high degrees of sulfonation increase membrane conductivity, but also can lead to uncontrolled swelling, loss of mechanical stability, or even dissolution of the membrane in water.

Compared to sulfonation of polymers, copolymerization of sulfonated and non-sulfonated monomers provides good control over the number of sulfonic acids in the polymer and some control over the distribution of the acid groups in the membrane. A representative example of this approach is the terpolymerization of disodium 3,3'-disufonate-4,4'-dichlorodiphenylsulfone (SDCDPS), 4,4'-dichlorodiphenyl sulfone, and 4,4'-biphenol reported by Wang and McGrath (**Figure 1.7**).[36] The conductivity at 30 °C for a 40% SDCDPS copolymer was 0.11 S/cm, comparable to Nafion. AFM images of a 60% SDCDPS copolymer showed obvious phase separation of the hydrophobic and hydrophilic regions in the membranes, however, at such a high degree of sulfonation, the membrane swelled dramatically and formed a hydrogel which was unsuitable for use as a PEM membrane. A recent topical review addressed the merits and problems of a series of sulfonated PEEK (polyether ether ketone) and PSU (polysulfone) copolymers and their application as PEMs.[37]

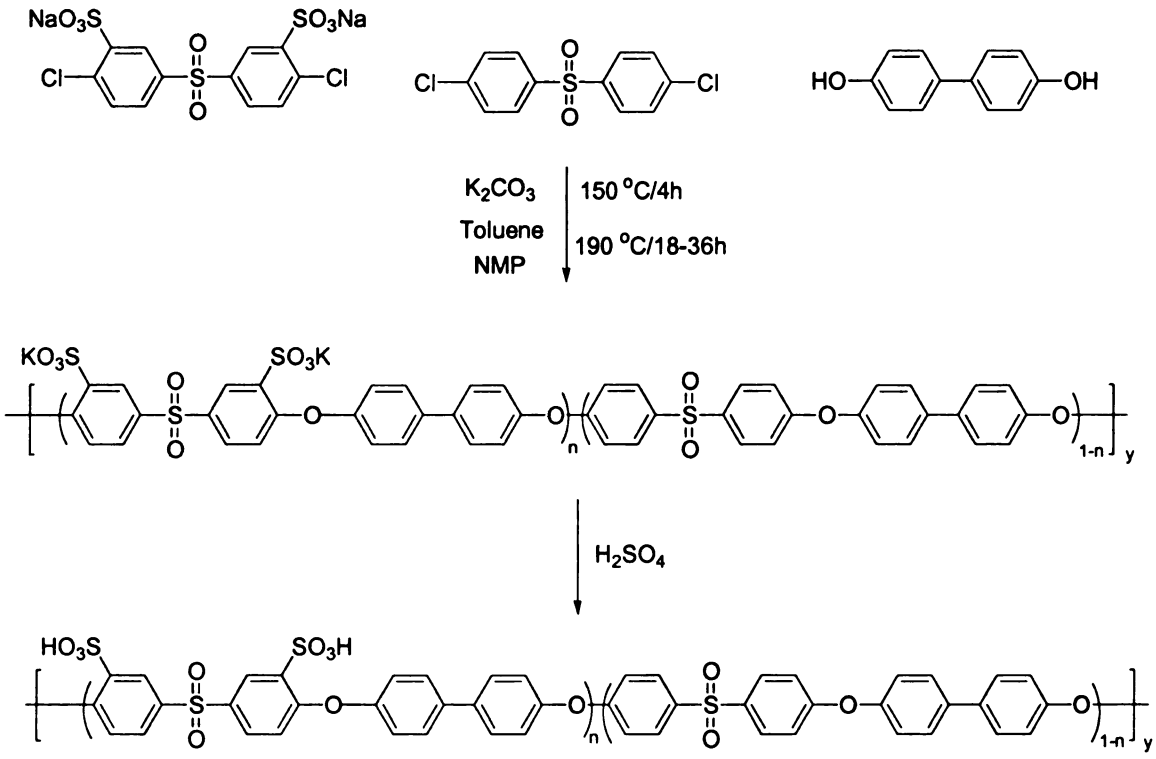

Figure 1.7. Direct copolymerization of sulfonated poly(arylene ether sulfone).

Neutral particles in proton-conducting polymers

The design of composite membranes generally follows the bi-continuous phase model. The membranes are comprised of two or more components, each providing different attributes to the membrane. The components are typically polymers and various particles, and can be in the form of mixtures of particles, polymer blends, or more commonly, polymer/particle composites. Particle-based composite membranes can be generated from non-conductive particles in a conductive matrix, conductive particles in a conductive matrix, and conductive particles in non-conductive matrix. The composite approach provides a simple route to PEMs since it eliminates the need to optimize the mechanical, chemical and physical properties in a single material.

Most early applications of the composite membrane approach were motivated by the need to improve membrane hydration at high temperatures. In an early attempt Mauritz et al.[68] soaked Nafion membranes in a silica precursor solution, and subsequently formed silica particles in membranes via a sol-gel process. However, the silica was concentrated near the membrane surface, decreasing to a minimum at the center of the membrane. Lvov et al. prepared Nafion/TiO_2 membranes by casting membranes from a mixture of pre-formed nanoparticles in a 5% Nafion solution. Compared to the unmodified membrane,[69] a composite PEM with 20% TiO_2 showed pronounced improvement at 120 °C under reduced humidity conditions. The authors attributed the improved performance to enhanced water retention due to the presence of absorbed pure water in the electrical double layer on the TiO_2 surface. Similar performance improvements at elevated temperatures and reduced humidity conditions were reported by Bocarsly and coworkers[70] for composite membranes prepared by adding metal oxide particles (SiO_2, TiO_2, Al_2O_3 and ZrO_2) to Nafion solutions. From the membrane characterization data, they suggested that coordination of metal ions to the oxygen of a SO_3^- group was directly correlated to the improved fuel cell current-voltage response. Metal-sulfonate cross-linking decreased proton conductivity slightly, and they also suggested that the loss of water in membrane at elevated temperatures might be caused by a change in polymer structure instead rather than direct evaporation of water.

TiO_2 nanoparticles were used as fillers in sulfonated polyethersulfone membranes. While the membrane conductivity decreased,[71] the fuel permeability through the membrane decreased and the water/methanol selectivity increased. A common advantage of composite membranes is decreased fuel permeation compared with polymer

membranes. Embedding nanoparticles in membranes increases the tortuosity or pathlength for fuel diffusion through the PEM. In general, inclusion of SiO_2 and other hygroscopic metal oxide nanoparticles in Nafion and other sulfonated polymer matrices increases membrane mechanical stability, decreases fuel permeability and improves water retention.[55-66]

Conducting particles in proton-conducting polymers

While the inclusion of non-conductive metal oxide particles in Nafion can improve some aspects of membrane performance, the effects are modest and often come with a loss in conductivity. In order to maintain high proton conductivity, the use of proton-conducting particles in Nafion and other polymer matrices were investigated.[72-80] Several types of conductive particles were investigated in composite membranes: heteropolyacids (such as phosphotungstic acid $H_3(W_{12}PO_{40})\bullet 29H_2O$, molybdo-phosphoric acid $H_3(Mo_{12}\ PO_{40})\cdot 29H_2O$), zirconium phosphate and its derivatives, cesium hydrogen sulfate ($CsHSO_4$) and sulfonated polystyrene beads.

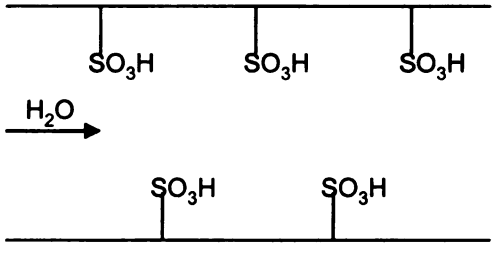

Figure 1.8. Schematic structure of layered zirconium phosphate.

α–Zirconium phosphate and its derivatives[53] are layered materials with pendant acid groups that extend into the interlayer region and form hydrogen bonds with water (**Figure 1.8**). These materials are widely used as proton sources in composite membranes at elevated temperatures (100 - 180 °C) because the crystallites are water soluble at lower temperatures. The conductivities of zirconium phosphate derivatives are dependent on hydration. Heteropolyacids such as phosphotungstic acid, molybdophosphoric acid and silicotungstic acid are crystalline inorganic compounds which provide protons when hydrated. They are highly soluble in water and their proton conductivity also is humidity dependent. Microcrystalline $CsHSO_4$ is comprised of hydrogen-bonded oxyanions. At 141 °C it undergoes a monoclinic to tetragonal phase transition. Reorganization of the SO_4 groups dramatically increases proton conduction,[54] making $CsHSO_4$ a stable proton conductor under anhydrous conditions at temperatures up to 250 °C. Sulfonated polymers such as cross-linked sulfonated polystyrene beads also have been used as conductive particles.

Traversa and coworkers[81] doped sulfonated polyether ether ketone (SPEEK) with hydrated tungsten oxide, an inorganic proton conductor. Compared to SPEEK, the doped membrane had a higher proton conductivity, improved heat resistance, and lower water solubility. While coordination of water molecules to the tungsten oxide and the SPEEK sulfonic acid groups was suggested, the membrane conductivity measurements were run at 60 °C and full humidity, conditions which would normally dissolve the inorganic acid. Lee et al.[72] modified montmorillonite with 3-mercaptopropyltrimethoxy silane, and then oxidized the thiol groups to sulfonic acid groups to obtain a modified clay with an IEC of 0.52 mmol/g. A Nafion membrane with 5 wt% sulfonated clay had better performance

than pristine Nafion when tested in a direct methanol fuel cell at 40 °C. However, the membrane conductivity decreased significantly when the modified clay loading increased, probably because of the low IEC content of clay.

When a sulfonated polymer is used as a matrix, the conductive particles could contribute to the overall conductivity of the composite membrane, and allow the use of polymers with moderate degrees of sulfonation, conductivity, and swelling. Because both particles and matrix are hydrophilic, the particles can disperse homogeneously, inhibiting direct permeation of reaction gases and improving the membrane's mechanical stability. Shaw and coworkers[83] prepared a composite membrane from lightly sulfonated poly(ether ketone ketone) (IEC < 1 mmol/g) and highly sulfonated cross-linked polystyrene particles (SXLPS) (IEC ~ 5 mmol/g). They suggested that the sulfonic acid groups of the matrix cluster around the particles, stabilizing the dispersed ~ 400 μm diameter SXLPS particles, and providing a highly acidic path for proton mobility. The crystallinity of the lightly sulfonated polymer matrix also improved the mechanical strength of the wet membrane and minimized swelling when exposed to water. Addition of the particles caused a four-fold increase in the conductivity of the base polymer, and the conductivity of membranes with 40 wt% particles was higher than Nafion.

Conducting particles in non-conducting polymers

Embedding proton-conducting particles in a non-conducting matrix allows complete separation of the proton conduction and mechanical stability functions during membrane design.[84-103] These systems naturally phase separate because of the opposite polarity of the two components. The role of the polymer matrix is to provide mechanical

and chemical stability while the particles provide a conductive path for protons. However, the distribution of the particles within the membrane is critical since high membrane conductivity depends on the formation of continuous conducting paths that connect both sides of the membrane. Simply increasing the particle volume fraction to high levels (>50% v/v) may not yield suitable membranes since the mechanical properties degrade at high particle contents.

Yamazaki et al.[95] prepared solvent-cast membranes from DMF solutions of polybenzimidazole containing zirconium tricarboxybutylphosphonate powder. The proton conductivity of a membrane with 50 wt% powder was 3.8×10^{-3} S/cm in fully humid conditions at 200 °C. Because of the relatively low conductivity, they treated the membrane with sulfuric acid, and the membrane conductivity increased to 8.13×10^{-3} S/cm under the same conditions. Though their membranes were conductive at high temperatures, full humidity at 200 °C can only be realized by pressurization, which complicates fuel cell design.

Heteropolyacids (HPA) were also investigated as a proton source in a hydrophobic matrix. Khan et al.[93] used solvent casting (DMF) to embed phosphotungstic acid in polysulfones. Membranes with 40 wt% HPA had adequate mechanical strength and a conductivity of 0.07 S/cm at 120 °C under full humidity conditions. However, the solubility of HPA in water indicates that the membranes were unsuitable for fuel cell applications. One strategy for preventing leaching of HPA and maintaining high conductivity is to use hydrogen bonding or van der Waals interactions to anchor HPA to the polymer matrix. Lin et al.[96] dissolved phosphotungstic acid in an aqueous solution of poly(vinyl alcohol) (PVA), which is a good methanol barrier. FTIR spectra of membranes

cast from water indicated hydrogen bonding interactions between phosphotungstic acid and PVA. The swelling of the hydrophilic polymer matrix decreased significantly with increasing HPA content, but the membrane conductivity did not exceed 10^{-4} S/cm, even when the HPA content reached 90 wt%.

Honma et al.[97] fabricated a composite membrane of zirconia and polytetramethylene oxide (PTMO) via a sol-gel process. When the molar ratios of metal alkoxide and PTMO were ~ 1:1 or 1:2, they obtained flexible and thermally stable membranes. Zirconias are expected to cross-link PTMO by hydrolysis and condensation reactions. Adding phosphotungstic acid rendered the membrane conductive. At 40 wt% phosphotungstic acid, the conductivity at 150 °C was 5×10^{-2} S/cm under full humidity conditions. The same group also prepared related membranes by substituting silica for zirconia, and reported a conductivity of $\sim 10^{-3}$ S/cm for a membrane with 50 wt% phosphotungstic acid.[89] The sol-gel process used in the above examples enables molecular level contact between the inorganic and organic phase and limits particle size to the nanometer scale; both could help retain phosphotungstic acid in the matrix.

Ferraris et al.[98] used an alternative strategy to prevent HPA from leaching from membranes, the synthesis of mesoporous tungstosilicate materials (WMM). These micron-sized particulates had conductivities of 4.0×10^{-2} S/cm, but the size of the particulates can complicate membrane processing. A stable 30 wt% WMM composite membrane was formed from polyethylene imine, 3-glycidlyoxypropyl trimethoxysilane (GLYMO), a cross-linker for polyethylene imine, and bis(trifluoromethanesulfonyl)imide (HTFSI). As HTFSI is a proton conducting liquid, the resulting membrane conductivity (6.12×10^{-2} S/cm) cannot be directly compared to other HPA containing membranes. In

more recent work, Shahi et al.[99] described membranes prepared by the hydrolysis of aminopropyltriethoxysilane in the presence of poly(vinyl alcohol). The membranes were cross-linked with formaldehyde and then phosphorylated with phosphonic acid. The highest conductivity measured was 5.22×10^{-2} S/cm for a membrane with 50 wt % silica. Although the ether bond connecting silica and PVA may not be stable enough to survive actual fuel cell conditions, this approach is a unique method for immobilizing acids in membranes. Narayanan et al.[91] prepared composite membranes by hot pressing mixtures of $CsHSO_4$ and PVDF above the melting point of PVDF. At temperatures above the 141 °C superprotonic phase transition, the conductivity of an anhydrous membrane with 60 vol% $CsHSO_4$ reached 10^{-3} S/cm.

In the above examples, a solid acid content of >40 % is necessary for composite membranes to reach high conductivity. The principal reason is the lack of proper particle-particle connectivity to form continuous conductive paths that connect both sides of the membrane at low acid contents. A potential solution to this problem is to fill a porous non-conductive polymer matrix with conductive particles. (The pores need to be interconnected to ensure continuous hydrophilic channels.) Direct insertion of particles into the matrix is difficult compared with *in situ* particle formation within the pores. Alberti et al.[94] used a soaking procedure to fill the pores of a porous polytetrafluoroethylene (PTFE) matrix with precursors to zirconium phosphate particles ($Zr(O_3P\text{-}OH)(O_3P\text{-}C_6H_4SO_3H)$). By repeating the soaking procedure 4-5 times, they were able to fill ~70-80% of the pore volume. At 100 °C, membranes with 20% and 40% particle contents had conductivities of 10^{-4} S/cm and 10^{-3} S/cm respectively at 95% relative humidity.

Another method for ensuring conductive paths in polymer membranes was developed by Oren's group.[100] By applying a strong ac electric field (1-100 kV/cm) during the synthesis of the membrane, the conductive particles aggregated into linear chains aligned along the applied field. The percolation threshold for high conductivity decreased from 40% particle content with no applied field to 10% for membranes prepared with the applied field. Although the actual membrane conductivity was not particularly high (10^{-3} S/cm), the work suggests approaches for reducing the percolation threshold while preserving the mechanical properties of composite membranes.

The use of organic particles such as cross-linked polystyrene sulfonic acid in membranes is gradually receiving more attention. Unlike heteropolyacids, these organic particles disperse but do not dissolve in water, and their size and IEC can be easily tuned. Their conductivity also is humidity-dependent. Shaw et al.[101] investigated membranes prepared by embedding different sized cross-linked polystyrene sulfonic acid beads in a cross-linked poly(dimethyl siloxane) matrix. They found that the size of particles and their IEC strongly influenced membrane properties such as water uptake and conductivity. As the particle size decreased, the equilibrium swelling increased. Conductivity increased with particle loading, but composite membranes prepared from smaller particles had lower conductivities because of the lower IEC of the particles.

Prakash and coworkers[102] designed semi-interpenetrating composite membranes by immersing PVDF films in a solution of styrene, divinylbenzene (cross-linker) and 0.3-0.4 wt% azobisisobutyronitrile (initiator). Heating the films in a press at 150 °C initiated polymerization within the PVDF matrix. The process was repeated until the membrane contained 15-20% cross-linked polystyrene. Sulfonation with chlorosulfonic acid

converted the cross-linked polystyrene to polystyrene sulfonic acid. The resulting membranes were homogeneous and their conductivities were comparable to Nafion measured under similar conditions. In addition, methanol crossover was greatly reduced comparable to Nafion. The interpenetrating polymerization process avoids extensive phase separation and results in films with good mechanical properties. However, inhomogeneous sulfonation and the extensive soaking steps complicate membrane fabrication. Hong et al.[103] directly blended PVDF with sulfonated polystyrene. The sulfonated polystyrene was introduced in the form of a methyl methacrylate copolymer to take advantage of PMMA's miscibility with PVDF. They found that the acid segments formed nanoscale domains distributed uniformly in the PVDF matrix. The conductivity of the membranes (IEC = 0.6 mmol acid/g) was ~ 10^{-3} S/cm, and the water uptake was as low as 26%.

Design of new composite PEM membranes

As described earlier, aromatic polymers and composites are the two major types of materials under consideration for the next generation of proton conducting polymer membranes. The membrane design strategies for both types of materials are consistent with the bi-continuous (or cluster network) model for proton conduction in Nafion. The current Department of Energy target for polymer membranes to be used in hydrogen fuel cells is a conductivity of 0.1 S/cm at 120 °C and 50% humidity,[35] but despite substantial research, these targets have not been met. A general problem has been the difficulty in obtaining high conductivities at elevated temperatures while maintaining dimensional and chemical stability in the membrane. These properties generally follow different trends, i.e. mechanically stability usually correlates with poor conductivity. In aromatic PEMs,

the degrees of sulfonation necessary for high conductivity result in significant membrane swelling or even dissolution of polymers in water. Membrane cost is another major challenge.

Three types of composite membranes were identified earlier: non conductive particles dispersed in a conductive matrix, conductive particles in conductive matrix, and conductive particles in non conductive matrix. Since the first two classes of composite membranes use existing membrane materials (Nafion or sulfonated aromatic polymers) as the conducting phase, the goal of adding particles is to improve mechanical properties or water retention at high temperatures. While some improvements have been made, there remain significant cost and thermal stability issues.

The third class of materials, proton conducting particles in hydrophobic polymer matrices, has received little attention, but may offer an opportunity to move beyond incremental improvements in membrane design. Since the matrix is non-conductive, a potentially broad range of polymers is available, and requirements such as mechanical stability or controlled swelling are easily satisfied. In general, adopting a two component approach simplifies membrane design by decoupling the problems of optimizing the physical and conductive properties of proton exchange membranes. Other advantages of a composite approach include simplification of membrane synthesis, rapid prototyping, and reduced cost.

Though the advantages of the "conducting particles in hydrophobic polymer" approach are obvious, the progress in this area has been slow. Successful membranes should be compatible with the bi-continuous phase model, and provide a continuous path to support proton transport through the membrane. The main challenges are the choice of

conductive particles and proper dispersion of the particles in the matrix. The most widely studied conductive particles are water soluble inorganic heteropolyacids which are not applicable in practical fuel cells. Conductive particles insoluble in water are required. Organic particles such as cross-linked polystyrene sulfonic acid have received some attention, but proper dispersion of large particles (μm range) is difficult to control.

We previously showed that modified hydrophobic fumed silica particles dispersed in a hydrophilic polymer matrix agglomerate and form a three dimensional network within the polymer matrix (**Scheme 1.1**).[106] Based on these results, we expect that the inverse, hydrophilic fumed silica particles dispersed in a hydrophobic polymer may form an analogous materials. However, in this case, the silica will correspond to the conductive phase and the non-conducting matrix will provide favorable mechanical properties. The silica networks in these materials might be considered as a crude analog of the channel structure believed to be important for ion conduction in Nafion.

A simple method to resolve the issue of solid acid solubility and particle size is to design composite particles which have polymers covalently attached to an inorganic core. In such a design, the surface properties of the particles are dominated by the attached polymers, and if sulfonated, the particle surface could bear enough acid groups to provide sufficient protons to support a high conductivity. The covalent bonds between the polymer and the inorganic particle surface ensure the polymers would not dissolve, thus resolving proton conductivity and solubility problems of solid acids. Properties such as particle size, and the concentration of acid groups can be easily tuned by modifying the surface properties of the inorganic particles.

The designed membrane consists of two major components: polymer matrix and modified composite silica particles. The following describes the design considerations for the conducting particle in polymer matrix approach to fuel cell membranes.

Polymer matrix. The polymer matrix must provide mechanical and chemical stability under the harsh conditions of fuel cells. Except for needing to be hydrophobic to induce phase separation, the polymer matrix is a tunable parameter. Because it is not involved in proton transport, there is broad flexibility in the choice of the matrix polymer and architectural features such as molecular weight, polydispersity, cross-linking, crystallinity and the glass transition temperature. The research described in this thesis uses commercially available PVDF (polyvinylidene fluoride) as the matrix since it is highly hydrophobic, has good mechanical properties, and can be easily be cast into membranes.

Composite particles. The nature of the particles used, their volume fraction, the particle distribution, and even their orientation in the polymer matrix affect the conductive properties of the membrane. Structures other than spheres such as porous rings, cylinders, or other geometries may prove useful in controlling the formed in the matrix. In principal, any particle that can modified with appropriate surface functional groups and are stable under fuel cell conditions could be used in a composite membrane. The particles used in this research have a core-shell structure, with acid groups coating the surface of silica particles. Silica has high thermal and chemical stability and the chemistry for attaching surface functional groups is well-developed.

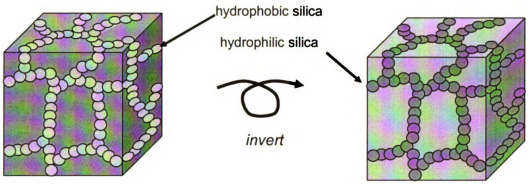

Scheme 1.1. Schematic diagram showing the structure of composite polymer electrolytes prepared by dispersing silica particles in a polymer matrix. At left, hydrophilic fumed silica is dispersed in a Li^+ conducting matrix to improve mechanical properties; at right, network formation polymer leads to a proton conducting network in a hydrophobic matrix.

Composite particle size. The particle size largely defines the available surface area and consequently the number of surface functional groups. Nanoparticles are preferred over larger particles because their higher surface to volume ratios enhance interfacial contact between polymer and dispersed particles. In ensembles of tightly packed aggregates, small particles also favor the formation of small conducting channels. A simplified schematic view of a composite membrane channel structure is shown in **Figure 1.9**.

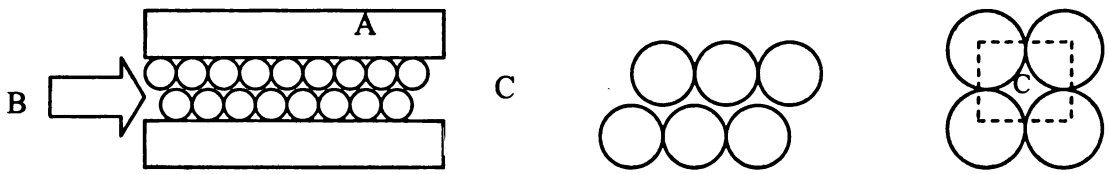

Figure 1.9. Simplified schematic diagram of the membrane microstructure. A, hydrophobic polymer matrix; B, hydrophilic phase; C, water channel between particles.

The smaller particle size also may favor retention of water at high temperatures due to capillary effects. If we view the space between particles as a capillary, we can apply the Laplace equation[107,108]

$$\Delta P = 2\gamma/r$$

where ΔP is the capillary pressure, γ is the surface tension and r is the radius of the capillary. Smaller capillary diameters strengthen the capillary effect and enhance the membrane's ability to retain water.

Particle aggregation and dispersion. The distribution of particles within the membrane has a major effect on conductivity and the onset of meaningful conductivity. A premise of the bi-phasic model is establishment of a continuous conducting phase that facilitates proton transport. Thus, understanding and controlling the particle-particle interactions is critical. For silica particles, the dominant interaction is through hydrogen bonding. Aggregation of particles functionalized with acid groups also may be driven by hydrogen bonding, but general methods for controlling the general architecture of the aggregates such as in Scheme 1.1 are not available.

The evolution of the conductivity as a function of particle content can be modeled as a percolation phenomena, where the conductivity rapidly rises when the particles establish a three-dimensional network of the conductive phase.[110-114] Kirkpatrick suggested a statistical percolation theory which relates the conductivity and volume fraction of the conductive fillers:

$$\sigma = \sigma_0 (V_f - V_f^*)^t$$

where σ is the conductivity of the mixture, σ_0 is the conductivity of the filler particles, V_f is the volume fraction of the filler, V_f^* is critical volume concentration at the percolation threshold, and t is an exponent that determines the increase in the conductivity above V_f^*. While this theory provides a good description of the experimental results near the transition point, it has limited predictive capabilities since V_f^* and t are sensitive to factors such as the size, shape and distribution of fillers, interactions between the matrix and the filler, and the quality of contacts (resistance) between filler particles.

Acid functional groups. Conductivity generally correlates with the pK_a of the acid. For example the pK_as of aromatic sulfonic acids, phosphoric acid, and acetic acid are approximately -2, 2.1, and 4.7, respectively. Carboxylic acid analogues of Nafion have much lower conductivities than its sulfonic acid form. Perfluorinated sulfonic acids have some of the lowest pK_as, -4. The nature of the acid groups also may influence phase separation.

Ion exchange capacity of composite particles. The IEC, expressed as mmol acid/g of sample directly contributes to a membrane's ability to absorb and retain water. While the IEC also defines the number of charge carriers in the membrane, the IEC, the conducting channel size, and channel distribution al influence the membrane conductivity. The interdependence of these factors could explain data for composite membranes prepared from conducting particles in conductive matrices. For example, When conducting particles are embedded in Nafion, the composite membranes usually have higher IEC numbers than pristine Nafion, but the conductivity is comparable or more commonly lower then that of pristine Nafion.[95]

Membrane fabrication methods

Membrane systems that incorporate both inorganic and organic components are usually prepared by direct mixing of pre-formed particles and a polymer solution followed by film casting or melt molding, *in-situ* growth of filler particles within a preformed membrane, or pore filling.

Direct mixing. In a direct mixing process, solids are ground into a fine powder and then dispersed with stirring in an organic solution of the ionomer. Membranes are obtained by casting films on substrates and followed by solvent elimination. As particles

tend to aggregate, the dried membranes typically contain a non-homogeneous dispersion of micron-sized particles.[106] Reducing the particle size maximizes contact with the polymer matrix and correlates with increased conductivity. [115] The membrane structure and properties are determined by the interactions between particles, polymer, and solvent during the solvent elimination, and it is not surprising that replicating the exact membrane structure at the microscale is difficult.

In-situ formation. *In-situ* formation of inorganic particles in a preformed membrane usually is effected by incorporating a filler precursor in the polymer matrix, and then adding acid or base to catalyze sol-gel process to form the inorganic filler in the matrix. The *in-situ* method affords nanometer sized colloidal particles homogeneously dispersed in the polymer matrix. Since the inorganic fillers grow concurrently with membrane formation, the interactions between the inorganic and organic components are much stronger than in a direct mixing process. Substantial effort has been focused on growing heteropolyacid particles in ionomers by sol-gel processes as this route limits particle size to the nanometer scale and allows molecular level contact between the inorganic and organic phase.[114] For example, Roziere et al. grew zirconium phosphate in sulfonated polyaryletherketones (sPEEK), but despite obtaining a reduced particle size, the electrochemical characteristics of the composite membranes were identical to those of pristine sPEEK membrane.[114]

Pore filling. [116-119] Membranes prepared by pore filling are composed of an inert porous substrate and a conductive polymer electrolyte that fills the pores of the substrate. The role of the porous substrate is to provide mechanical stability to the membrane. The pores within the matrix must be interconnected to ensure a continuous hydrophilic

channel for proton conductivity. As the conductivity and mechanical stability are provided by two separate phases, pore filled membranes avoid the excess swelling commonly found in single component sulfonated polymer membranes. The membrane structure at the microscale is repeatable and controllable, and filling porous structure with conductive particles can be as simple as *in-situ* filtration of finely dispersed nanoparticles through the membrane. Yamagushi et al.[126] used poly(acrylamide-*tert*-butylsulfonic acid) (PATBS) with an IEC of 4.5 mmol/g to fill porous cross-linked high density polyethylene (CLPE) substrates. The resulting membrane had a proton conductivity of 0.15 S/cm at 25 °C. Though the resulting membranes may not be ideal for practical fuel cells, the high conductivity shows the promise of the controlled membrane structure/high IEC electrolyte strategy.

Chapter 2

Electrolytes based on fumed silica modified with monolayers of sulfonic acids

Fumed silica is a nanoparticulate SiO_2 material prepared by the continuous flame hydrolysis of silicon tetrachloride at high temperatures. Fumed silicas have excellent thermal and chemical stability and are widely used as low cost fillers in polymers and as viscosity modifiers in low molecular weight polymers and oils. AEROSIL A200 (Degussa) is representative of commercially available fumed silicas. A200 particles are amorphous and nonporous, and have a specific surface area of ~200 m^2/g. A TEM image of the 14 ~16 nm diameter particles,[120] **Figure 2.1**, shows agglomeration of the primary particles into large-scale aggregates.

Because of their large surface area relative to their mass, nanoparticle surface chemistry plays a significant role in determining their physical properties. The surface of A200 is populated by hydrophobic siloxane (Si-O-Si) and hydrophilic silanol groups (Si-OH). The surface silanol groups are easily functionalized to tailor the interfacial properties of A200 for specific applications. The density of silanol groups limits the maximum concentration of groups which can be attached to the silica surface in a single layer. The most reliable analytical method for quantifying the surface silanol groups is titration with $LiAlH_4$, and monitoring the volume of hydrogen gas evolved from the reaction of $LiAlH_4$ with silanol groups.[121] Typical analyses of A200 yield 1.0 mmol of SiOH/g, or 3 OH groups per nm^2.[103]

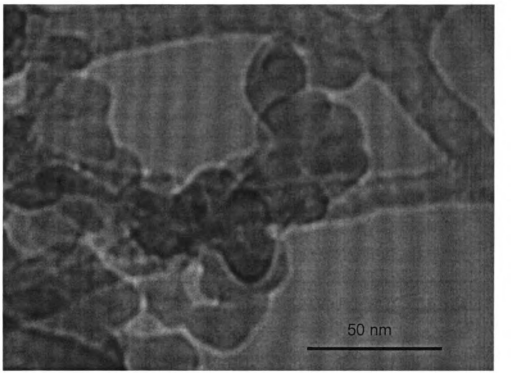

Figure 2.1. TEM image of pristine A200 particles. The sample was prepared by deposition of a methanol suspension of A200 particles onto a lacey formvar/carbon support coated on a 300 mesh copper grid.

Table 2.1. Useful IR absorptions for characterizing silica surfaces

Functional group	IR absorption (cm^{-1})
isolated SiOH	3747
bridged SiOH	3200-3800
SiOSi combination	1860
HOH	1620

Anchoring sulfonic acid monolayers to A200

Using organic groups, typically alkoxysilanes or chlorosilanes, to replace silanols on silica surfaces is termed silylation. The details of their reactivity and reaction mechanisms have been described previously.[122] In our initial attempt to convert silica particles to solid acids, we attached a single layer of sulfonic acid groups to the silica surface as shown in **Scheme 2.1**. The changes in the surface chemistry are conveniently followed by IR spectroscopy,[123] and **Table 2.1** lists important IR absorption bands of A200.[133] **Figure 2.2** shows the IR spectra of A200 and a series of surface-modified A200 derivatives described in this chapter. All of the silicas have two common characteristic absorptions, the Si-O-Si combination band at 1860 cm^{-1} and a broad peak at 3200 - 3800 cm^{-1} from hydrogen bonded SiOH. A sharp peak at 3747 cm^{-1} from isolated SiOH groups on the silica is apparent in A200 and less so in other silicas. Disappearance of this prominent band is a clear indication of successful surface modification of A200.[123]

Scheme 2.1. Attachment of sulfonic acid monolayers to A200 fumed silica

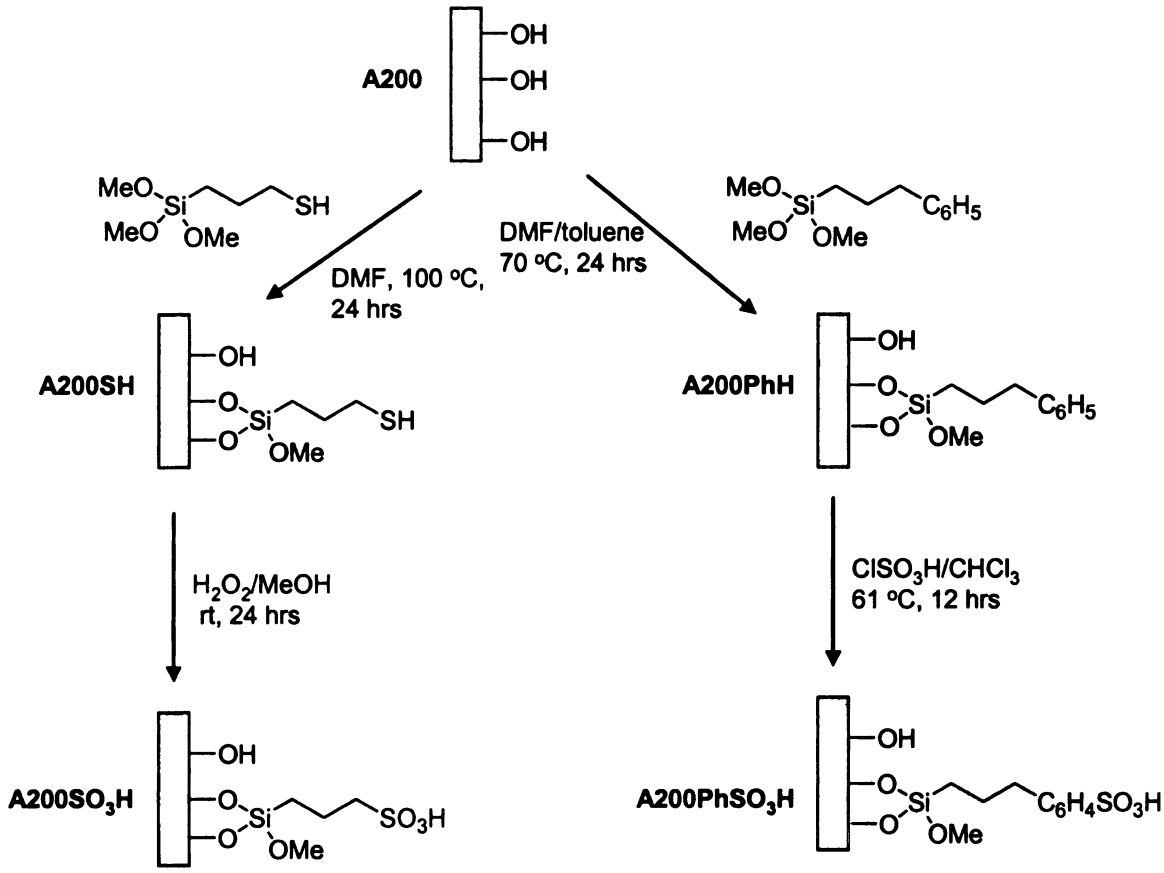

We introduced alkyl and arylsulfonic acids onto the surface of A200. In both cases, a precursor group was added to the surface which was eventually converted to the acid. Reaction of A200 with mercaptopropyl trimethoxysilane in DMF for 24 hours at 100 °C, followed by washing with toluene and isolation by centrifugation yielded ***A200SH***. The IR spectrum of ***A200SH*** shows the expected bands for CH_2 stretching at ~ 2950 cm^{-1} and methoxy C-H stretching at 2850 cm^{-1}. A weak band at 2620 cm^{-1} (S-H stretching) confirmed the presence of the thiol. Oxidizing ***A200SH*** with H_2O_2 at room temperature for 24 hours followed by washing with acetone and H_2O yielded ***A200SO$_3$H***. Successful oxidation was indicated by disappearance of the thiol band and an increase in the intensity of the bridged hydroxy band (3200-3800 cm^{-1}). The intensity of the alkyl bands decreased which may indicate loss of some alkyl groups (e.g. methoxy groups) or errors in normalizing the spectra. As silica absorbs strongly below 1400 cm^{-1}, we could not observe the expected SO_2 stretching peaks of the sulfonic acid (1100-1300 cm^{-1}).

To tether arylsulfonic acids to A200, (2-phenylethyl)trimethoxysilane was stirred for 24 hours in a slurry of A200 in DMF at 70 °C. ***A200Ph*** was isolated by washing with toluene and acetone, and drying under vacuum. The IR spectrum of ***A200Ph*** shows the expected C-H stretching bands above and below 3000 cm^{-1} for the aryl sp^2 C-H and alkyl sp^3 C-H groups respectively. Also obvious were sharp bands at 1610, 1460, and 1500 cm^{-1} from benzene ring, and a methoxy band at 2850 cm^{-1}. After sulfonation with chlorosulfonic acid in $CHCl_3$, ***A200PhSO$_3$H*** was washed with $CHCl_3$ and acetone until the supernatant was neutral, and dried under vacuum. The most significant change in the IR was a strong increase in the intensity of the broad hydroxy band, especially its extension to below 3000 cm^{-1}. The bands from the benzene ring were retained, but the

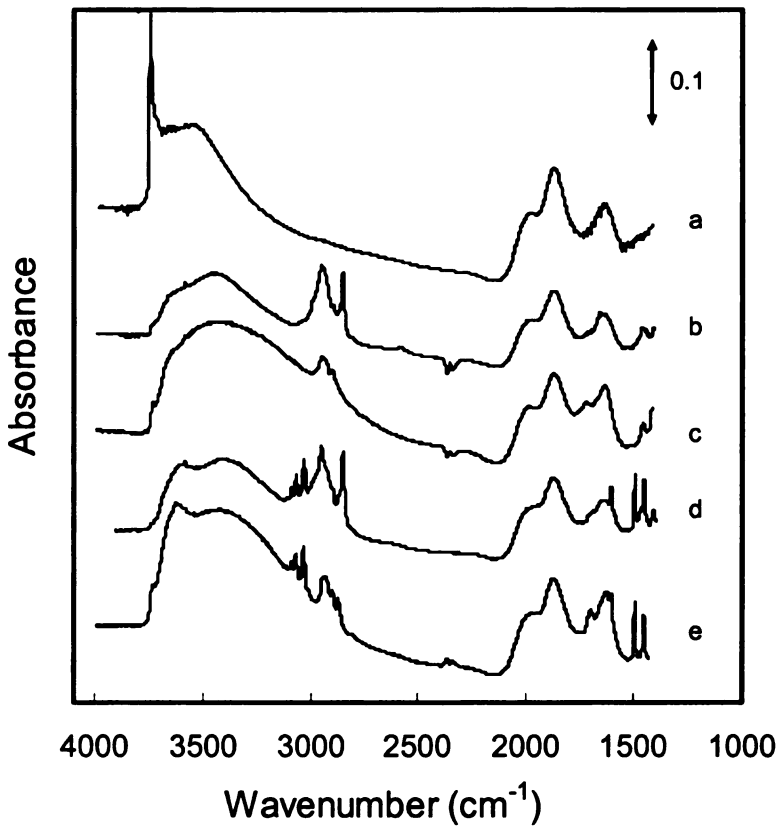

Figure 2.2. IR spectra of surface-modified A200 particles. a, A200; b, A200-SH; c, A $200SO_3H$; d, A200PhH; e, $A200PhSO_3H$

methoxy band was almost completely lost, presumably due to the acidic sulfonation conditions. **Figure 2.3** shows TGA data for A200 and the four modified A200 silicas. All showed some loss of water at the beginning of the run despite being held at 110 °C for 30 min prior to initiating the analysis. This behavior was more pronounced for ***A200SO$_3$H*** and ***A200PhSO$_3$H*** which showed earlier loss of water than corresponding ***A200SH*** or ***A200PhH*** and is consistent with sulfonic acid containing polymers retaining water to ~130 °C.[82]

The IR spectra of **Figure 2.2** showed that a substantial population of silanols remained on the surface after functionalization. These unreacted silanol groups can complicate further characterization of the silicas and composite membranes prepared from them. In particular, quantifying the number of acid groups on the surface would be simplified if the silanols could be eliminated. As shown in **Scheme 2.2**, we masked the residual silanols in functionalized silicas by dispersing them in a solution of trimethylsilyl chloride (TMSCl), diethylamine, and toluene. After stirring for 2 hours, the silica was washed with toluene and dried under vacuum. IR spectra of the "TMS capped" silicas are shown in **Figure 2.4**. Strong 2964 cm^{-1} bands for the added methyl groups are obvious in the spectra of all silicas treated with TMSCl, indicating that a large fraction of the surface silanols are chemically accessible. However, the 3400-3600 cm^{-1} hydroxy bands diminished but did not disappear, since some silanols in A200 are embedded in the silica and inaccessible.

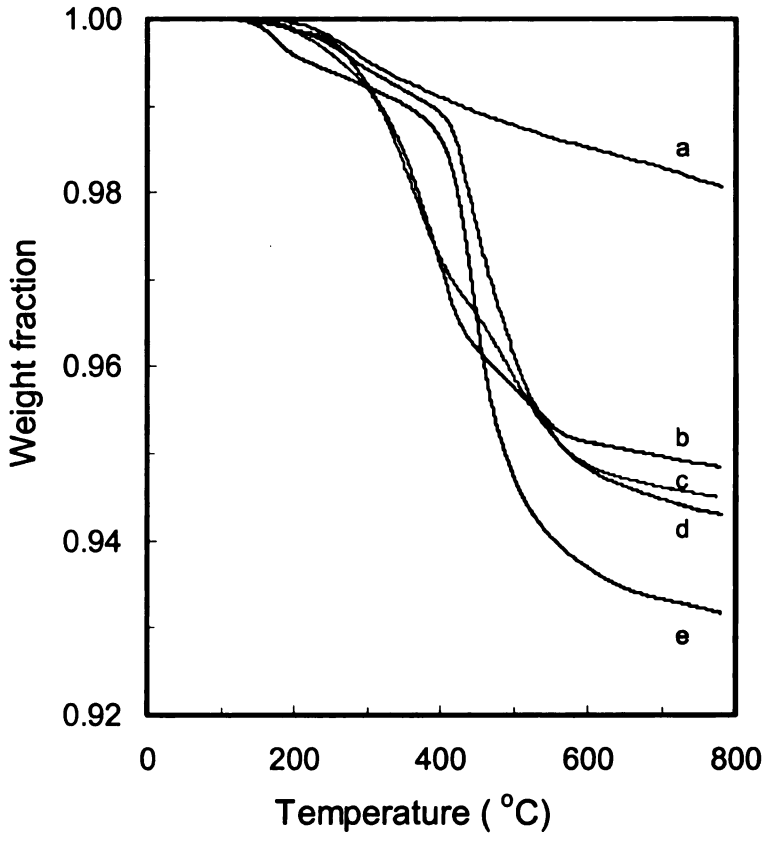

Figure 2.3. Thermogravimetric analysis results for surface-modified A200 particles. The experiments were run in dry air at a rate of 10 °C/min. Prior to initiating the run, all samples were stabilized at 110 °C for 30 min. a, A200; b, A200SH; c, $A200SO_3H$; d, A200PhH; e, $A200PhSO_3H$.

Scheme 2.2. TMS capping of silanols on modified fumed silicas.

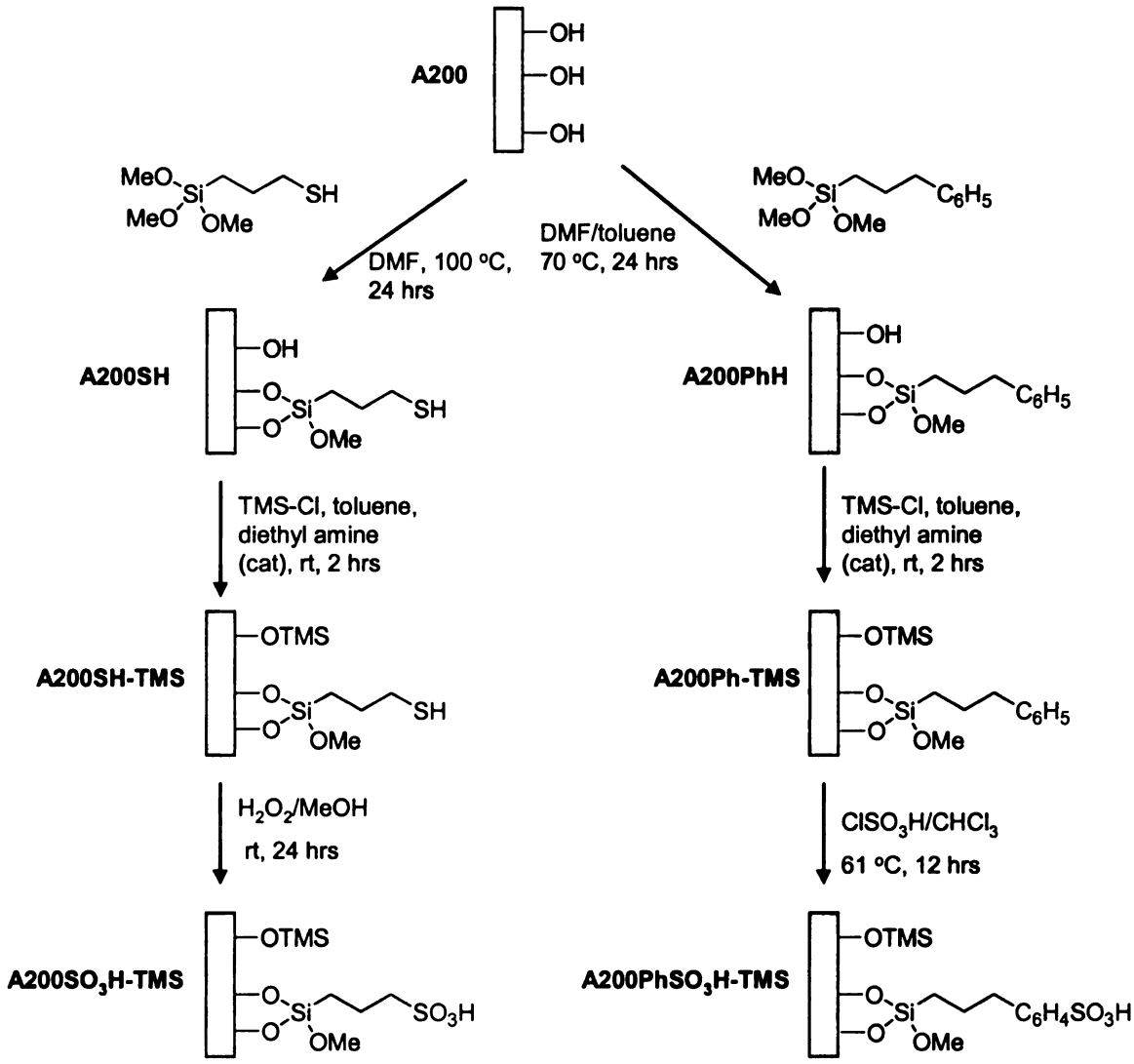

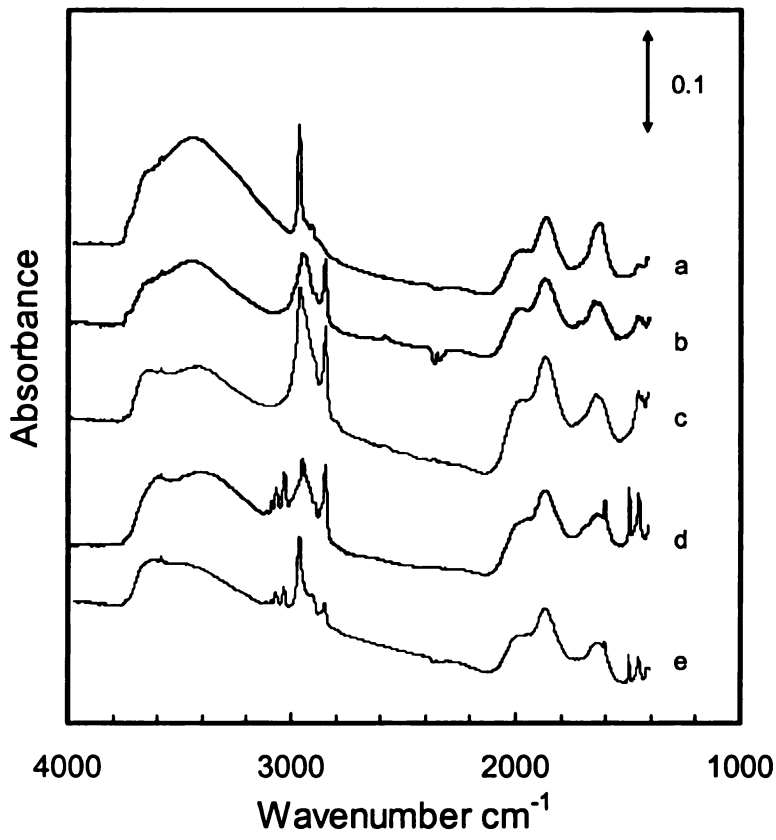

Figure 2.4. IR spectra of surface-modified A200 particles before and after treatment with trimethylsilyl chloride. a, A200-TMS; b, A200SH; c, A200SH-TMS; d, A200PhH; e, A200Ph-TMS

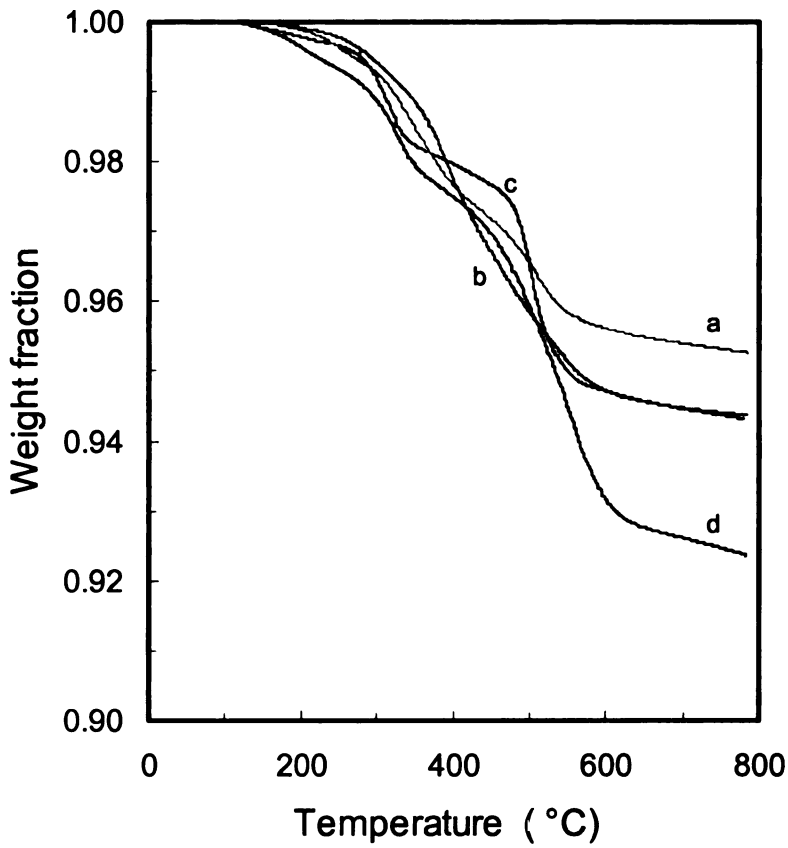

Figure 2.5. Thermogravimetric analysis results for surface-modified A200 particles following treatment with trimethylsilyl chloride. The experiments were run in dry air at a rate of 10 °C/min. Prior to initiating the run, all samples were stabilized at 110 °C for 30 min. a. A200SO_3H-TMS ; b, A200SH-TMS; c, A200Ph-TMS; d, A200PhSO_3H-TMS.

TGA analysis of the "capped" silicas (**Figure 2.5)** showed that the thermal stability was largely unaffected. This is consistent with the <2% weight loss calculated for a full monolayer of TMS on A200.

The ion exchange capacity (IEC, moles of acid functional groups per unit mass) should be directly related to the sulfur content in the silicas. The thiol content of silicas were determined by UV/vis using Ellman's reagent (5,5'-dithio-bis(2-nitrobenzoic acid)).[124] The data in **Table 2.2** show that ***A200SH*** and ***A200SH-TMS*** have comparable thiol contents, ~0.38 mmol/g. After oxidation, the IEC measured by titration is 0.33 mmol/g for ***A200SO$_3$H*** and 0.26 mmol/g for ***A200SO$_3$H-TMS***. The lower IEC for ***A200SO$_3$H-TMS*** may reflect less efficient oxidation of the more hydrophobic ***A200SH-TMS***. The IEC of the aromatic system ***A200PhSO$_3$H*** is comparable to that of the alkyl systems.

Table 2.2. Measured thiol contents and ion exchange capacities

	A200SH	**A200SH-TMS**	**A200SO$_3$H-TMS**	**A200SO$_3$H**	**A200PhSO$_3$H**
Thiol [1] (mmol/g)	0.39	0.36	0.00	0.00	0.00
IEC [2] (mmol/g)	0.00	0.00	0.26	0.33	0.27

1. Measured by titration with Ellman's reagent (5,5'-dithio-*bis*(2-nitrobenzoic acid)), and 0.01M EDTA in 100 mL of pH 8.0 buffer.
2. Measured by titration of 0.50 g of silica after conversion of the sulfonic acids to the corresponding Na salt using a mixture of 30mL of 2M NaCl and 5 mL of 2-methoxyethyl ether. Dried A200 was titrated under same conditions as blank. The IEC results were average of three measurements.

Composite membranes were prepared by mixing ***A200SO$_3$H*** or ***A200PhSO$_3$H*** samples with polyvinylidene (PVDF). The functionalized silicas were stirred in DMF until homogeneous and then the solution was combined with a DMF solution containing the desired amount of PVDF. The mixture was stirred overnight until the silica powder was dispersed homogeneously in polymer solution. To cast films, solutions were poured onto glass slides heated to ~ 50 °C on hot plate. Round membranes ~1 cm in diameter were obtained after solvent evaporation and were further dried in a vacuum oven at 80 °C overnight to remove residual solvent. Membranes with <50 wt% particles were hydrophobic, and water deposited on the membrane surface remained spherical and did not spread. The membranes were pretreated with boiling in 8% HNO_3 and then deionized water. For conductivity measurements, the round membranes were sandwiched between 2 stainless steel discs, 0.5 cm diameter, which contacted two platinum electrodes. However, the membrane resistance was too high and outside the operational range of the instrument.

Conclusion

Alkyl and aryl sulfonic acid monolayers were successfully anchoring on the surface of A200 fumed silica. Titration of the sulfonic acid groups on the silica indicated ~ 0.3 mmol/g. Membranes prepared by dispersing the modified silicas in PVDF proved to be non-conductive. At the highest particle loadings, the mechanical properties of the membranes were poor and the membranes cracked. Increasing the concentration of acid groups tethered to particle surfaces is needed to increase the number of charge carriers and the conductivity of the membranes.

Experimental

Aerosil 200 (A200), a gift from Degussa AG, Frankfurt, Germany, was dried under vacuum at 130 °C for 2 h before use. (2-Phenylethyl)trimethoxysilane, (3-mercaptopropyl)trimethoxysilane (95%), H_2O_2 (30% solution in water), $ClSO_3H$ (99%), trimethylchlorosilane (98%) and butyl lithium (2.5M in hexanes) were purchased from Aldrich and used as received.

^1H and ^{13}C NMR spectra were obtained at room temperature in $CDCl_3$ using a Varian Gemini-300 spectrometer, with the solvent proton and carbon signals used as chemical shift standards. The chemical shifts are reported in ppm relative to α,α,α-trifluoromethylbenzene. A Nicolet IR/42 spectrometer purged with dry nitrogen was used to obtain infrared spectra. Samples used were 1 cm^2 pressed pellets prepared from ~ 100 mg of various modified silica. All spectra reported were acquired by signal averaging 32 scans at a resolution of 4 cm^{-1}. Thermogravimetric analyses (TGA) were performed in dry air at heating rate of 10 °C/min on a Perkin Elmer TGA 7 instrument. Samples were held at 110 °C for 30 min before the run was started. Dynamic light scattering (DLS) measurements were performed with a Protein Solutions Dyna Pro-MS/X system with temperature control. Samples were sonicated for 20 min, filtered and allowed to equilibrate in the instrument for 25 minutes at 25 °C before taking measurements.

AC impedance data were obtained from an HP 4192A LF impedance analyzer scanning from 5Hz to 13MHz with an applied voltage of 10 mV under the control of an in-house designed LabView application. Round membranes (~1 cm diameter) were sandwiched between 2 stainless steel electrodes in a Teflon cell isolated in an oven equipped with a gas inlet and outlet. Humidity control was obtained by bubbling dry N_2

into 75 °C deionized water under atmospheric pressure. TEM images were taken using a JEOX 100CX transmission electron microscope. Membrane samples for TEM were prepared by cryosectioning using a PowerTome-XL by BAL-TEC RMC with thickness control of ~80 nm.

***Mercaptopropyl functionalized silica* (A200SH).** Mercaptopropyl trimethoxysilane (1.7 mL, 8.6 mmol) was added to a slurry of 4.5 g of A200 (4.5 mmol silanol groups) in 120 mL DMF at 100 °C. After stirring for 24 h at 100 °C under N_2, the solvent was removed by distillation. The functionalized silica was washed with toluene (3 × 30 mL) acetone (30 mL), and then dried under vacuum at 80 °C for 2 h to yield 4.1g of **A200SH** (90%).

Propanesulfonic acid modified silica. (A200SO$_3$H). A slurry of 2 g of mercaptopropyl functionalized silica in 40 mL of a 1:3 (v/v) solution of H_2O_2/MeOH was stirred under N_2 for 24 h at room temperature. The modified silica was collected by filtration, and after washing with water (3 × 30 mL) and acetone (30 mL), the modified silica was dried under vacuum at 80 °C for 2 h to yield 1.9 g of ***A200SO$_3$H*** (95%).

2-Phenylethyl modified silica (A200PhH). (2-Phenylethyl)trimethoxysilane (3.3 mL, 14.7 mmol) was added to a slurry of 4.5g of A200 (4.5 mmol silanol groups) in 120 mL of a 4:1 (v/v) mixture of DMF and toluene at 70 °C of. After stirring for 24 h at 70 °C under N_2, the solvent was removed by distillation. The functionalized silica was washed with toluene (3 × 30 mL) acetone (30 mL), and dried under vacuum at 80 °C for 2 h to yield 4.1 g of ***A200PhH*** (90%).

Sulfonated (2-phenylethyl) modified silica (A200PhSO$_3$H). Under a blanket of nitrogen, chlorosulfonic acid (1.0 mL, 15 mmol) was added drop-wise to stirred slurry of 2 g of ***A200Ph*** in 60 mL $CHCl_3$. After refluxing overnight, the solvent was removed by rotary evaporation. The functionalized silica was washed with $CHCl_3$ (3 × 30 mL) and acetone (30 mL), and then was dried under vacuum at 80 °C for 2 h to yield 1.95 g of ***A200 PhSO$_3$H*** (98% yield).

Trimethylsilane functionalized silica (A200TMS). Under a blanket of nitrogen, *n*-butyllithium (1.0 mL of a 2.5 M solution in hexanes) was added to a vigorously stirred slurry of the silica (2.0 g) in 40 mL of ice-cold THF. After 15 min, the silica was collected by vacuum filtration, washed with THF (3 × 10 mL), and dried under vacuum. After re-suspending the sample in 20 mL THF, trimethylchlorosilane (0.3 mL, 2.4 mmol) was added and the mixture was stirred for 20 min. The silica was collected by filtration, washed with THF (3 × 10 mL), and dried under vacuum at 80 °C for 2h to yield 1.9 g of ***A200TMS*** (98% yield).

Mercaptopropyl functionalized silica end capped with TMS (A200SH-TMS). To a slurry of 2g ***A200SH*** in 40 mL toluene and 0.2 mL diethylamine (2.0 mmol), 0.50 mL trimethylchlorosilane (TMSCl, 4.0 mmol) were injected under nitrogen and the mixture was stirred for 2 hours at room temperature. The functionalized silica was collected by filtration and washed with toluene (3 × 30 mL) followed by vacuum drying at 80 °C for 2h to yield 1.8 g of ***A200SH-TMS*** (90% yield).

Propanesulfonic acid silica end-capped with TMS (A200SO$_3$H-TMS). A slurry of 2 g of ***A200SH-TMS*** in 40 mL of a 1:3 (v/v) solution of H_2O_2/MeOH was stirred under N_2 for 24 h at room temperature. The modified silica was collected by filtration,

and after washing with water (3 × 30 mL) and acetone (30 mL), the modified silica was dried under vacuum at 80 °C for 2 h to yield 1.9 g of ***A200SO$_3$H-TMS*** (95%).

2-Phenylethyl modified silica end-capped with TMS (A200Ph-TMS.) to a slurry of 2g ***A200PhH*** in 40 mL toluene and 0.2 mL diethylamine (2.0 mmol), 0.50 mL trimethylchlorosilane (TMSCl, 4.0 mmol) were injected under nitrogen and the mixture was stirred at room temperature for 2 hours. The functionalized silica was collected by filtration and washed with toluene (3 × 30 mL) followed by vacuum drying at 80 °C for 2h to yield 1.8 g of ***A200Ph-TMS*** (90%).

2-Phenylethyl sulfonated silica end capped with TMS (A200PhSO$_3$H-TMS.) Under a blanket of nitrogen, chlorosulfonic acid (1.0 mL, 15 mmol) was added drop-wise to a stirred slurry of 2 g of ***A200Ph-TMS*** in 60 mL $CHCl_3$. After refluxing overnight, the solvent was removed by rotary evaporation. The functionalized silica was washed with $CHCl_3$ (3 × 30 mL) and acetone (30 mL), and then was dried under vacuum at 80 °C for 2 h to yield 1.9 g of ***A200PhSO$_3$H-TMS*** (95%).

Ion-exchange capacity (IEC) measurements. Silica (0.50 g) substituted with sulfonic acid groups was added to a mixture of 5 mL of 2M NaCl and 5 mL of 2-methoxyethyl ether with stirring. After soaking for 24 h, the silica was collected by filtration, washed 3 times with 5 mL of 1:1 (v/v) of NaCl and 2-methoxyethyl ether. The combined liquid filtrate was titrated to the phenolphthalein end point with 0.0112 M NaOH solution. Dried A200 titrated under same conditions was used as a blank.

Determination of thiol contents. A linear calibration curve was generated by using a Perkin-Elmer Lambda 40 UV/VIS spectrometer to measure the absorbance of

standard solutions (1.0×10^{-4} M, 1.5×10^{-5} M, and 5.0×10^{-5} M) of Ellman's reagent in 0.01M EDTA in pH 8.0 phosphate buffer. To measure the thiol content of sample, functionalized silica (0.014 g) was added to 100 mL of 1.5×10^{-4} M solution of Ellman's reagent and 0.01M EDTA in pH 8.0 phosphate buffer. The absorbance of these solutions was measured after 16 h, and the thiol content was inferred from the calibration curve.

Membrane preparation. PVDF (0.01g) and 0.4 mL DMF were added to a vial and stirred at room temperature until the PVDF dissolved. The desired amount of ***A200SO$_3$H*** or ***A200PhSO$_3$H*** particles were weighed in another vial with 1.0 mL DMF and stirred for 12 hour until homogeneous. The two solutions were combined and stirred for 12 hours. Membranes were cast by pouring the final solution onto glass slides heated to ~ 50 °C on a hot plate. Round membranes ~1 cm in diameter were obtained after solvent evaporation and were further dried in a vacuum oven at 80 °C overnight to remove residual solvent.

Hybrid membrane pretreatment. The round membranes were peeled from the glass plate and their size and thickness were measured with a micrometer. Membranes were first boiled in 8% HNO_3 for 30 min, rinsed with water, and then boiled in deionized water for 30 min. The pretreated membranes were stored in deionized water at room temperature before measurements.

Membrane conductivity measurements. The membranes were sandwiched between 2 stainless steel discs (0.5 cm diameter) which were in contact with two platinum electrodes. AC impedance measurements were conducted with an applied voltage of 10 mV over a frequency range of 5 Hz to 13 MHz.

Chapter 3

Sulfonic acid multilayer tethered to silica nanoparticle surfaces

Chapter 2 described successful anchoring of alkyl and aryl sulfonic acid monolayers on A200 fumed silica. The maximum number of acid groups that can be immobilized on silica surfaces is ~1 functional group/nm^2. A200 has a surface area of 200 m^2/g, which corresponds to a maximum surface loading of ~0.3 mmol/g. Membranes prepared by dispersing the modified silicas in PVDF proved to be non-conductive. At the highest particle loadings, the mechanical properties of the membranes were poor and the membranes cracked. Increasing the concentration of acid groups tethered to particle surfaces will increase the number of charge carriers and should improve the conductivity of the membranes. A convenient method for anchoring multiple ions to a single surface site is the use of polymer chains as supports.

Two general strategies are particularly effective for attaching organic groups to nanoparticles. In "grafting to" processes on silica surfaces, preformed polymers that have been end-functionalized with either chloro or alkoxysilane groups are reacted with silanols on silica surfaces to form a covalently bound polymer layer. The advantages of this method are that the properties and purity of the polymers can be controlled and characterized before they are anchored to the surface. However, the areal density of the tethered polymers is usually low since macromolecules must diffuse through an existing polymer layer to reach the silica surface.[125-128] This problem is exacerbated for nanoparticles since the size of the polymer and nanoparticles may be comparable.

The "grafting from" approach, commonly termed surface initiated polymerization,[129,130] involves growth of polymers from surfaces. Initiators are

covalently attached to the particle surface and then polymerization is initiated from the surface. The small size of monomers compared to macromolecules enables their facile diffusion to particle surfaces, enabling the growth of dense brush layers. The application of controlled polymerization techniques to the growth of polymer chains from surfaces provides control over the polymer's grafting density, composition, structure and molar mass. Atom Transfer Radical Polymerization (ATRP) is one of the most popular strategies for controlled polymerizations from surfaces since radical polymerizations are tolerant to a wide range of functional monomers and experimental conditions, and ATRP provides polymers of predictable molecular weights and low polydispersities.[131-136]

The ATRP reaction mechanism is shown below. Radicals are generated through a reversible redox process catalyzed by a transition metal complex (M^n-X/Ligand, where X is a halogen atom) which undergoes a one-electron oxidation with concomitant abstraction of X from the dormant chain, R-X. Polymer chains grow by addition of the intermediate radicals to monomers in a manner similar to a conventional radical polymerization, with a rate constant k_p. Termination reactions with a rate constant k_t, also occur in ATRP, mainly through radical coupling and disproportionation. The equilibrium between the active free radicals and dormant species ensures a low concentration of radicals thereby limiting termination reactions.[137]

$$\text{R-X} + \text{M}^n\text{-X / Ligand} \rightleftharpoons \text{R}^{\bullet} + \text{X}_2\text{-M}^{n+1} \text{ / Ligand}$$

$$\text{termination} \xleftarrow{k_t} \text{R}^{\bullet} \xrightarrow[\text{monomer}]{k_p} \text{polymerization}$$

Results and Discussion

Composite particles using A200 as cores. **Scheme 3.1** shows the synthetic approach used to attach sulfonic acid polymers to silica particles. A200 was selected as the particle source to enable direct comparison of the data presented in this chapter with those reported in Chapter 2. The growth of polystyrene from particles via ATRP is based on the work of Paten and coworkers.[136] 4-Vinylbenzyl chloride (4-VBC) was hydrosilylated with dimethylchlorosilane using Karstedt's catalyst (**Scheme 3.2**). ^{1}H NMR analysis of the reaction of 4-VBC with dimethylchlorosilane showed a 4.6:1 ratio of the endo and exo products (**Figure 3.1**).

Scheme 3.1. Synthetic route used to tether acids to silica surfaces

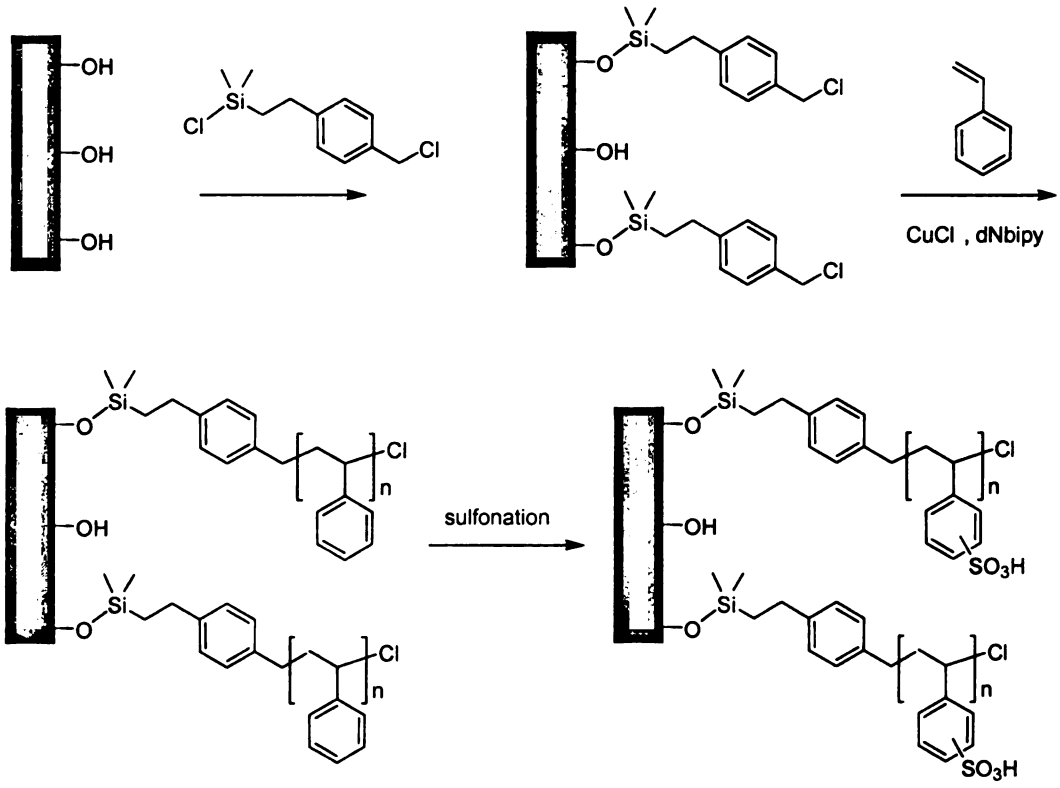

The initiator was anchored to dried A200 by stirring a DMF/toluene slurry of the particles and chlorosilane overnight, and then washing the product with solvent and drying under vacuum. **Figure 3.2** shows IR spectra of A200 (trace a) and A200 after anchoring the initiator layer (trace b). The disappearance of the sharp peak at 3740 cm^{-1} in the A200 spectrum, the appearance of bands above and below 3000 cm^{-1} from the aromatic and alkyl C-H bonds, and weak bands from the aryl ring at 1400-1500 cm^{-1} confirm successful attachment of the chlorosilane initiator. Thermogravimetric analysis (TGA) of pristine and modified A200 (**Figure 3.5**) support the IR data. Prior to initiating the runs, each sample was equilibrated at 110 °C for one hour in the TGA apparatus, and then was heated at 10 °C/min in air. Pristine A200 lost 2.5% of its original weight at 600°, which is consistent with the loss of adsorbed water and some dehydration of surface silanols. The weight loss of A200 with an attached initiator layer was ~ 8%. Considering the surface area of A200 and the additional 5.5% weight loss, we estimate a grafting density of 1 initiator/nm^2 and ~ 0.30 mmol initiator/g silica.

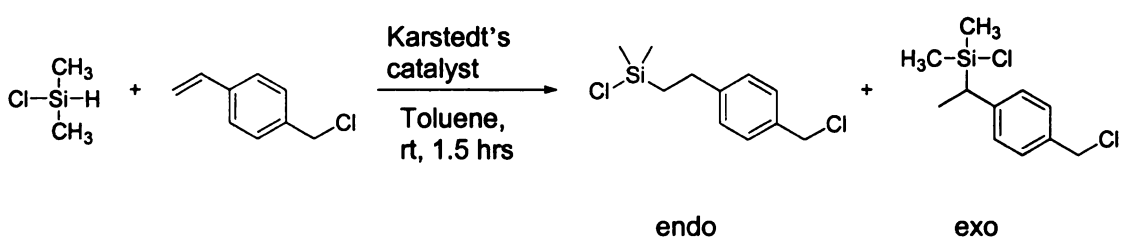

Scheme 3.2. Synthesis of the chlorosilane initiator via hydrosilylation.

Figure 3.1. ^{1}H NMR spectrum of 2-(4-chloromethylphenyl)-ethyldimethylchlorosilane **2**

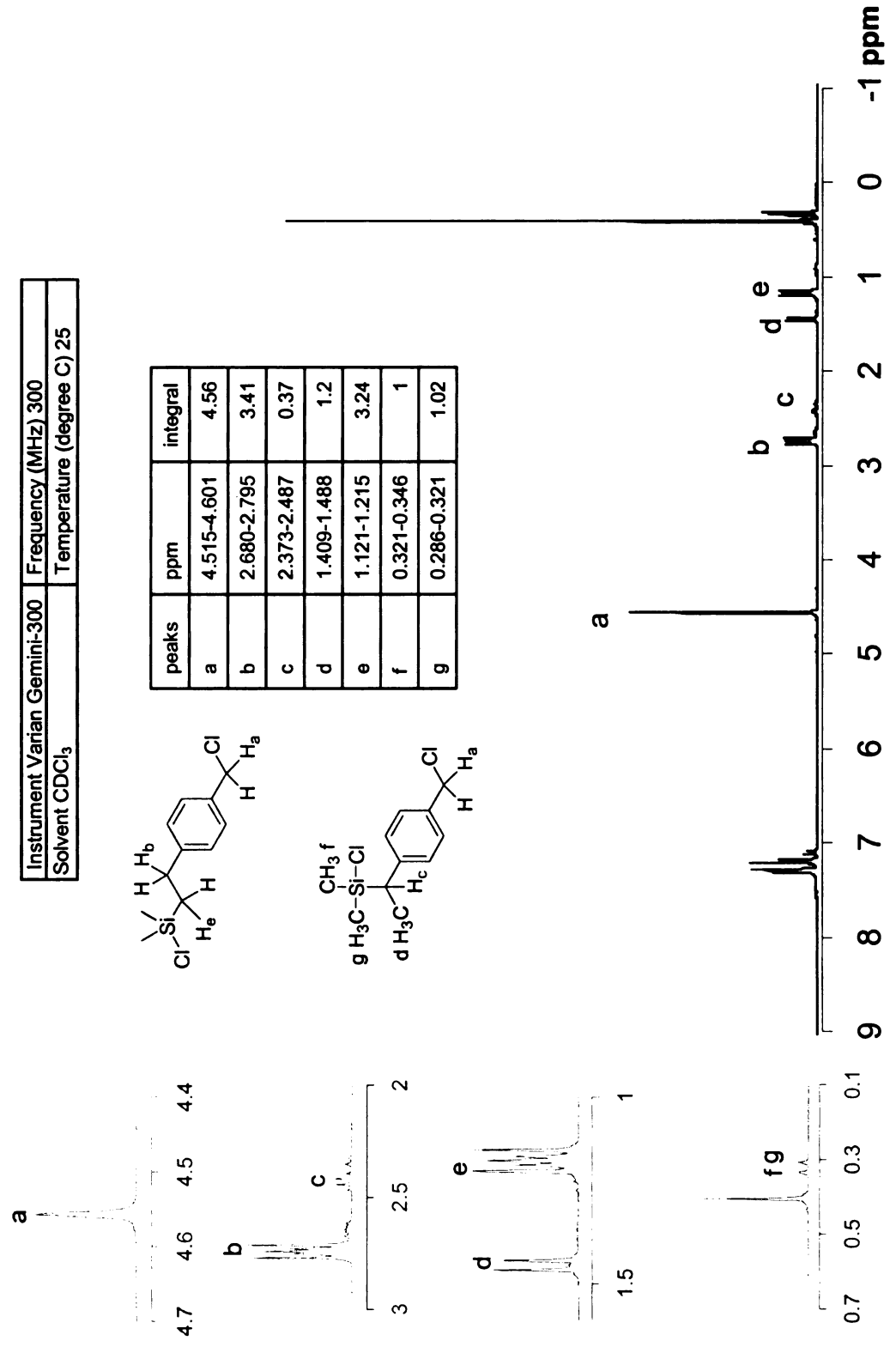

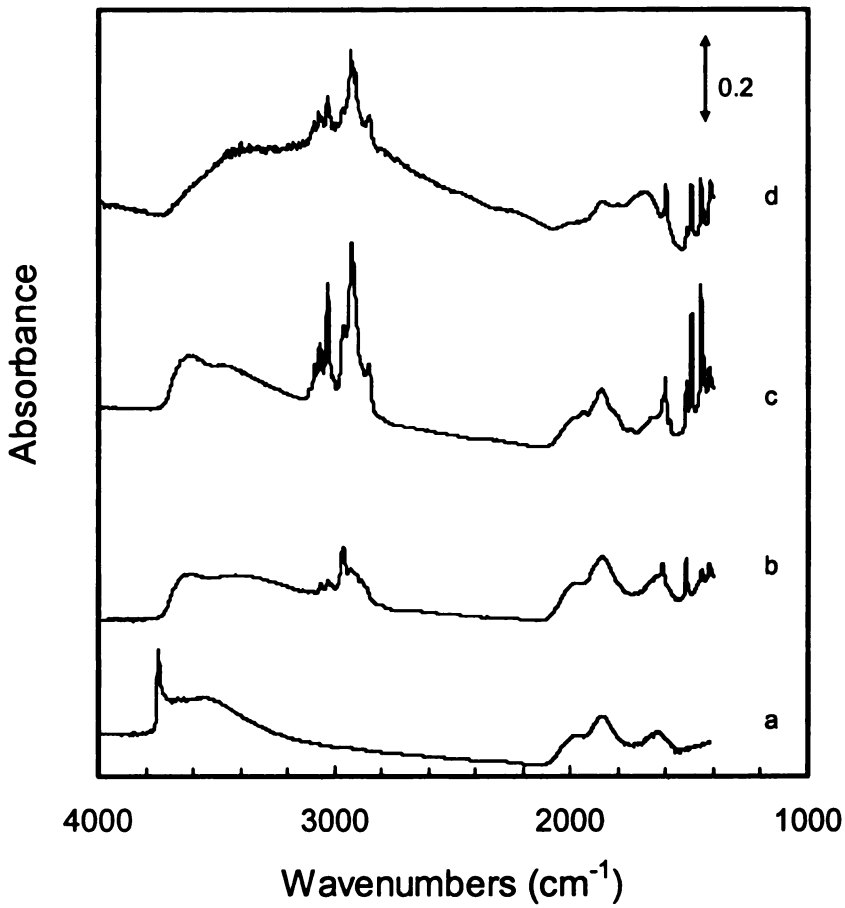

Figure 3.2. IR spectra of A200 (a); A200 with an attached initiator layer (b); A200 after ATRP of styrene from the surface (c); polystyrene anchored to A200 after sulfonation (d).

Polymerization was initiated from the particle surface by adding styrene, CuCl, and one equivalent of di-*n*-nonylbipyridine (dNbpy), a ligand for Cu. The polymerization was run at 110 °C in xylenes for 2 hours, and then the particles were sequentially washed with toluene and ethanol. The IR data (**Figure 3.2**, trace c) show a dramatic increase in the intensity of the aromatic and aliphatic bands after polymerization. The changes in IR intensity caused by the growth of polymer from the surface are clearly shown in **Figure 3.3,** where the IR data are normalized with respect to the weight of silica in each sample as determined from TGA results. Because of the structural similarity of the initiator and polymer, the IR bands in both spectra are similar, but after polymerization the bands are much more intense. Several absorbance are due to the silica particles. A substantial band at 3700 ~ 3400 cm^{-1} from O-H stretching **(Figure 3.4)** suggests silanols trapped within the fumed silica matrix, or residual surface silanols that did not participate in the initiator anchoring step. Broad bands between 1600 and 2000 cm^{-1} also are characteristic of silica particles.[123]

The TGA weight loss for the polystyrene/A200 particles **(Figure 3.5)** increased to 28% and the onset for weight loss increased by 30°. (The increased the decomposition temperature for polystyrene attached to silica may represent the higher volatility of the initiator compared to polystyrene.) These measurements were taken after continuously extracting the particles with toluene overnight under Soxhlet conditions to ensure that no polystyrene was physically absorbed in the particles. A 5% HF solution was used to cleave the polymers from the silica surface, and analysis of the polystyrene by GPC gave M_w = 14,900 with a polydispersity of 1.42. Combining both TGA and GPC results, we estimate the number of polymer chains on the silica surface was ~0.02 mmol/g sample.

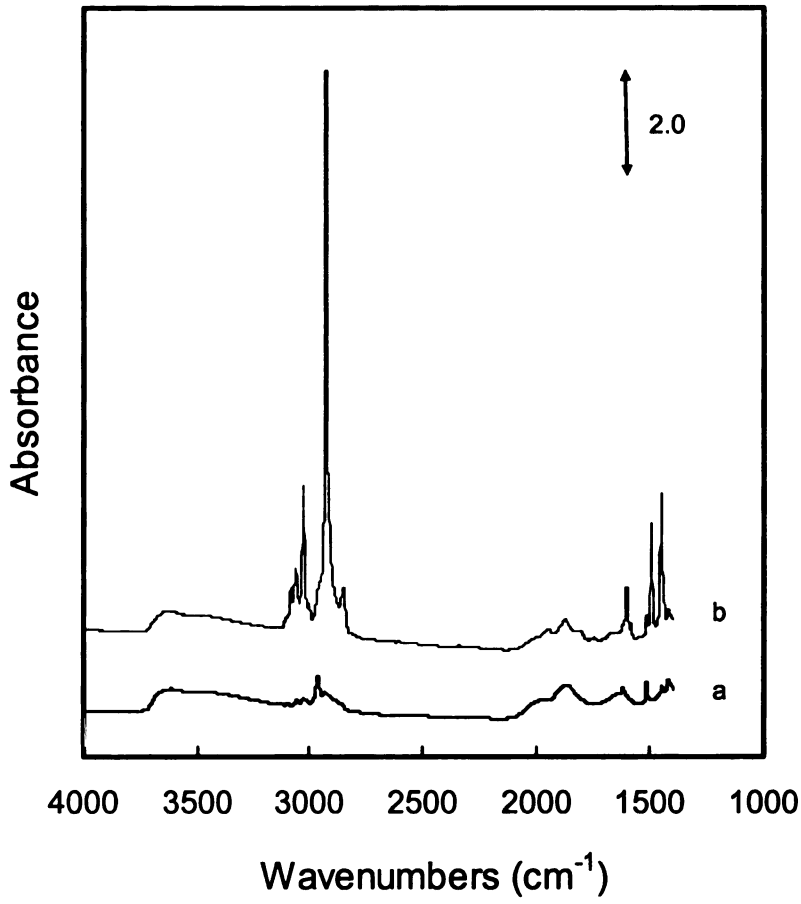

Figure 3.3. IR spectra of A200 (a); A200 with an attached initiator layer (b); A200 after ATRP of styrene from the surface. The spectra were normalized with respect to the silica particle content using the TGA data. The samples were 1 cm diameter disks prepared by pressing 120 mg of sample into pellets.

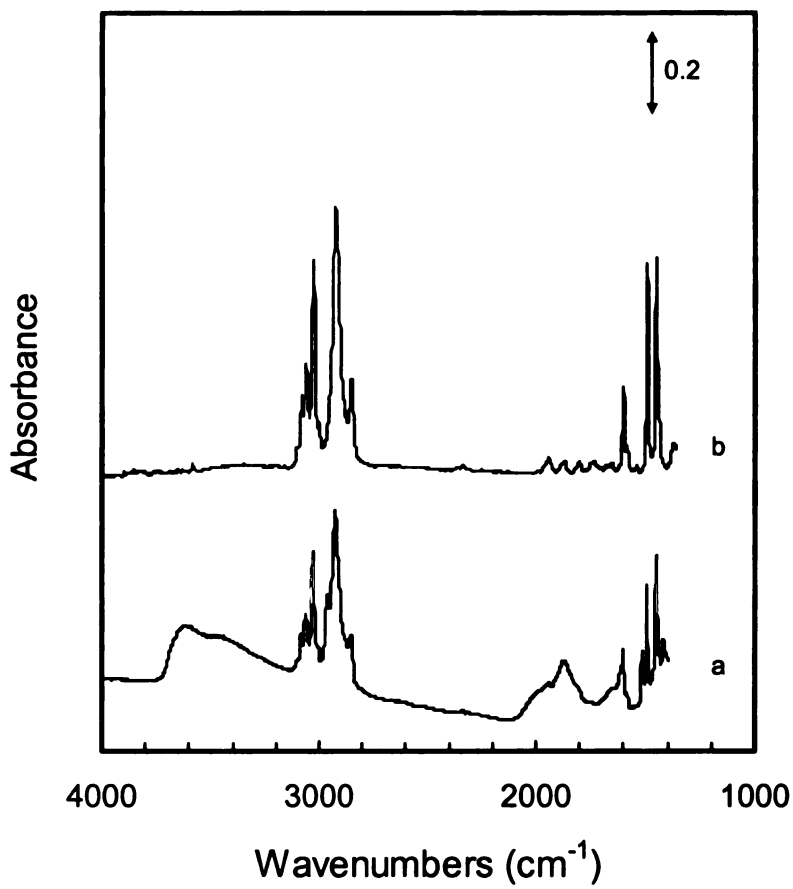

Figure 3.4. IR spectra of A200 after ATRP of styrene from the surface, (a); and pure polystyrene, (b).

Sulfonation of the particle-bound polystyrene with chlorosulfonic acid at room temperature introduced the arylsulfonic acids. The sulfonated particles were very hydrophilic. After washing the particles until neutral and drying under vacuum to remove residual acid, the sulfonated particles were titrated resulting in an Ion Exchange Capacity (IEC) of 3.2 mmol/g of sample. IR shows a broad absorption above 2400 cm^{-1}, consistent with the presence of the sulfonic acid. S-O stretching bands were obscured by bands from the silica particles and were not observed.

Figure 3.6 compares TGA data for sulfonated polystyrene attached to silica with sulfonated polystyrene cross-linked with 2% divinylbenzene. A sulfonated version of the crosslinked polystyrene, used as a control, is shown in trace c. Both sulfonated materials show an early onset of weight loss followed by a gradual weight loss that extends to high temperatures. The difference in traces a and c are due to the inert silica cores of the particle-bound polymers; normalization of the data gave nearly identical results. The data are consistent with the sulfonated materials having poorer inherent thermal stabilities, but transforming via crosslinking and rearrangements into more thermally stable residues. At 600 °C, the surface-bound carbon is oxidized and lost leaving SiO_2.

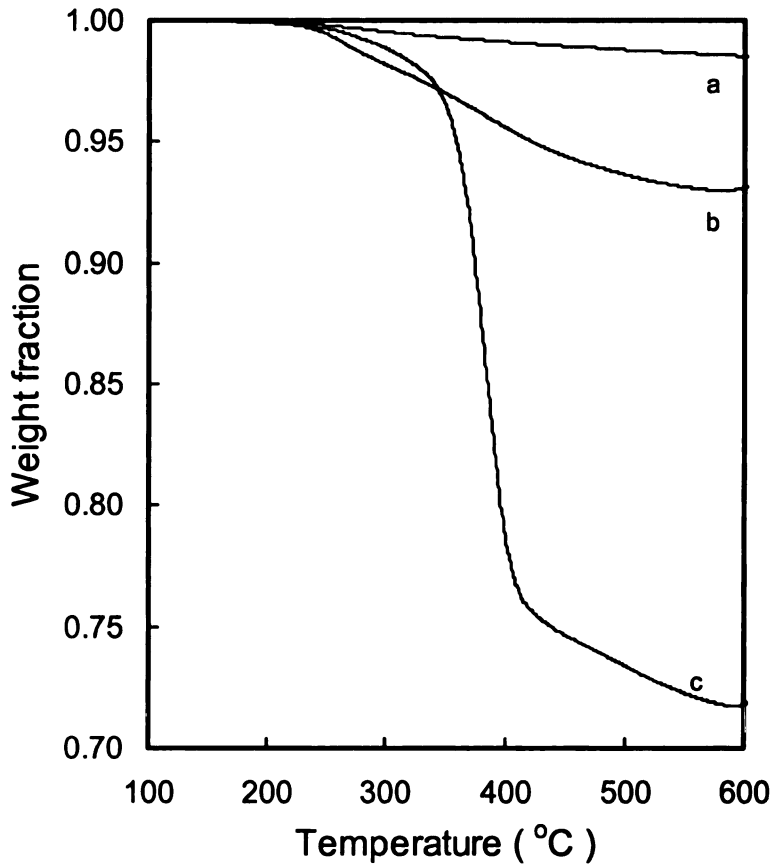

Figure 3.5. TGA analyses of A200 (a); A200 with an attached initiator layer (b); and A200 after ATRP of styrene from the surface (c). The samples were run at 10°/min in air following a 1 h equilibration at 110 °C.

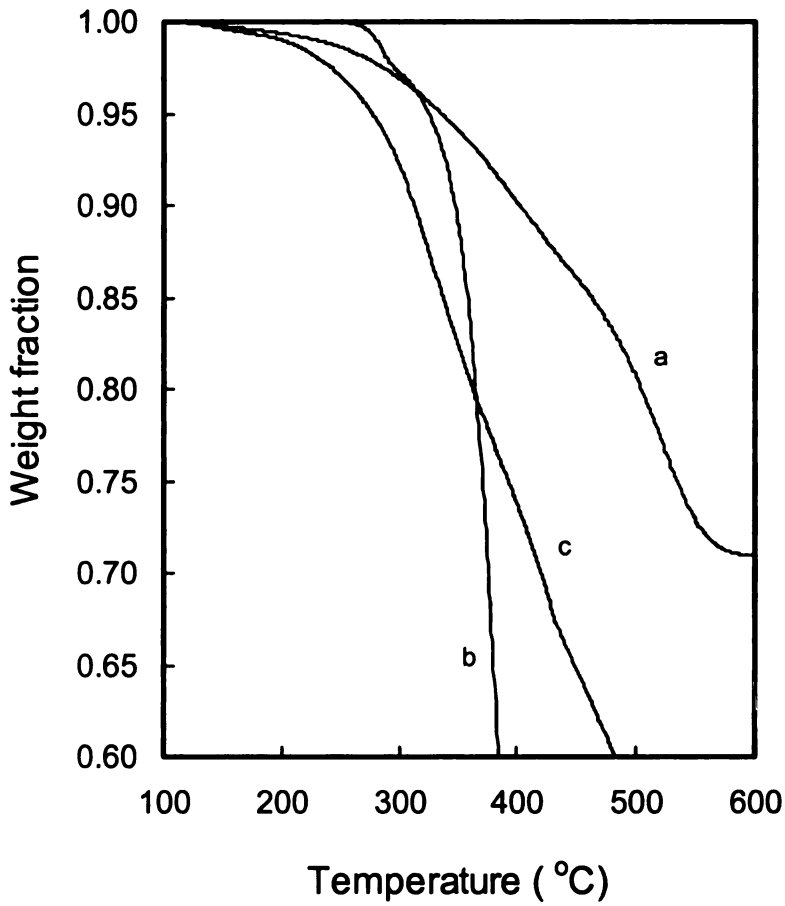

Figure 3.6. TGA analyses of A200/polystyrene after sulfonation (a); polystyrene crosslinked with 2% divinylbenzene (b); and polystyrene crosslinked with 2% divinylbenzene after sulfonation (c). The samples were run at 10°/min in air following a 1 h equilibration at 110 °C.

Characterization of composite membranes Composite membranes were fabricated by casting mixtures of sulfonated nanoparticles and PVDF in DMF (~2 wt% solids) on glass slides. The casting solution was stirred overnight to ensure a homogeneous dispersion of particles prior to membrane casting. Because the particles are highly hydrophilic and PVDF is hydrophobic, the particles agglomerated during solvent evaporation. The interactions between particles, solvent, and polymer define the internal structure of the membranes and can lead to formation of a continuous path of particles that enables proton transport. Sample membranes were cut into ~ 2 × 0.5 cm rectangular strips and the membrane thickness was measured with a micrometer. Membranes were pretreated by boiling in 8% HNO_3 solution for 30 min followed by boiling in deionized water for 30 min. The pretreated membranes were rinsed with deionized water and sandwiched between 2 Teflon blocks so that the ends of the membrane were in contact with platinum electrodes. The membranes were characterized by AC impedance and the membrane resistance was deduced from the real part of impedance when the phase angle is near zero at high frequency. The membrane conductivity was calculated from the relationship $\sigma = t/(R \times S)$ which t is the thickness of membrane, R is the membrane resistance, S is the membrane area.

Figure 3.7 shows the membrane conductivity as a function of particle content. The results suggest a percolation phenomenon with a threshold at ~ 20 wt% particles. At low particle contents, the membranes are hydrophobic and poorly conductive, but above the percolation threshold, the membranes were hydrophilic and highly conductive. The highest conductivity measured was 0.077 S/cm for membranes with 56 wt% particles. For comparison, the conductivity of Nafion 117 measured under the same conditions was

0.086 S/cm. The composite membranes were mechanically robust, but became increasingly fragile when the particle content exceeded 60 wt%.

We examined the aqueous swelling behavior of several membranes since their dimensional stability in water is important for the successful operation fuel cell membranes. Equilibrium water absorption by membranes with ≤40 wt% particles increased nearly linearly with particle content as shown in **Figure 3.8**. A membrane with 56 wt% particles absorbed 1.5× its weight in water but did not dissolve. As the PVDF matrix is not cross-linked, these data illustrate an advantage that two-phase materials have over homogeneous materials. The observed swelling suggests that the hydrophilic particles are connected within the membrane, which is consistent with the high conductivity measured for these membranes. Membranes with 3 wt% particles were hydrophobic and did not absorb a measurable amount of water. The particles in these films are likely isolated in the PVDF matrix.

We used TEM and confocal microscopy to gain some insight about the particles and their distribution in the membranes. A representative TEM image of A200/polystyrene particles is shown in **Figure 3.9**. The sample was prepared by evaporation of a toluene solution of A200/polystyrene onto a formvar carbon support. Most particles agglomerated and formed large aggregates, but we observed a few isolated particles comprised of a ~14 nm dark center surrounded by a ~22 nm thick light gray region. The ~14 nm black features are the approximate diameter of pristine A200 particles, and we interpret the surrounding the core as the attached polystyrene.

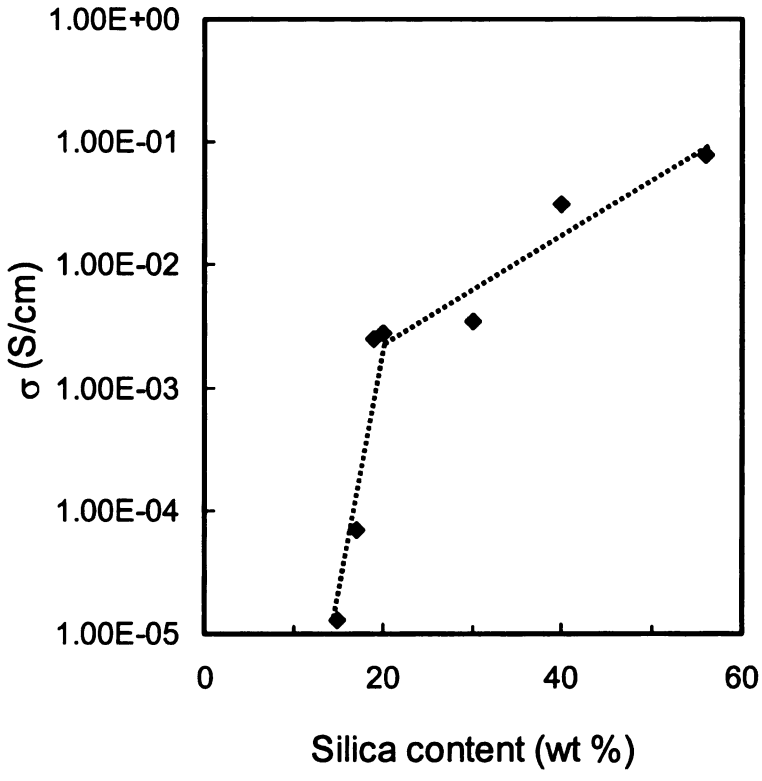

Figure 3.7. The relationship between conductivity and particle content for composite membranes prepared from PVDF and sulfonated polystyrene anchored to A200 silica particles. Measurements were taken at room temperature and full humidity. Each data point was average of two independent samples.

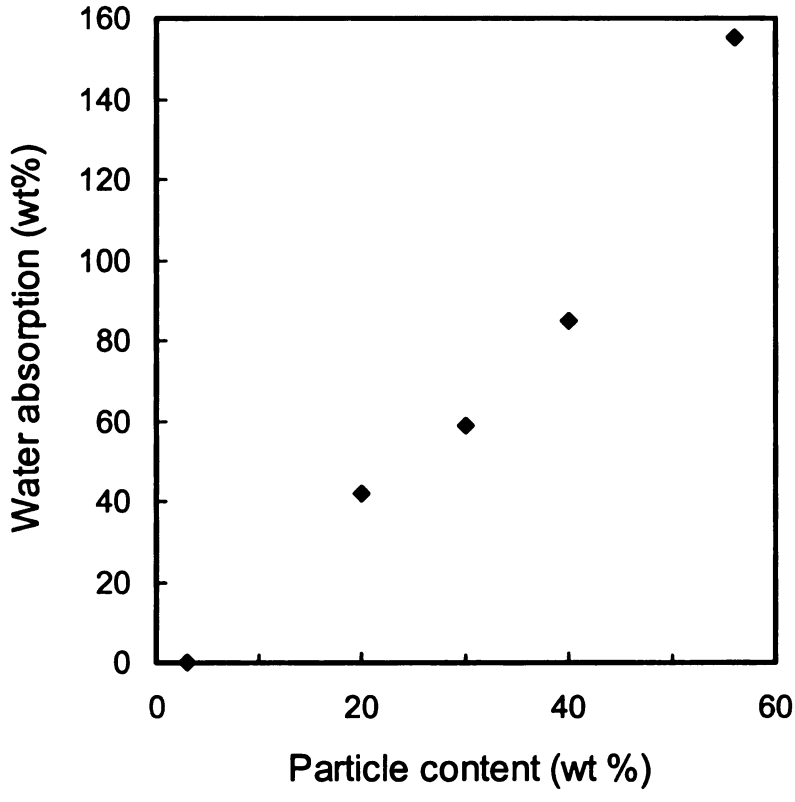

Figure 3.8. Water absorption (water absorbed/dry membrane wt.) for composite membranes as a function of particle content. Each data point is the average of three independent measurements.

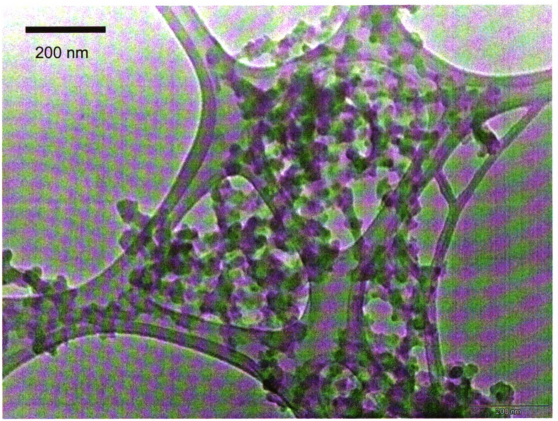

Figure 3.9. TEM images of composites prepared from PVDF and sulfonated polystyrene anchored to A200 silica particles. The scale bar is 200 nm. Samples were prepared by deposition of a suspension prepared from 1 mg composite powder in 5 mL toluene onto lacey formvar/carbon supported on a 300 mesh copper grid.

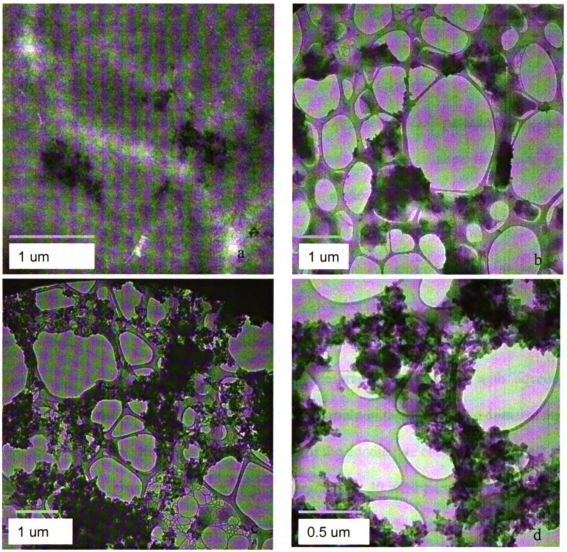

Figure 3.10. TEM images of composites prepared from PVDF and sulfonated polystyrene anchored to A200 silica particles. Particle content: a, 3%; b, 20%; c, 30%; d, 56%.

Figure 3.10 shows TEM images of PVDF/sulfonated particle composites prepared by casting solutions onto a formvar carbon film supported by a TEM grid. While the samples are not actual membranes, the images provide a plausible structural hypothesis for understanding the proton conductivity of composite membranes. The TEM images in **Figure 3.10** show materials with different PVDF/particle ratios, and support the notion of isolated particle aggregates below the percolation threshold, and continuous networks at > 20 wt% particles. Image **a** shows a film with 3 wt% particles indicating that the particles (black dots) are aggregated in the gray polymer matrix even at low particle contents. As the particle content increases, the area covered by aggregates increases, and for 30 and 56 wt% particles, the aggregates appear to be continuous.

Controlled swelling also offers the possibility of imaging the proton conducting pathways in membranes. When conductive membranes are swollen with aqueous solutions of fluorescent dyes, the dyes should concentrate in the hydrophilic domains and fluorescence imaging should reveal some details of the conductive channels. **Figure 3.11** shows a confocal microscopy image of a membrane with 30 wt% particles after soaking in a solution of 0.1% solution of Cy3, a cyanine dye with 3 carbon atoms in the conjugated polyene linkage. The structure of Cy3 is shown below.

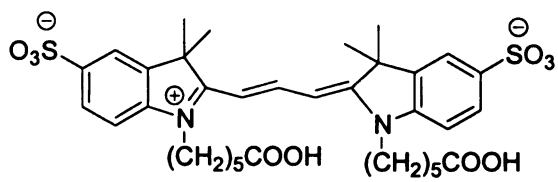

In the confocal microscopy image, the red regions indicate hydrophilic regions accessible to the fluorescent probe. The distribution of red emission is inhomogeneous, with a granularity >10 μm, and emission from all regions of the film is consistent with

continuous hydrophilic channels in the membrane. These data confirm the basic premise of the composite membrane design, that a network of hydrophilic particles in a hydrophobic matrix should provide membranes with both high conductivities and good mechanical properties.

Conclusion

ATRP was used to grow polystyrene from silica particles. Subsequent sulfonation resulted in highly hydrophilic particles with an IEC of 3.2 mmol/g. When particles were embedded in hydrophobic PVDF, the composite membranes were hydrophilic and conductive. Confocal microscopy showed continuous hydrophilic channels in the membrane, in agreement with our initial membrane design hypothesis.

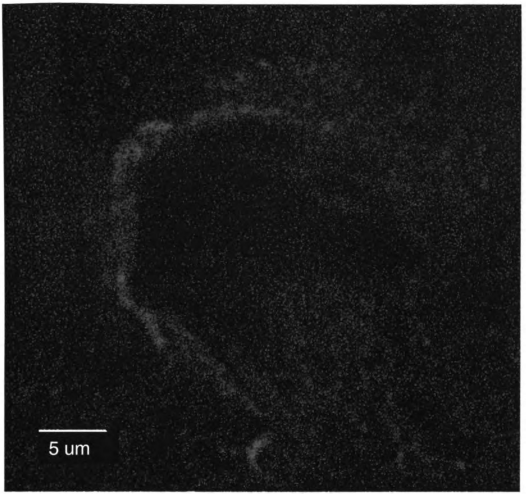

Figure 3.11. Confocal microscopy image of a conductive composite membrane with 30 wt% ***A200polystyrene acid*** particles. The bright red colors indicate hydrophilic domains accessible to the fluorescent dye. The image shows a 2D section parallel to surface inside the membrane. The sample was a film deposited on a glass slide prepared by soaking the membrane in an aqueous solution of Cy3 (1:1000) for 5 min. The film was covered with aluminum foil and stored at 4 °C until measured.

Experimental

Unless otherwise noted, all chemicals and reagents were obtained from Aldrich and used as received. Styrene (99%) and 4-vinylbenzyl chloride (>90%, Fluka) were passed through alumina and purged with argon before use. Xylenes (>98.5%) were dried over sodium. CuCl, dimethylchlorosilane (>97%, Gelest), 4,4'-di-(5-nonyl)-2,2'-bipyridyl (dNbpy) (Reilly Industries), cetyl trimethylammonium bromide (CTAB, 99%) and chlorosulfonic acid (99%), Karstedt's catalyst were used as received. A200 samples were gifts from Degussa Company, Germany. Cy3 fluorescent dyes were obtained from Jackson ImmunoResearch Laborotary, Inc.

^{1}H and ^{13}C NMR spectra were obtained at room temperature in $CDCl_3$ using a Varian Gemini-300 spectrometer and are reported relative to TMS, with the solvent proton and carbon signals used as chemical shift standards. A Nicolet IR/42 spectrometer purged with dry nitrogen was used to obtain infrared spectra. Samples used were 1 cm^2 pressed pellets prepared from ~100 mg of various modified silica. All spectra reported were acquired by signal averaging 32 scans at a resolution of 4 cm^{-1}. DRIFT IR (Diffuse reflectance infrared Fourier transform spectroscopy) data were collected from a computer-controlled Nicolet Protégé 460 equipped with a DRIFTS Auxiliary experiment module. All spectra were acquired by signal averaging 100 scans at a resolution of 4 cm^{-1}. Thermogravimetric analyses (TGA) were performed in dry air at heating rate of 10 °C/min on a Perkin Elmer TGA 7 instrument. Samples were held at 110 °C for 30 min before initiating the run. TEM images were taken using a JEOX 100CX transmission electron microscope. Membrane samples for TEM were prepared by cryosectioning using a PowerTome-XL by BAL-TEC RMC with thickness control of ~80 nm. Dynamic light

scattering (DLS) measurements were performed with a Protein Solutions Dyna Pro-MS/X system with temperature control. Samples were sonicated for 20 min, filtered and allowed to equilibrate in the instrument for 25 minutes at 25 °C before measurements. Confocal microscopy images were taken using LSM 5PASCAL using He-Ne laser light at an exciting wavelength of 543 nm.

2-(4-Chloromethylphenyl)-ethyldimethylchlorosilane. Karstedt's catalyst (0.1 g) and 4-vinylbenzene chloride (7.1 mL, 50 mmol) were added to 25 mL toluene in a round bottomed flask. The solution was stirred for 20 min, and dimethylchlorosilane (5.0 mL, 50 mmol) was then added drop-wise to the solution. The solution immediately turned yellow and eventually became dark brown, with stirring continued for 1 hour at room temperature. The brown solution was eluted through a carbon black column under nitrogen to remove the catalyst. The product, 2-(4-chloromethylphenyl)ethyldimethyl chlorosilane was confirmed by ^{1}H NMR and was used without further purification. ^{1}H NMR revealed two regioisomers (endo/exo 50/9). ^{1}H NMR δ: 7.1-7.4 (m, 4H), 4.6 (s, 2H), 2.7-2.8 (m, 2H endo), 2.4-2.5 (q, 1H, exo), 1.4-1.5 (d, 3H, exo), 1.1-1.2 (m, 2H, endo), 0.5 (s, 6H), 0.39 (s, 1H, exo), 0.36 (s, 1H, exo).

A200initiator. Toluene (30 mL) and DMF (10 mL) were added under N_2 to a 100 mL round bottom flask containing dried A200 (2.5 g). The mixture was stirred for 30 min, and then a solution of 2-(4-chloromethylphenyl) ethyldimethylsilane in 10 mL toluene (10 mmol of mixture of *endo* and *exo* hydrosilation products) was syringed into the flask solution with continuous stirring. After stirring at room temperature overnight, the reaction mixture was precipitated with pentane and isolated by centrifugation. The

solids were re-dispersed in 10 mL toluene and re-precipitated with 50 mL pentane. After repeating the process 4 times, the particles were dried under vacuum at 80 °C for 12 hours to yield 2.0 g of ***A200initiator*** (80% yield).

A200polystyrene. A 25 mL Schlenk flask was charged with 2 mL of *p*-xylene, styrene (4 mL, 34.9 mmol), CuCl (19.1 mg, 0.19 mmol), 4,4'-di-(5-nonyl)-2,2'-bipyridyl (0.236g, 0.38 mmol), and 0.52g of ***A200initiator*** (0.19 mmol initiator sites). The flask was sealed and the mixture was de-gassed using three freeze-pump-thaw cycles. The flask was heated with stirring for 2 hours at 110 °C, and then the silica/polystyrene nanoparticles were precipitated by addition of ethanol and isolated by centrifugation. The silica/polystyrene nanoparticles were re-dissolved in 2 mL toluene, precipitated into 30 mL of ethanol, and isolated by centrifugation. This process was repeated 4 times until the nanoparticles were white. The solids were dried vacuum at 80 °C for 12 hours to yield 0.52 g of ***A200polystyrene***, (100% yield).

A200polystyrene acid. Under N_2, $ClSO_3H$ (0.25 mL, 3.8 mmol) was injected drop by drop into in a flask containing 0.5 g ***A200polystyrene*** in 35 mL of refluxing CH_2Cl_2. After refluxing overnight, the particles were isolated from the yellow-brown solution by centrifugation, and washed with THF (4×20 mL) until the THF was neutral. The product was dried under vacuum at 80 °C for 12 h to yield 0.4g, (80%yield).

Measurement of the ion exchange capacity (IEC). A200polystyrene acid silica (0.10 g) was added to a 5 mL mixture of 1:1 DMF and 2M NaCl with stirring. After soaking for 24 h, the silica was collected by filtration, washed 3 times with 5 mL of 1:1 (v/v) DMF and 2M NaCl. The solution was ultrasonicated for 1h, and allowed to soak overnight. The solids were collected and washed with 1:1 DMF and 2M NaCl several

times. The combined liquid filtrate was titrated to the phenolphthalein end point with 0.010 M NaOH. Dried A200 initiator titrated under same conditions was used as a blank. The reported IEC result is the average of 3 measurements

Membrane preparation PVDF (0.01g) and 0.4 mL DMF were added to a vial and stirred at room temperature until the PVDF dissolved. The desired amount of ***Silica/polystyrene acid*** particles, previously ground in a mortar and pestle, was weighed into a second vial with 0.2 mL DMF and stirred for 12 hour until homogeneous. The two solutions were combined and stirred for 12 hours. Membrane were cast by pouring the final solution onto glass slides heated to ~ 50 °C on a hot plate. Round membranes ~1 cm in diameter were obtained after solvent evaporation and were further dried in a vacuum oven at 80 °C overnight to remove residual solvent.

Hybrid membrane pretreatment. Membranes cast on glass plates were cut into ~ 2.0 × 0.5 cm rectangular strips with a razor blade and their size and thickness was measured. The cut membrane was released from its support by immersion in water, and was boiled in 8% HNO_3 for 30 min, rinsed with water, then boiled in deionized water for 30 min. The treated membranes were stored in deionized water at room temperature.

Absorption of phosphoric acid in hybrid membranes. Pretreated membranes were blotted dry with filter paper and immersed in various concentrations of phosphoric acid for 2 days at 50 °C. The treated samples were stored in phosphoric acid at room temperature.

Membrane conductivity measurements. Rectangular strips of the membrane (~ 2.0 × 0.5 cm) were sandwiched between 2 Teflon blocks with two membrane ends in

contact with platinum electrodes. The blocks and membrane were isolated in an oven which was equipped with a gas inlet and outlet. Humidity control was obtained by bubbling dry N_2 into 75 °C deionized water under atmosphere pressure.

Cleaving polystyrene chains from silica. Silica/polystyrene nanoparticles (0.2 g) were dispersed in 10 mL of toluene in a polyethylene flask. Aliquot 336 (50 mg) was added as phase transfer catalyst, along with 10 mL of 5% HF. The mixture was stirred overnight. The organic layer was removed and the polymer was precipitated by adding 20 mL of ethanol. The polymer was isolated by centrifugation and dried under vacuum.

Membrane samples for confocal microscopy Rectangular strips of the membrane (~ 2.0 × 0.5 cm) were soaked in 0.1% aqueous solution of Cy3 for ~5 min, and then the membrane was removed from the solution, spread on a clean glass slide, and soft paper tissues were applied gently to absorb excess solution on both sides of the membrane. The membrane was sandwiched between a cover glass and glass slide, wrapped with aluminum foil and stored at 4 °C before measurements.

Chapter 4

Composite particles with Snowtex-XS cores

Composite membranes prepared by dispersing a solid acid (polystyrene sulfonic acid tethered to A200 fumed silica) in PVDF have conductivities comparable to Nafion. However, a limitation of these new membranes is that the high conductivity is restricted to full humidity conditions, and high temperature operation could be problematic. The poor high temperature behavior may reflect a too low concentration of acid groups on the particles, or that the conducting channels are too large for capillarity to be effective in retaining water. The use of smaller particles may solve both problems. The large surface area per unit mass characteristic of small nanoparticles provides a simple approach to tethering high concentrations of acid groups on surfaces, and since the conductive channels in membranes are defined by particle size, smaller particles should increase capillary effects and improve water retention. This chapter describes the use of functionalized colloidal silica nanoparticles as a solid acid in fuel cell membranes.

Snowtex-XS is a commercial colloidal silica available as an aqueous dispersion of ~ 4-6 nm diameter particles at pH 9.2. The particles have a net negative charge due to the deprotonated silanols, resulting in a clear dispersion stabilized by the repulsion of particles of the same charge. Decreasing the pH or adding a surfactant to the dispersion decreases the charge-induced repulsion and causes the particles to agglomerate as a white powder.[138] Particles precipitated by addition of surfactants are somewhat hydrophilic, and the agglomerated silica can be re-dispersed in organic solvents for further chemical modifications such as those described previously for A200 (**Scheme 3.1**). **Figure 4.1**

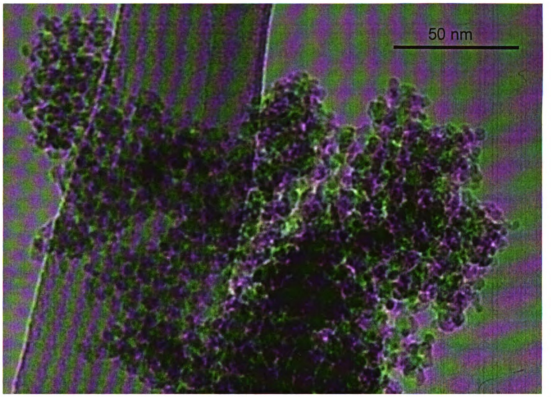

Figure 4.1. TEM image of Snowtex particles precipitated from a colloidal suspension by addition of surfactant. The TEM sample was prepared by deposition of a Snowtex particle suspension in liquid nitrogen onto a lacey formvar/carbon film supported on a 300 mesh copper grid.

shows a TEM image of Snowtex particles precipitated from an aqueous colloidal suspension.

Chemical modification of Snowtex particles. The Snowtex nanoparticles were modified as described earlier for A200. Cetyl trimethylammonium bromide (CTAB) was added to the colloidal silica, and the precipitated particles were collected by centrifugation, washed with deionized water and dried under vacuum. The particles were re-dispersed in 3:1 (v/v) toluene/DMF and the chlorosilane initiator (prepared by hydrosilylation of 4-vinylbenzylchloride with dimethylchlorosilane using Karstedt's catalyst[136]) was anchored to the Snowtex surface, converting the particles into a macroinitiator for ATRP (**Scheme 3.2**). Characterization by FTIR and TGA verified attachment of the ATRP initiator to the Snowtex surface, the amount of polymer grown from the surface, and successful sulfonation of the particles.

The IR spectrum of Snowtex (trace a, **Figure 4.2**) shows broad OH stretching at 3100 - 3700 cm^{-1}. Other characteristic IR bands for silica[123] appear at 1625 cm^{-1} (O-H bending) ~2000 cm^{-1} (Si-O-Si combination band) and 1100 cm^{-1} (Si-O-Si); the latter dominates the spectrum and is not shown for clarity. The weak bands below 3000 cm^{-1} are from the surfactant layer on the surface of precipitated Snowtex. After anchoring the initiator to the surface, the O-H stretching band deceased in intensity and the C-H stretching band increased as expected.

TGA experiments were run on these samples at a heating rate of 10 °C/min in air after being equilibrated at 110 °C for one hour (**Figure 4.3**). The weight loss for Snowtex was about 4% which corresponds to the loss of surface adsorbed water, dehydration of surface silanols, and degradation of the surfactant layer. After adding the

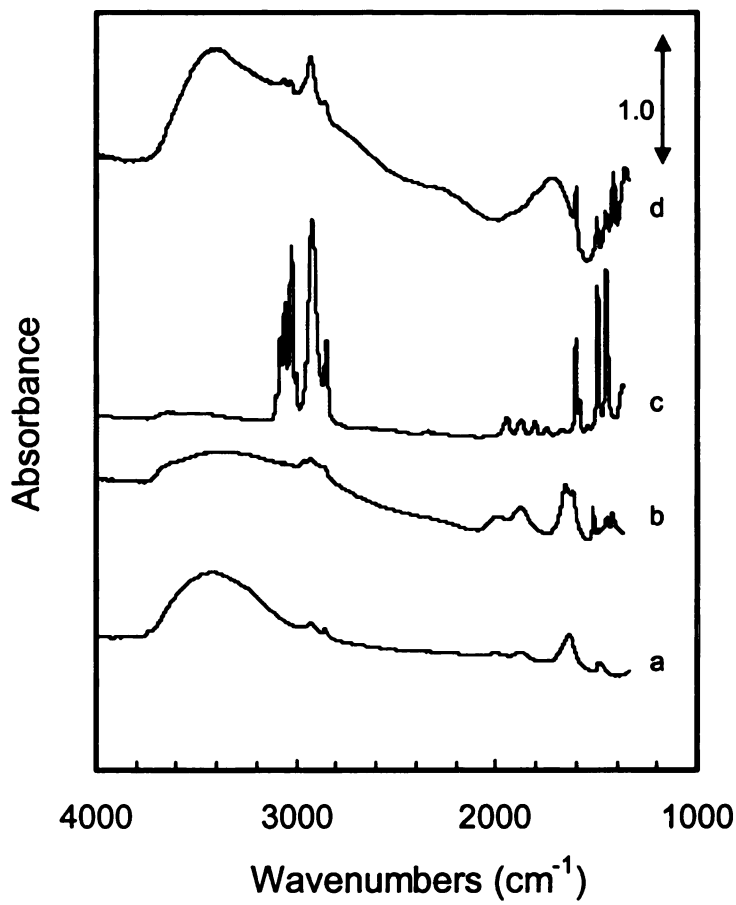

Figure 4.2. Infrared spectra of **a**, Snowtex precipitated from solution; **b**, Snowtex after anchoring initiator on the surface; **c**, Snowtex after growing polystyrene from the surface; and **d**, Snowtex/polystyrene after sulfonation with chlorosulfonic acid. Samples were prepared by pressing particles into 1 cm diameter pellets.

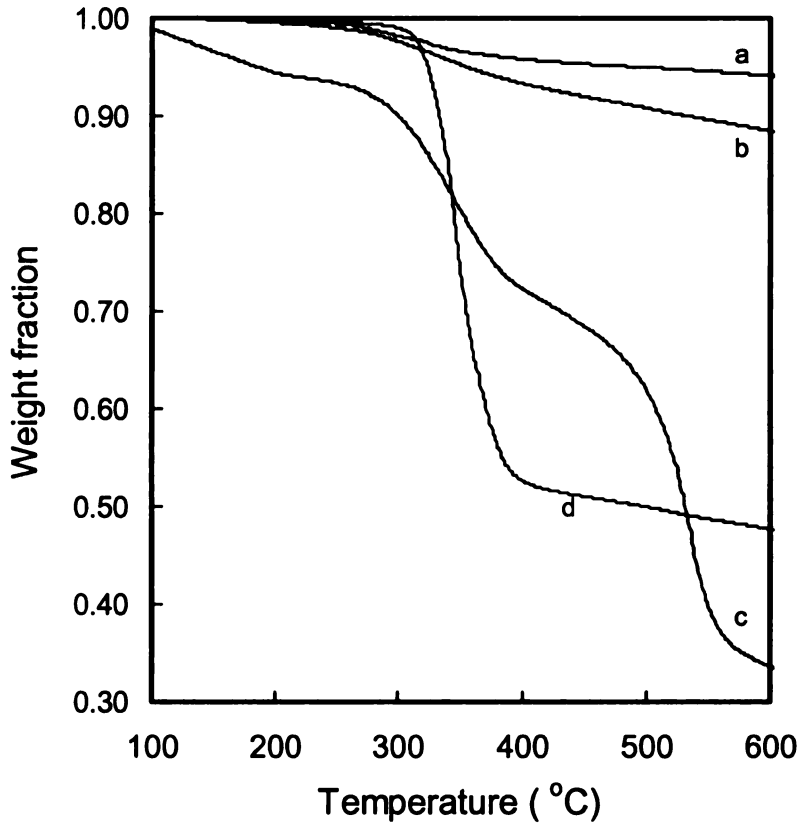

Figure 4.3. TGA measurements of modified Snowtex particles in dry air. **a**, Snowtex precipitated from solution; **b**, Snowtexinitiator; **c**, Snowtexpolystyrene; **d**, Snowtexpolystyrene acid. All samples were stabilized at 110 °C for 30 min prior to initiating the run.

initiator layer, the weight loss increased to 8%. Because we do not know the amount of surfactant retained after the initiator anchoring step, we cannot reliably quantify the amount of initiator on the surface of the particles.

Styrene, solvent, and the ATRP catalyst were added to the macroinitiator to effect growth of polystyrene from Snowtex. The IR spectrum shows prominent bands for polystyrene at 2800-3200 cm^{-1} (C-H stretching), 1800-2000 cm^{-1} (combination and overtones), and 1600 cm^{-1} (aromatic ring). TGA analyses taken after washing particles with toluene overnight under Soxhlet conditions to remove adsorbed polymer showed a 45% weight loss, which reflects the growth of a significant polystyrene film from the particle surface. The polystyrene was detached from the particles using 5% HF and analyzed by GPC, resulting in M_w = 60,279 and a polydispersity (PDI) of 1.8. The PDI is higher than expected for a controlled polymerization, given Paten's report of a PDI of 1.3-1.4 for the growth of polystyrene from 70 nm diameter silica particles.[136] The number of polymer chains on the silica surface can be estimated from the TGA and GPC results. We find ~0.008 mmol/g sample, much lower than the 0.02 mmol/g obtained using A200 particles as the support. It is possible that the surfactant layer on the Snowtex particle surface limited efficient anchoring of initiators.

After sulfonation using chlorosulfonic acid, the particles were very hydrophilic, and again the O-H stretching band dominates the spectrum. The signals from both alkyl and aromatic groups appeared much smaller, and possibly some polymer chains were detached from the particles under the strong sulfonation conditions.

The TGA data show substantial loss of water below 300 °C, followed by loss of a portion of the polystyrene. A second weight loss at >450 °C may reflect cross-linking or

polystyrene structural rearrangements during the TGA run that led to more thermally stable residues. Titration yielded an IEC of 2.3 mmol acid/g, compared to 3.2 mmol/g when A200 was used as the nanoparticle support.

Particle imaging by TEM. **Figure 4.4** shows a TEM image of particles after sulfonation. These hydrophilic particles agglomerated rapidly and we were unable to identify isolated particles in the image. The dark black dots are ~4 nm in diameter, the approximate size of pristine Snowtex nanoparticles. The dots are separated by gray areas, which we interpret as sulfonated polystyrene. DLS measurements (**Figure 4.5**) provide an average particle diameter of ~17 nm in methanol.

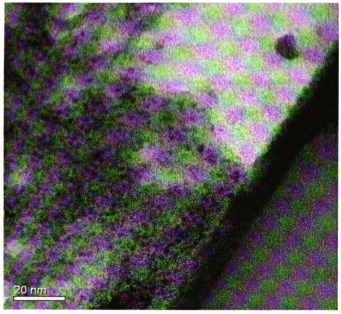

Figure 4.4. TEM image of sulfonated polystyrene grafted to Snowtex particles. Samples were prepared by deposition of a suspension of particles in liquid nitrogen onto a lacey formvar/carbon film supported on a 300 mesh copper grid.

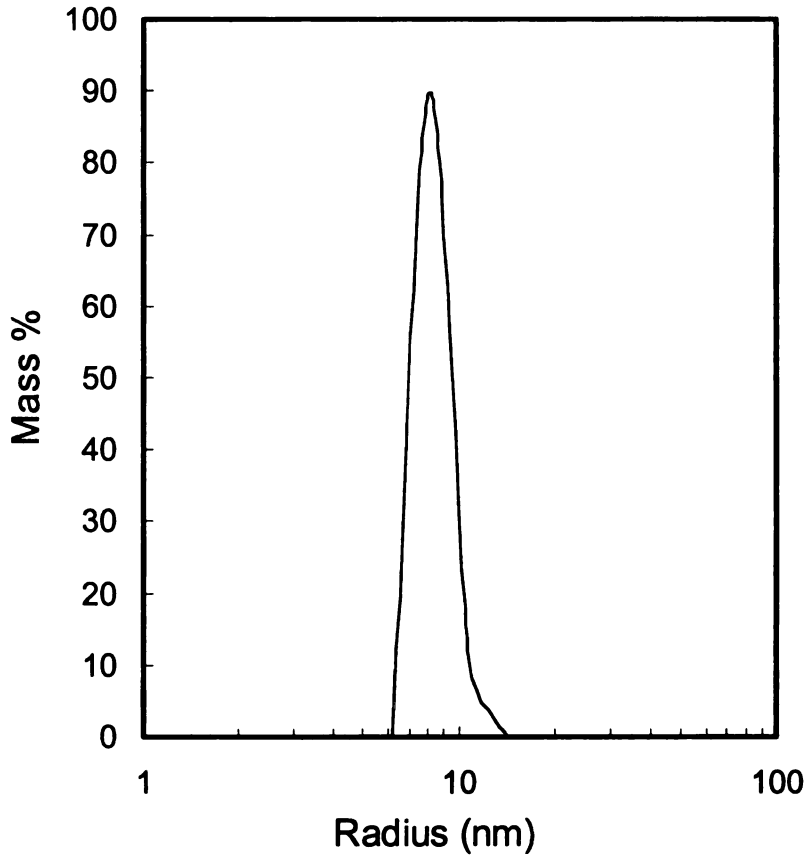

Figure 4.5. Dynamic light scattering data from sulfonated polystyrene grafted to Snowtex particles at a concentration of 2 mg/mL. The solutions were sonicated for 20 min in methanol, and passed through 0.02 μm filter prior to taking measurements at 25 °C.

Membrane properties. Composite membranes were fabricated by pouring a suspension of sulfonated nanoparticles and PVDF in DMF (~2 wt% solids) onto glass slides warmed on a hot plate at ~50 °C. Sample membranes were cut into ~ 2 × 0.5 cm rectangular strips and the membrane thickness was measured with a micrometer. The membranes treated with 8% HNO_3, and rinsed with deionized water. The membrane resistance was deduced from the real part of the impedance, when the phase angle at high frequency is near zero. The membrane conductivity was calculated from the relationship $\sigma = t/(R \times S)$ where t is the thickness of membrane, R is the membrane resistance, and S is the membrane area. **Figure 4.6** shows the relationship between membrane conductivity and particle content. The conductivity of a membrane with 15 wt% particles was ~10^{-4} S/cm. Increasing the particle content to 20 wt% increased the membrane conductivity to 10^{-3} S/cm, and the maximum conductivity of 0.09 S/cm was realized with membranes prepared with a 50 wt% particles.

In order to have a better understanding of their structure, a membrane with 30 wt% particles was cryosectioned by cutting perpendicular to membrane surface, and was examined by TEM (**Figure 4.7**). The image shows two phases, a comparatively smooth phase corresponding to the PVDF matrix, and a rough phase that appears torn. This area is populated by large aggregates, presumably comprised of Snowtex cores embedded in sulfonated polystyrene. While the image shows obvious phase separation and revealed the heterogeneous character of membrane, it does not provide information on the connectivity of the domains that we assume to be present.

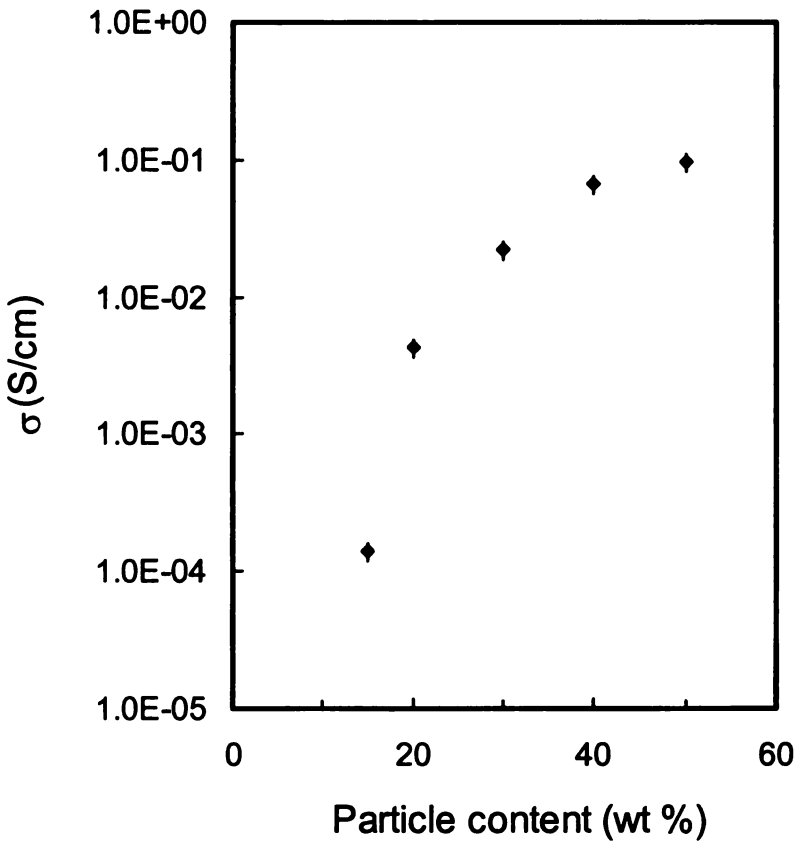

Figure 4.6. Room temperature proton conductivity of composite membranes as a function of particle content. Measurements were run at 100% humidity. Each data point represents the average of three independent samples, and the error bars shown are the standard deviation.

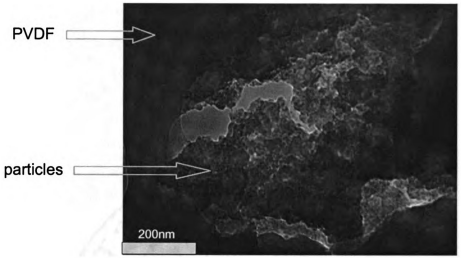

Figure 4.7. TEM image of a thin layer from a composite membrane with a 30 wt% particles. The sample was prepared by cryosectioning perpendicular to membrane surface, with a thickness control of about 85 nm.

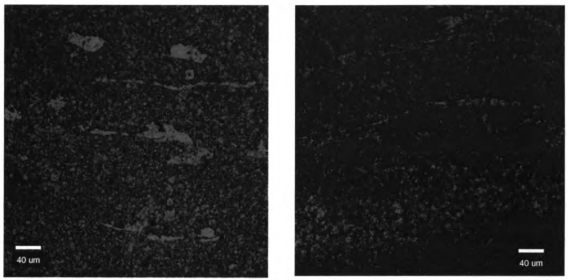

Figure 4.8. Confocal microscopy images of composite membranes with 30 (left) and 15 wt% particle contents (right) after soaking for 5 minutes in a 0.1% solution of the water soluble fluorescent Cyanine dye Cy3. The red fluorescence identifies hydrophilic domains accessible to the dye. The images show areas inside membrane parallel to surfaces. The membranes were supported on glass slides, and were covered with aluminum foil and stored at 4 °C before measurement.

We soaked two fresh membranes in an aqueous solution of Cy3, a cyanine dye with 3 carbons in conjugated polyene segment, one with 15 wt% particles and the other 30%, and then examined the membranes using confocal microscopy. **Figure 4.8** shows images of the two membranes, where the red areas correspond to dye fluorescence from hydrophilic domains. The membrane with 30 wt% particles shows a mixture of intense red "lines", aggregates >40 μm, and a diffuse red background indicating substantial penetration of the dye into the membrane. In contrast, the membrane with 15 wt% particles had far fewer domains, and no obvious connectivity between domains. The images of **Figure 4.8** are consistent with the conductivity data shown in **Figure 4.6**. The membrane with 15 wt% particles was poorly conductive and showed little connectivity between domains, while the 30 wt% sample displayed obvious connectivity and a 100× higher conductivity.

H_3PO_4 soaked membranes. The ability to operate PEMs above 100 °C would reduce problems related to catalyst poisoning and water management. However, as the temperature approaches 100 °C, water is lost from membranes as vapor and the membrane conductivity drops severely. One solution is to replace water with less volatile electrolytes such as phosphoric acid as conducting media. The most studied phosphoric acid-doped membranes are polybenzimidazoles (PBIs) (**Figure 4.9**).

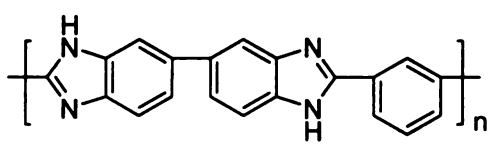

Figure 4.9. Chemical structure of PBI

PBI is an amorphous thermoplastic polymer with a glass transition temperature of 425-436 °C. It has good chemical, thermal and mechanical stability and low methanol permeability. PBI received much attention in the fuel cell community because of the work by Savinell and Litt et al.[104,105] They showed that the conductivity of PBI membranes doped with 11 M phosphoric was 2×10^{-2} S/cm at 130 °C and 30% humidity. The nitrogen atoms of PBI make the polymer slightly basic, and the strong interaction between PBI and the acid helps immobilize the absorbed acid. The conductivity of PBI/H_3PO_4 is attributed to formation of H_3PO_4 domains. Using phosphoric acid as the electrolyte enables fuel cell operation at elevated temperatures and under low humidity conditions, however, the high doping level needed to reach high conductivities presents potential problems with acid leaching and corrosion.

Following a membrane doping protocol similar to that used for PBI, we soaked membranes with 8M H_3PO_4. The quantity of acid absorbed, listed in **Table 4.1**, was determined by drying samples in vacuum at 80 °C for 2 days. The weight fraction of acid absorbed by the membrane was calculated by

$$H_3PO_4 \text{ absorbed} = (W_v - W_d)/W_d$$

where W_d is the weight of the pristine dry membrane and W_v is the weight of the membrane after soaking in 8M H_3PO_4 and drying in a vacuum oven. Generally, absorption of acid correlated with particle content. For example, when the silica content increased from 20% to 50%, the absorbed H_3PO_4 increased from 0.7 to 3.3× the dry membrane weight. (Membranes with 10 wt% particles were hydrophobic). The number of H_3PO_4 molecules absorbed per SO_3H group also increased with particle content.

Table 4.1. H_3PO_4 absorption by composite membranes.

	Particle content (wt%)				
	10%	20%	30%	40%	50%
H_3PO_4/membrane (w/w) [a]	2%	70%	140%	210%	330%
H_3PO_4/SO_3H [b]	0.76	15	20.2	23.4	29

a. Samples were soaked with 8M H_3PO_4 for 48 hrs at 50 °C, and then dried under vacuum at 80 °C for 2 days. The weight difference between the dry membrane before H_3PO_4 doping and the membrane doped with H_3PO_4 after drying under vacuum is defined as quantity of the acid absorbed. The results are average of three independent membrane measurements.

b. The SO_3H quantity was calculated from the ion exchange capacity of the particles and their wt% in the membrane.

Figure 4.10 shows the dependence of conductivity on the concentration of H_3PO_4 used in the soaking process for membranes with 50 wt% particles. The conductivities of the H_3PO_4 solutions are shown for comparison. The peak conductivity for H_3PO_4 solutions occurred between 4 and 8M H_3PO_4, and then dropped slightly, which may indicate increased viscosity offsetting the effects of higher acid concentrations.

The membranes show a similar pattern in their conductivity, but the conductivities were much higher. The difference in conductivity between H_3PO_4 and membranes soaked with same concentration of acid increased from 2M to 5M, and reached a maximum at 8M. This may be related to the interaction of SO_3H groups on the silica surface with H_3PO_4, creating more H^+ defects as suggested by Liu et al.[139]

Figure 4.11 shows the conductivity of membranes soaked in 8M of H_3PO_4 at various temperatures and 0.3 atmosphere humidity. The humidity was controlled by bubbling dry N_2 into 75 °C deionized water under atmosphere pressure. **Table 4.2** shows the vapor pressure of water at different temperatures. At constant temperature, membrane conductivity increased almost linearly with particle content, which suggests a contribution form the surface SO_3H groups to the conductivity. For the same membrane, conductivity decreased with increased temperature, possibly due to loss of water from the membrane. The conductivity gradually stabilized at temperatures above 100 °C.

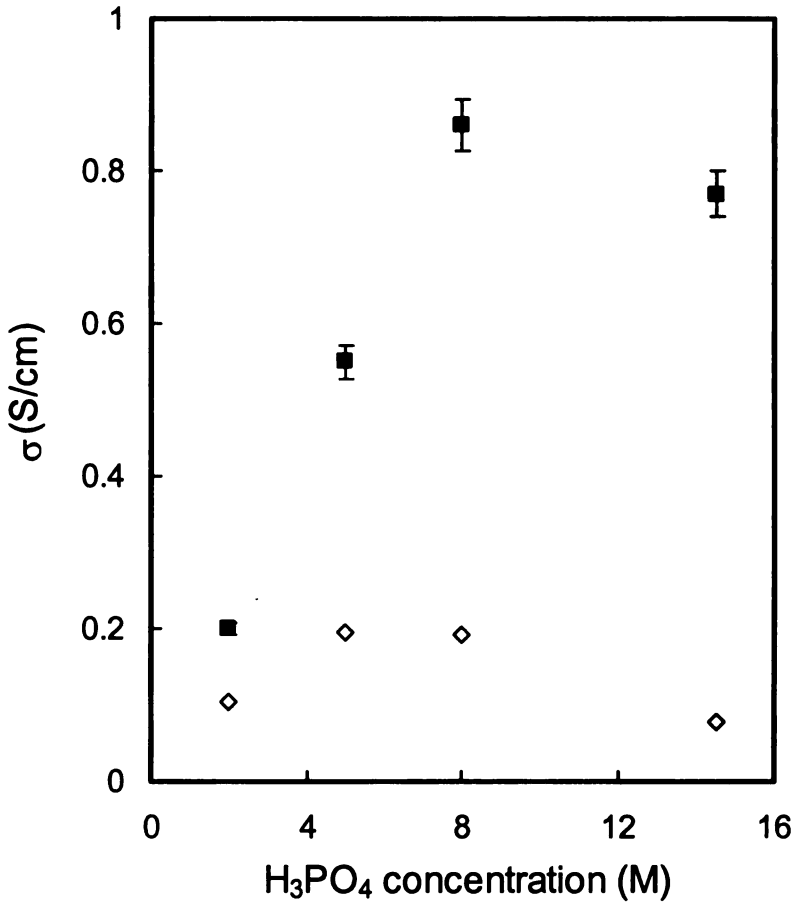

Figure 4.10. Dependence of the room temperature conductivity with [H_3PO_4] for: ■ a composite membrane with 50 wt% particles; ◊ aqueous solutions of H_3PO_4. Each data point is the average of measurements from three independent samples. The standard deviations are comparable to the size of the symbols for aqueous solutions of H_3PO_4.

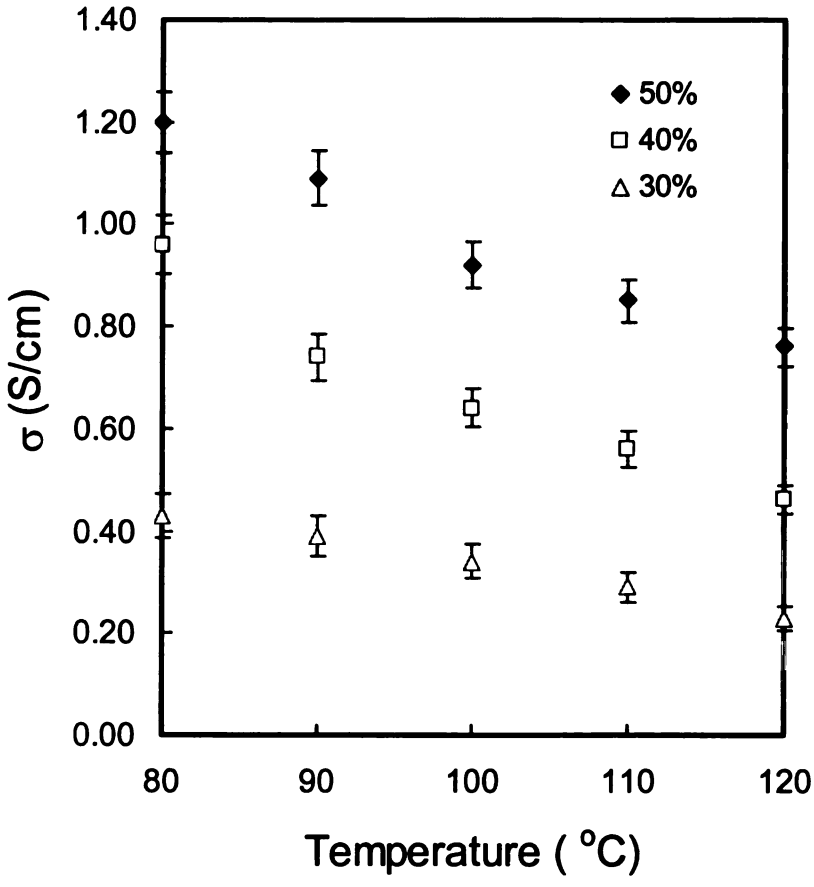

Figure 4.11. Temperature dependent proton conductivity of composite membranes with different particle contents. Membranes were soaked in 8M H_3PO_4 for 48 hrs at 50 °C before measuring at 0.3 atmosphere humidity. Each data point was average of three independent samples. The error bars show the standard deviations for the average.

Table 4.2. Vapor pressure of water below 100 °C

Temperature (°C)	50	60	70	80	90	100
Vapor pressure (mm Hg)	92.51	149.38	233.7	355.1	525.76	760.00

* from Handbook of Chemistry and Physics, College Edition, 49th Edition, 1968-1969

Conclusion

ATRP was used to grow polystyrene from Snowtex, a commercial colloidal silica with particle diameters of 4-6 nm. After sulfonation with chlorsulfonic acid, the particles were highly acidic with an IEC of 2.3 mmol/g. Embedding the particles in PVDF provided membranes that were conductive under fully hydrated or partial water vapor conditions, demonstrating the effect of particle size (or channel size) on membrane properties. Confocal microscopy of highly conductive membranes showed continuous hydrophilic domains, which confirms our initial membrane design strategy. Controlling the distribution of particles in the films should further improve the membrane structure as well as membrane properties.

Experimental

Unless otherwise noted, all chemicals and reagents were obtained from Aldrich and used as received. Styrene (99%) and 4-vinylbenzyl chloride (>90%, Fluka) were passed through basic alumina and purged with argon before use. Xylenes (>98.5%) were dried over sodium. Dimethylchlorosilane (>97%, Gelest), and 4,4'-di-(5-nonyl)-2,2'-bipyridyl (dNbipy, Reilly Industries) were used as received. Snowtex-XS was a gift from Nissan Chemical Company. A200 was a gift from Degussa Company, Germany. Cy3 fluorescent dyes were purchased from Jackson ImmunoResearch Laborotary, Inc.

^{1}H and ^{13}C NMR spectra were obtained at room temperature in $CDCl_3$ using a Varian Gemini-300 spectrometer, and are reported relative to TMS, with the proton and carbon signals from the solvent used as chemical shift standards. A Nicolet IR/42 spectrometer purged with dry nitrogen was used to obtain infrared spectra. Samples used were 1 cm^2 pressed pellets prepared from ~ 100 mg of various modified silica. All spectra were acquired by signal averaging 32 scans at a resolution of 4 cm^{-1}. DRIFT IR (Diffuse reflectance infrared Fourier transform spectroscopy) data were collected from a computer-controlled Nicolet Protégé 460 equipped with a DRIFTS Auxiliary experiment module. All spectra were acquired by signal averaging 100 scans at a resolution of 4 cm^{-1}. Thermogravimetric analyses (TGA) were performed in dry air at heating rate of 10 °C/min on a Perkin Elmer TGA 7 instrument. Samples were held at 110 °C for 30 min before the run was started. TEM images were taken using a JEOX 100CX Transmission Electron Microscope. Membrane samples for TEM were prepared by cryosectioning using a PowerTome-XL by BAL-TEC RMC with thickness control of ~80 nm. Dynamic light scattering (DLS) measurements were performed with a Protein Solutions Dyna Pro-

MS/X system with temperature control. Samples were sonicated for 20 min, filtered and allowed to equilibrate in the instrument for 25 minutes at 25 °C before measurements. Confocal microscopy images were taken using LSM 5PASCAL using He-Ne laser light at an exciting wavelength of 543 nm.

AC impedance data were obtained from an HP 4192A LF Impedance Analyzer controlled by an in-house designed LabView application, scanning from 5 Hz to 13 MHz with an applied voltage of 10 mV. Rectangular strips of membrane were sandwiched between 2 Teflon blocks with the ends of the membranes in contact with platinum electrodes. Both the Teflon blocks and membrane were isolated in an oven equipped with a gas inlet and outlet. Humidity control was obtained by bubbling dry N_2 into 75 °C deionized water under atmospheric pressure.

2-(4-Chloromethylphenyl)-ethyldimethylchlorosilane. Karstedt's catalyst (0.1 g) and 4-vinylbenzene chloride (7.1 mL, 50 mmol) were added to 25 mL toluene in a round bottomed flask. The solution was stirred for 20 min, and dimethylchlorosilane (5.0 mL, 50 mmol) was then added drop-wise to the solution. The solution immediately turned yellow and eventually became dark brown, with stirring continued for 1 hour at room temperature. The brown solution was eluted through a carbon black column under nitrogen to remove catalyst. The product, 2-(4-chloromethylphenyl)-ethyldimethylchlorosilane was confirmed by ^{1}H NMR and was used without further purification. ^{1}H NMR revealed two regioisomers (endo/exo 50/9) NMR. ^{1}H NMR δ: 7.1-7.4 (m, 4H), 4.6 (s, 2H), 2.7-2.8 (m, 2H endo), 2.4-2.5 (q, 1H, exo), 1.4-1.5 (d, 3H, exo), 1.1-1.2 (m, 2H, endo), 0.5 (s, 6H), 0.39 (s, 1H, exo), 0.36 (s, 1H, exo).

Pristine Snowtex particles With stirring, cetyl trimethylammonium bromide (CTAB) (3 g) was added to a beaker containing 100 mL of Snowtex-XS in a 50 °C water bath. A copious amount of a white precipitate formed, and stirring was continued for 30 min. The solids were isolated by centrifugation at 2000 rpm for 10 min, and re-dispersed in 100 mL of 50 °C deionized water. The process was repeated until foaming was not observed while stirring (3-4 times). The solids were collected by centrifugation, washed with ethanol, and dried under vacuum at 80 °C for 12 h to yield 20 g of ***Snowtex***.

Snowtexinitiator. Toluene (15 mL) and DMF (5 mL) were added to dry Snowtex particles (1.4 g) in a 100 mL round bottom flask. The solution was stirred and purged with N_2 at room temperature until the powders dispersed and the solution became clear (~10 min). A 10 mL toluene solution of 2-(4chloromethylphenyl)ethyldimethylsilane (10 mmol of the hydrosilation product) was syringed into the mixture with stirring. The reaction was allowed to proceed at room temperature under N_2 overnight, and then the silica was precipitated with 50 mL pentane and isolated by centrifugation. The solids were collected, re-dispersed in 10 mL toluene and re-precipitated with 50 mL pentane. After repeating the process 4 times, the particles were dried under vacuum at 80 °C for 12 hours to yield 1.1 g of ***Snowtexinitiator*** (78% yield).

Snowtexpolystyrene Styrene (5.45g, 6 mL) and ***Snowtexinitiator*** (0.6 g) were added to a 50 mL Schlenk flask and the mixture was degassed by 3 freeze-pump-thaw cycles. The flask was transferred into a dry box and Cu(I)Cl (14.3 mg, 0.145 mmol), dNbipy (0.120 g, 0.29 mmol) and 1.5 mL of xylenes were added to the mixture. The flask was sealed, removed from the dry box, and heated under N_2 to 110 °C in an oil bath.

After stirring for 8 h, the reaction mixture was cooled and then precipitated into 50 mL ethanol. The solids were isolated by centrifugation at 2000 r/min for 10 min, re-dispersed in 5 mL THF and precipitated with 30 mL EtOH. The process was repeated 4 times and particles were dried under vacuum for 12 h at 80 °C to yield 0.69 g of ***Snowtexpolystyrene.***

Snowtexpolystyrene acid Under N_2, $ClSO_3H$ (0.1 mL) was syringed drop-wise into a refluxing solution of ***Snowpolystyrene*** (0.2 g) in 30 mL CH_2Cl_2. The reaction mixture immediately turned pink red and eventually the color grew deep red. The agglomerated particles were isolated by centrifugation, and washed with THF (4 × 20 mL) until the THF was neutral. The product was dried under vacuum at 80 °C for 12 h to yield 1.8 g of ***Snowtexpolystyrene acid*** (90% yield).

Measurement of the ion exchange capacity (IEC). Snowtexpolystyrene acid silica (0.10 g) was added to a 5 mL mixture of 2M NaCl and 5 mL of 2-methoxyethyl ether with stirring. After soaking for 24 h, the silica was collected by filtration, washed 3 times with 5 mL of 1:1 (v/v) DMF and 2M NaCl. The solution was ultrasonicated for 1h, and allowed to soak overnight. The solids were collected and washed with 1:1 DMF and 2M NaCl several times. The combined liquid filtrate was titrated to the phenolphthalein end point with 0.0112 M NaOH. Dried A200 titrated under same conditions was used as a blank.

Membrane preparation PVDF (0.01g) and 0.4 mL DMF were added to a vial and stirred at room temperature until the PVDF dissolved. The desired amount of ***Snowtexpolystyrene acid*** particles, previously ground in a mortar and pestle, was

weighed into a second vial with 0.2 mL DMF and stirred for 12 h until homogeneous. The two solutions were combined and stirred for 12 h, and then the membrane was cast by pouring the final solution onto a glass slide heated to ~ 50 °C on a hot plate. Round membranes ~1 cm in diameter were obtained after solvent evaporation and were further dried in a vacuum oven at 80 °C overnight to remove residual solvent.

Hybrid membrane pretreatment. Membranes cast on glass plates were cut into ~ 2.0 × 0.5 cm rectangular strips with a razor blade and their size and thickness was measured. The cut membrane was released from its support by immersion in water, and was boiled in 8% HNO_3 for 30 min, rinsed with water, then boiled in deionized water for 30 min. The treated membranes were stored in deionized water at room temperature.

Absorption of phosphoric acid in hybrid membranes. Pretreated membranes were blotted dry with filter paper and immersed in various concentrations of phosphoric acid for 2 days at 50 °C. The treated samples were stored in phosphoric acid at room temperature.

Membrane conductivity measurements. Rectangular strips of the membrane (~ 2.0 × 0.5 cm) were sandwiched between 2 Teflon blocks with two membrane ends in contact with platinum electrodes. The blocks and membrane were isolated in an oven which was equipped with a gas inlet and outlet. Humidity control was obtained by bubbling dry N_2 into 75 °C deionized water under atmosphere pressure.

Cleaving polystyrene chains from silica. Silica/polystyrene nanoparticles (0.2 g) were dispersed in 10 mL of toluene in a polyethylene flask. Aliquot 336 (50 mg) was added as phase transfer catalyst, along with 10 mL of 5% HF. The mixture was stirred

overnight. The organic layer was removed and the polymer was precipitated by adding 20 mL of ethanol. The polymer was isolated by centrifugation and dried under vacuum.

Membrane samples for confocal microscopy Rectangular strips of the membrane (~ 2.0 × 0.5 cm) were soaked in 0.1% aqueous solution of Cy3 for ~5 min, and then the membrane was removed from the solution, spread on a clean glass slide, and soft paper tissues were applied gently to absorb excess solution on both sides of the membrane. The membrane was sandwiched between a cover glass and glass slide, wrapped with aluminum foil and stored at 4 °C before measurements.

Chapter 5

Sol-gel nanoparticles with surface functional groups

Chapter 4 described the synthesis of nanoparticles with sulfonated polystyrene chains attached to their surface. Membranes cast from DMF solutions of PVDF and nanoparticles had conductivities comparable to Nafion. Microscopy indicates agglomeration of nanoparticles to form continuous channels within a hydrophobic PVDF polymer matrix. However, the introduction of sulfonic acids by electrophilic aromatic substitution can be reversible under acidic conditions, especially at high temperatures. This raises potential long term stability issues for membranes in operating fuel cells. An alternative is to replace aromatic sulfonic acids with alkyl sulfonic acids.

The surface functionalization of silica nanoparticles can be effected either by grafting functional alkoxysilanes to the surface of preformed silica nanoparticles, a "grafting to" method as described in Chapter 2, or by a sol-gel process, the condensation of silicon alkoxides with one or more organoalkoxysilanes.[140] However the number of organic groups that can be added by a post-grafting processes is constrained by the number of reactive silanols on the surface and possibly by diffusion limitations. As described in Chapter 2 and in previous literature,[141-143] grafting alkyl thiols directly to silica particles such as A200 results in a limited amount of acid groups on the surface, ~ 0.3 mmol/g for A200. These restrictions may be overcome by sol-gel syntheses of small nanoparticles.

Sol-gel reactions are based on the acid or base catalyzed condensation of alkoxide precursors such as tetraethyl orthosilicate ($Si(OEt)_4$, or TEOS), followed by aging and

drying under ambient conditions. The chemical steps for forming silica via a sol-gel process are shown below.

$$Si(OR)_4 + 4H_2O \rightleftharpoons Si(OH)_4 + 4ROH \quad \text{hydrolysis}$$

$$SiOH + SiOH \rightleftharpoons Si\text{-}O\text{-}Si + H_2O \quad \text{condensation}$$

Sol-gel processes provide a wide range of silica-based materials under mild conditions. A breakthrough in materials science was the introduction of molecular templating techniques to build mesoporous silica structures around self-assembled organic templates. The resulting mesoporous silicas have large surface areas and well-defined pore sizes and shapes.[140]

Silica particles with surface alkyl sulfonic groups can be prepared via sol-gel processes. As controlling pH is important in sol-gel syntheses, the sulfonic acid groups are typically introduced as alkyl thiols, and then oxidized to the acids upon completion of the sol-gel synthesis. There are several examples of one-step syntheses of mesoporous silica with organosulfur groups.[144,145] For example, Stein et al. reported 4.7 mmol of S/g SiO_2 and an IEC of 1.76 mmol/g after oxidation,[145] confirming that a high density of functional groups can be grafted to a silica surface by a one step process. However, formation of composite membranes also depends on suitable particle-particle interactions in a polymer matrix to enable proton transport through the membrane. Nanoparticulate systems are the most promising because of their high surface area.

Microemulsion sol-gel techniques provide control over particle size in the nanometer range. Microemulsions[146-152] are thermodynamically stable, optically clear dispersions of two immiscible liquids such as oil and water. Microemulsions are formed

when a surfactant, or a mixture of surfactants are added to two immiscible phases, lowering the oil/water interfacial tension and allowing thermal motions to spontaneously disperse the phases. Water droplets dispersed in a continuous oil phase is termed a water-in-oil (w/o) microemulsion. These dispersed droplets can serve as micro or nanoreactors to control particle size. **Figure 5.1** shows Schulman's model for the reverse micelles of a w/o microemulsion,[153] in which the surfactant forms spherical aggregates with the polar ends oriented toward the center through ion-dipole interactions with the polar co-surfactant. The co-surfactant acts as an electronegative spacer minimizing repulsions between the positively charged surfactant heads. The droplet sizes are usually determined by the ratio of water and surfactants used.

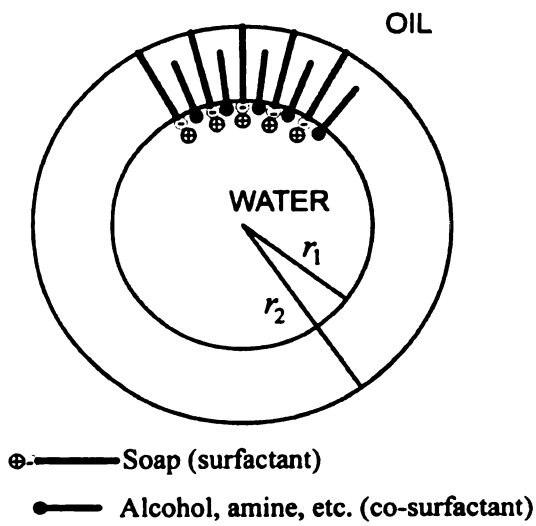

Figure 5.1. Schulman's model of the reverse micelle.[163]

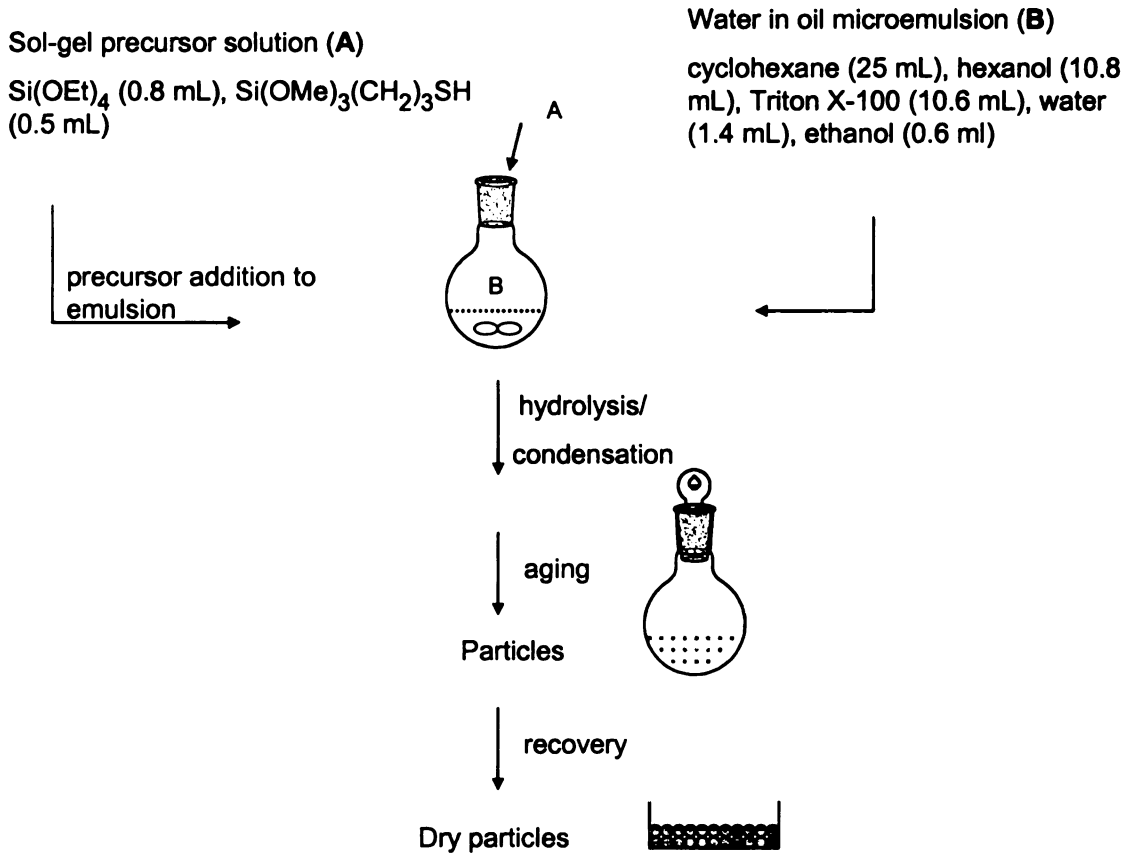

Figure 5.2. Schematic showing the synthesis of sol-gel particles via water in oil microemulsion mediated sol-gel processing.

Results and discussion

Figure 5.2 shows the synthesis of nanoparticles via the w/o microemulsion mediated sol-gel process. The w/o microemulsion was established by mixing cyclohexane, hexanol, Triton X-100, water and ethanol until the water droplets were homogeneously dispersed in the organic phase. Triton X-100 (shown below) is a nonionic surfactant where n is ~10. A precursor solution of TEOS and mercaptopropyl trimethoxysilane was introduced into the microemulsion system, followed by the slow addition of ammonium hydroxide to catalyze the hydrolysis reaction. The condensation was completed at room temperature with constant stirring, and after 24 hours the particles were recovered by centrifugation and dried under vacuum at 80 °C. The thiols in the isolated particles were treated with H_2O_2 at room temperature and after a series of washing steps, the nanoparticles were dried under vacuum.

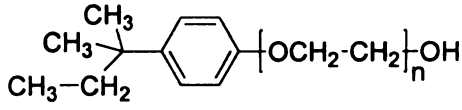

Triton X-100

The sol-gel reaction and further chemical modifications of the resulting particles are conveniently followed by IR spectroscopy. The particles obtained from the sol-gel reaction were analyzed by DRIFT IR (diffuse reflectance infrared Fourier transform spectroscopy). **Figure 5.3** shows data for nanoparticles containing alkyl thiol groups (***sol-gelSH***), and particles obtained after oxidation of the thiols to sulfonic acids (***sol-gelSO$_3$H***). Both spectra have a broad peak from 3700 - 3400 cm^{-1} characteristic of O-H stretching. In addition, both spectra showed substantial C-H stretching bands at 2800-3000 cm^{-1} confirming that they were due to the mercaptopropyl fragment. More

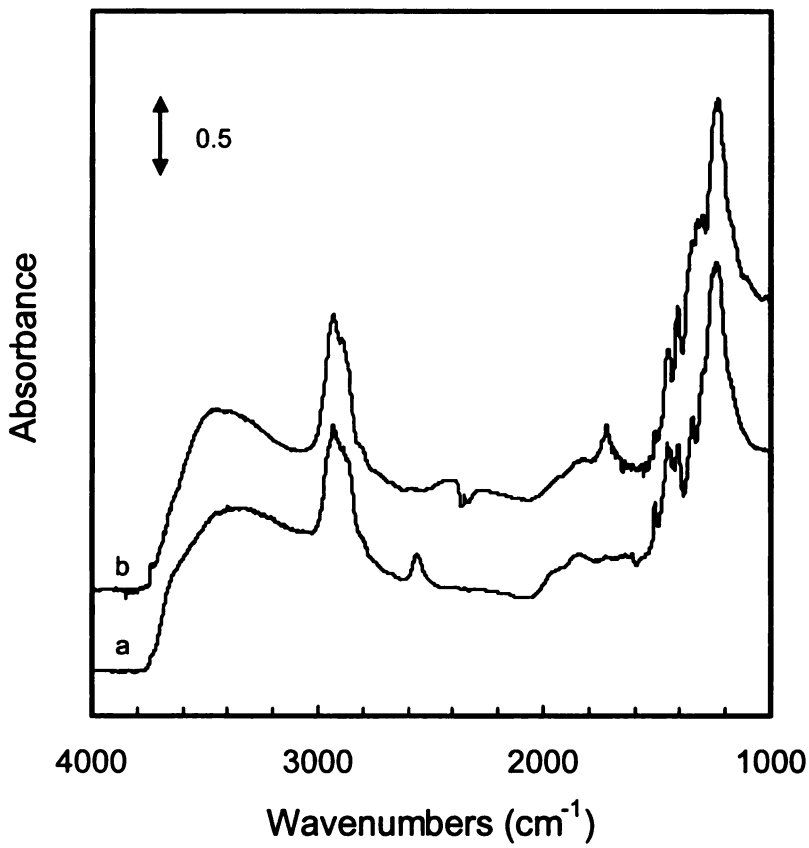

Figure 5.3. DRIFT IR spectra of sol-gel nanoparticles. **a**, sol-gelSH; **b**, sol-gelSO_3H

diagnostic was the weak peak at ~2600 cm^{-1} in ***sol-gelSH*** which confirmed the presence of the thiol groups. After oxidation with H_2O_2, this peak disappeared and the spectrum of ***sol-gelSO_3H*** suggests that most of the thiols were accessible and oxidized. The sharp peaks at 1240 cm^{-1} in both ***sol-gelSH*** and ***sol-gelSO_3H*** were assigned to Si-O-Si asymmetric stretching.[123]

TGA measurements run in air provide information about the thermal stability of the particles and the relative amounts of organic components in the particles. Also shown is ***sol-gelTEOS***, particles prepared solely from TEOS for comparison. The weight loss onset for ***sol-gelTEOS*** was at ~ 200 °C, with a ~13% loss by 600 °C. Under similar conditions, ***A200***, a dense silica with only OH groups on its surface lost 3%. The relatively high weight loss for sol-gelTEOS may be from surface silanol groups and residual ethoxy groups which appear in solid state carbon NMR spectra. The weight losses for ***sol-gelSH*** and ***sol-gelSO_3H*** were ~ 32% and 40% of total weight, respectively. The profile of the ***sol-gelSO_3H*** was as expected, an early onset of weight loss followed by a gradual weight loss that extends to high temperatures. Being more hydrophobic than ***sol-gelSO_3H***, we anticipated that the gradual weight loss at low temperatures for ***sol-gelSH*** would be absent, and the rapid loss at ~ 260 °C is consistent with the loss of the alkyl groups. ***Sol-gelTEOS*** showed the same thermal characteristics of both as ***sol-gelSH*** and ***sol-gelSO_3H***, loss of surface bound water followed by loss of residual alkoxy groups.

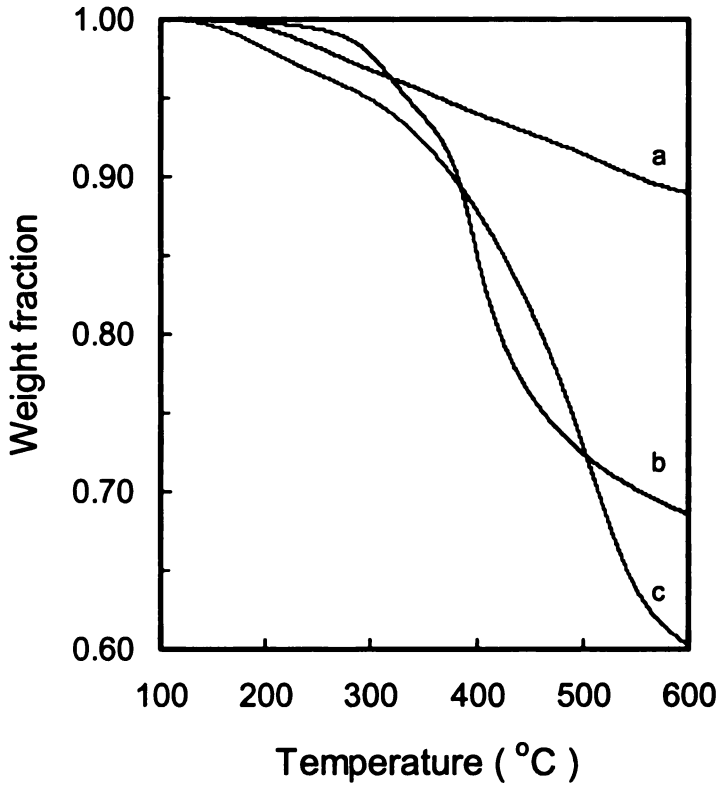

Figure 5.4. TGA data for sol-gel nanoparticles in dry air. **a**, sol-gelTEOS; **b**, sol-gelSH; **c**, sol-gelSO_3H. All samples were stabilized at 110 °C for 30 min prior to initiating the run.

Table 5.1. Elemental analysis of sulfur in sol-gelSH and titration results after oxidation.

Expected S content [a]	S analysis of Sol-gelSH [b]	Titratable S after oxidation [c]
4.8 mmol/g	3.2 mmol/g	2.2 mmol/g

a. Calculated from the reactant ratios used in the sol-gel synthesis.
b. Based on elemental analysis.
c. Sample powder was ion exchanged with1:1 DMF and 2M NaCl and the aqueous solution were titrated with 0.010M NaOH. Results were average of three measurements. Sol-gelSH, titrated under same conditions, was used as a blank.

Table 5.1 presents data from elemental analyses for S in ***sol-gelSH***. The expected sulfur content calculated from the reactants was 4.8 mmol/g. However, the analysis results, 3.2 mmol/g of S, suggests the thiol precursor may have a lower reactivity in the sol-gel reaction. After oxidation to ***sol-gelSO_3H***, the sulfonic acids were ion exchanged with 1:1 DMF and 2M NaCl and the aqueous layer was titrated with 0.010M NaOH. The titration yielded 2.2 mmol acid/g (average of three titrations).

We used solid state ^{13}C NMR experiments to further confirm the composition of the particles. **Figure 5.5** shows ^{13}C NMR spectra of the two precursors and the co-surfactant used in the synthesis of the sol-gel nanoparticles, and **Figure 5.6** shows solid state ^{13}C NMR spectra of the sol-gel products. Two small peaks at 68 ppm and 27 ppm in the solid state spectrum of ***sol-gelTEOS*** are particularly interesting. These resonances are consistent with ethoxy groups. Since the particles were heated to 130 °C at 20 mtorr for 4 hours, physisorbed ethanol seemed unlikely. A plausible explanation is that resonances are due to residual ethoxysilyl groups. The spectrum of ***sol-gelSH***

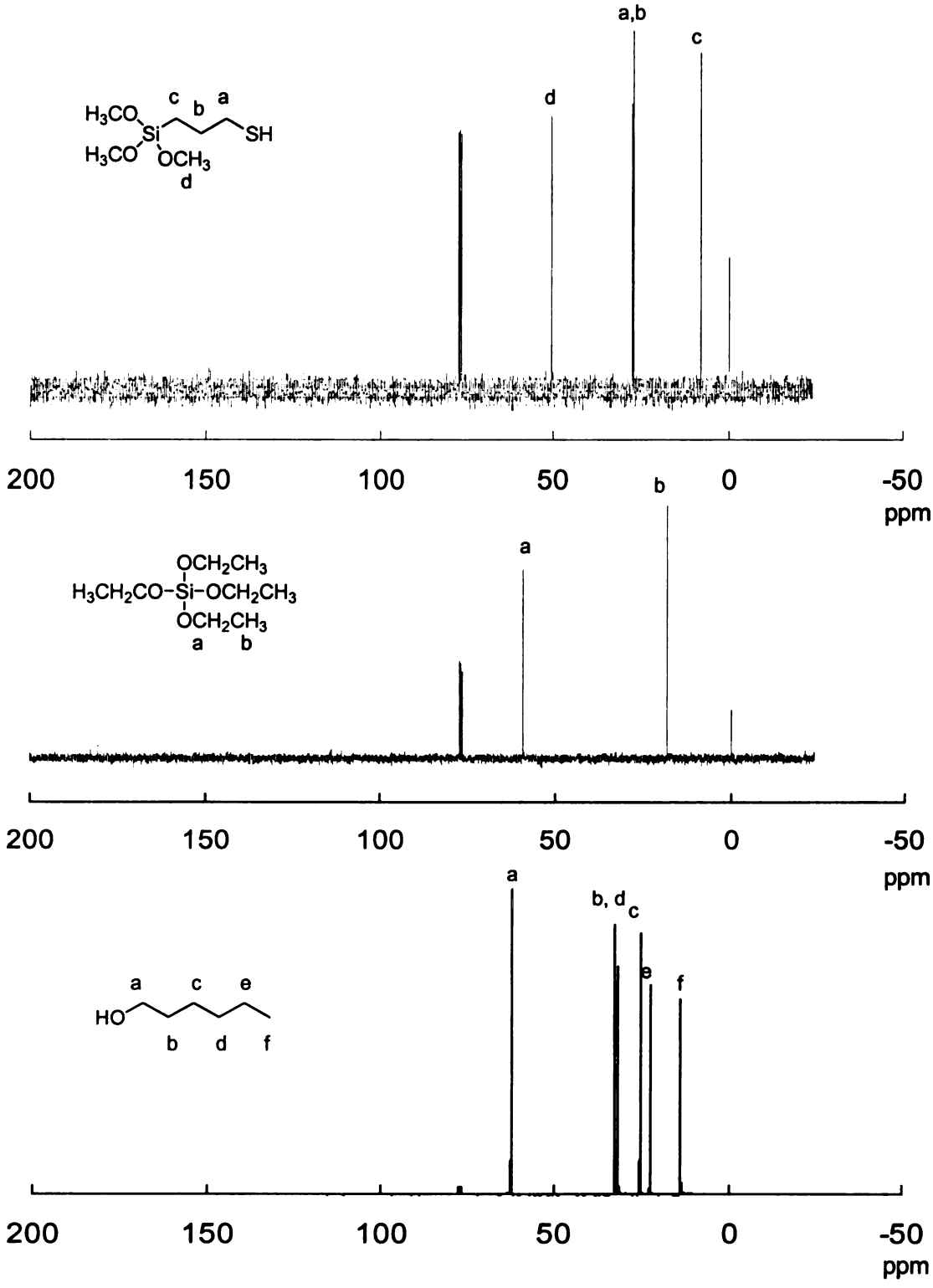

Figure 5.5. ^{13}C NMR spectra of the precursors and cosurfactant used in the synthesis of sol-gel nanoparticles.

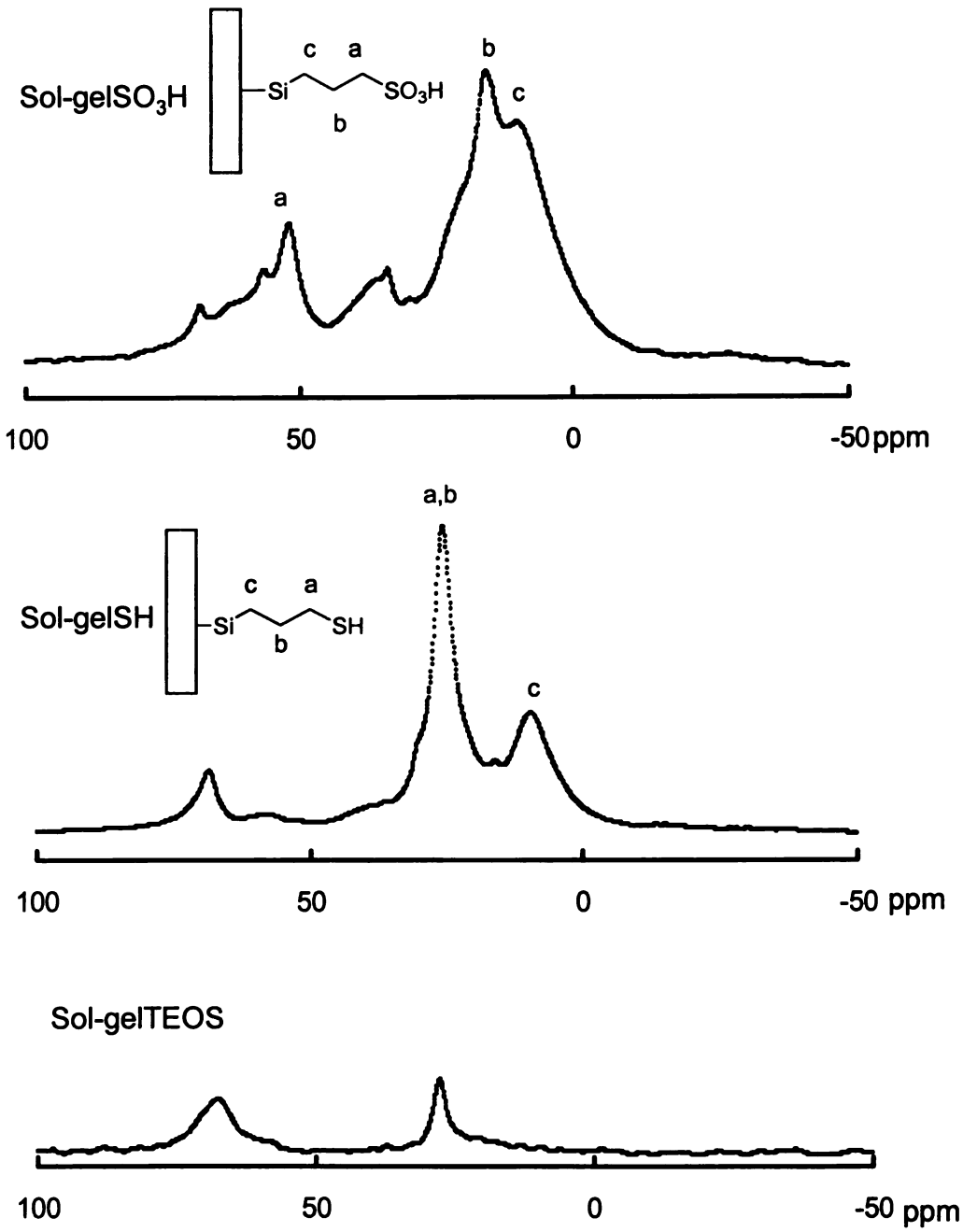

Figure 5.6. ^{13}C solid state NMR spectra of sol-gel nanoparticles

had peaks at 8 ppm and 24 ppm which was in agreement with its liquid precursor and literature reports.[143-145] After oxidation, the resonance for the carbon adjacent to the sulfur atom shifted to 51 ppm and the beta carbon to 15 ppm. A broad peak at ~35 ppm was assigned to carbon atoms alpha to other oxidation products such as sulfinate groups.[145] The sol-gelSO_3H nanoparticles were characterized by TEM (**Figure 5.7**) and dynamic light scattering (DLS) (**Figure 5.8**). For the TEM measurements, the particles were dispersed in liquid nitrogen, and then deposited on an amorphous carbon film supported by a Cu TEM grid. A representative TEM image, shown in **Figure 5.7,** reveals a collection of poorly resolved particles, roughly 4-6 nm in diameter, while DLS measurements of sonicated particles in methanol provide a 4-8 nm particle diameter.

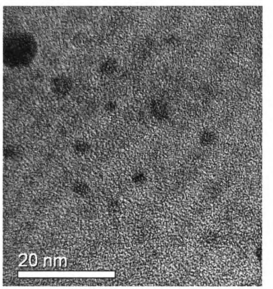

Figure 5.7. TEM image of sol-gelSH particles. Samples were prepared by deposition of a sol-gelSH suspension in liquid nitrogen onto a lacey formvar/carbon supported on a 300 mesh copper TEM grid.

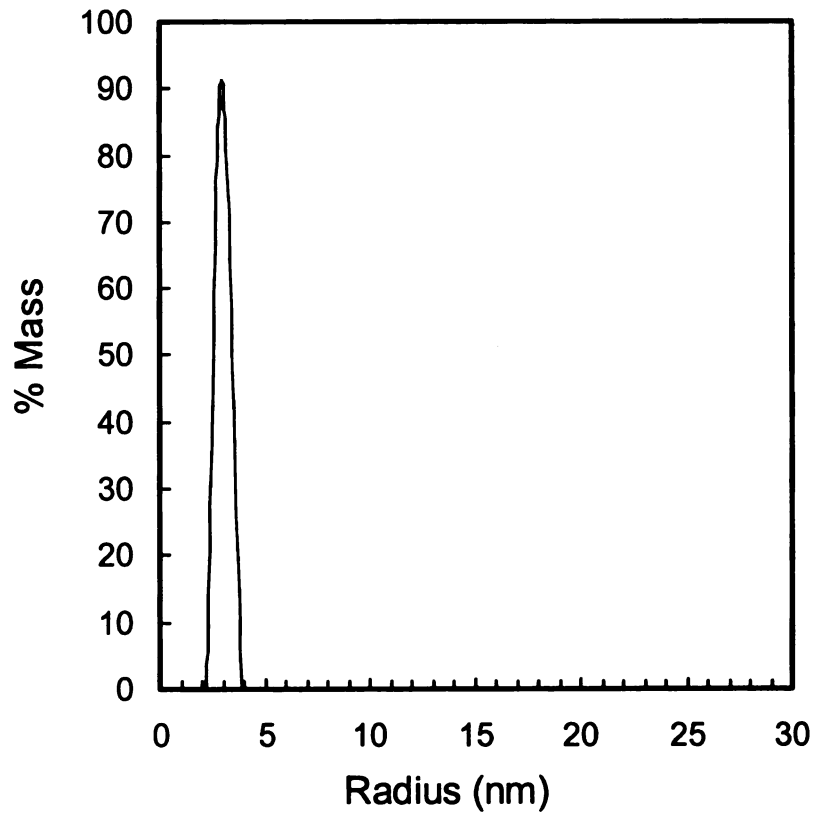

Figure 5.8. Dynamic light scattering data obtained from sol-gelSO_3H particles at a concentration of 2 mg/mL. The solutions were sonicated for 20 min in methanol, and passed through 0.02 μm filter prior to taking measurements at 25 °C.

Characterization of composite membranes. Smooth, flexible membranes were cast from ***sol-gelSO_3H*** nanoparticles dispersed in DMF solutions of PVDF. The casting solutions were prepared by combining a 25 wt% solution of PVDF in DMF with a DMF dispersion of the appropriate amount of ***sol-gelSO_3H*** particles. After combining the two solutions, the mixture was stirred for 12 hours, and then cast onto glass plates warmed to 50 °C on a hot plate. Sample membranes were cut into 1.5 × 0.5 cm rectangular strips. Membranes were pretreated by first boiling in 8% HNO_3 solution for 30 min followed by boiling in deionized water for 30 min. The pretreated membranes were rinsed with deionized water and sandwiched between 2 Teflon blocks with the ends of the membrane in contact with platinum electrodes. The membranes were characterized by AC impedance spectroscopy, with the membrane resistance deduced from when the phase angle is near zero in the high frequency portion of the data. The membrane conductivity was calculated from the relationship $\sigma = t/(R \times S)$ where t is the thickness of membrane, R is the membrane resistance, and S is the membrane area.

Figure 5.9 shows that the membrane conductivities were strongly dependent on the particle content. The room temperature conductivities of membranes with 30 and 40 wt% particles were $<10^{-4}$ S/cm at full humidity, but those with 50 wt% particles were more than two orders of magnitude higher, 0.02 S/cm. We believe the poor conductivity at 30 and 40 wt% stem from particle agglomeration, and poor connectivity between the agglomerates. For comparison, the conductivity of a densely packed sample of fully hydrated particles (no polymer) was 0.053 S/cm at room temperature.

The cause of the low conductivity seen for the 30 and 40% membranes is not that the particles agglomerate. Instead, poor conductivity results from *how* they

agglomerate. A200 fumed silica forms a continuous network structure and its effects in materials are observable at 10 wt%. The ***sol-gelSO_3H*** nanoparticles apparently form isolated dense aggregates rather than networks. During membrane casting, strong particle-particle interactions favor rapid aggregate formation rather than the preferred network structure, and thus, the percolation threshold (and high conductivity) occurs at high particle contents.

Shown in **Figure 5.10** are the results of confocal microscopy experiments designed to probe the size and connectivity of aggregates in the membranes. A conductive membrane with 50 wt% particles was soaked in an aqueous solution of Cy3, a fluorescent cyanine dye with 3 carbon atoms in the conjugated polyene. The hydrophilic domains selectively adsorb dye and appear bright red in the image. The domains are irregular in shape and are not connected to adjacent domains. Some aggregates were > 50 μm in size. The image is consistent with formation of an ensemble of aggregates rather than a network structure. A better understanding of the conditions that lead to aggregation and network formation is needed to reliably obtain conducting membranes at lower particle contents.

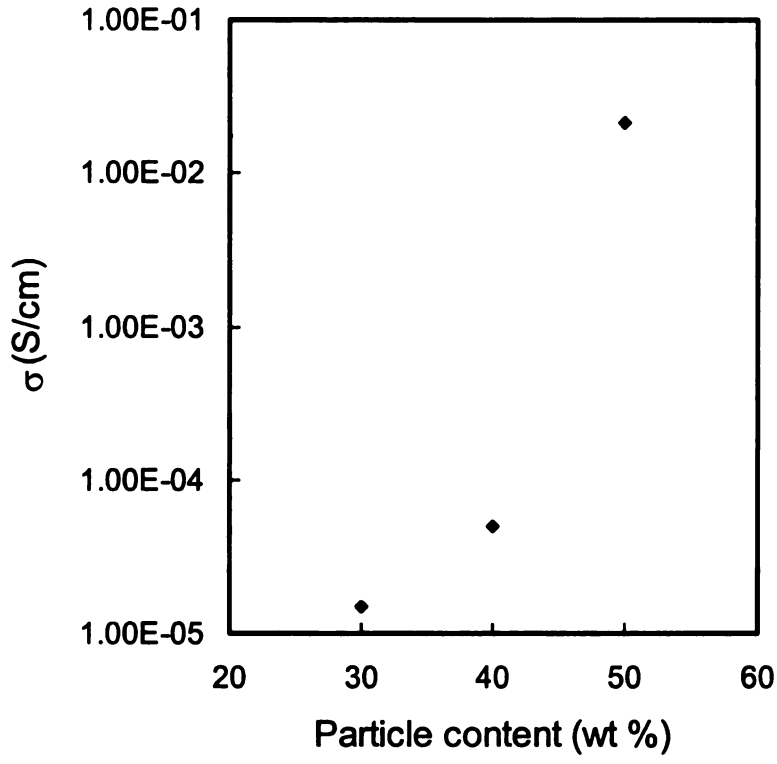

Figure 5.9. The conductivity of composite membranes with various particle contents. Each data point was average of two independent samples.

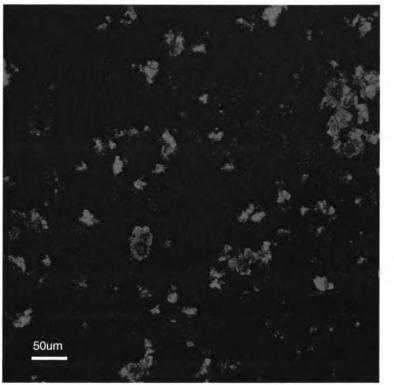

Figure 5.10. Confocal microscopy image of a membrane with a 50 wt% ***sol-gelSO_3H*** particle content. The membrane conductivity was 0.02 S/cm at room temperature, under full humidity conditions. The image is from a 2D section inside the membrane parallel to surface. The bright red regions indicate a high concentration of fluorescent dye in hydrophilic domains.

Operating PEMs at high temperatures is preferred as catalyst poisoning is reduced and water management problems are simplified above 100 °C. Replacing water with less volatile H_3PO_4 is approach to high temperature fuel cells. As described in Chapter 4, soaking Snowtexpolystyrene/PVDF composite membranes in phosphoric acid greatly enhanced the membrane conductivity. We carried out the same protocol on membranes containing 50% Sol-gelSO_3H, soaking the membranes in 8M H_3PO_4 at 50 °C for two days.

Figure 5.11 shows the temperature dependent conductivity for membranes doped with 8M phosphoric acid measured under 0.3 atmosphere humidity conditions. Generally, doping with H_3PO_4 enhanced the membrane conductivity. At high temperature, the conductivity decreased and then stabilized above 100 °C. The initial drop in conductivity was likely due to loss of water from the membrane. After aging the membrane for 300 hours at 120 °C and 0.3 atmosphere humidity, the conductivity dropped from 0.2 to 0.1 S/cm **(Figure 5.12). Figure 5.12** also shows long term aging data for a membrane with 50 wt% Snowtex particles under same conditions. (The Snowtex particles had sulfonated polystyrene attached to the surface of the particles.) In the first 100 hours of testing, the conductivity of the Snowtex membrane abruptly dropped from 0.8 S/cm to 0.2 S/cm, and then stabilized. Both membranes showed similar aging profiles after 100 hours of testing. The similarity of the long term aging trends for membranes containing ***Sol-gelSO_3H*** and sulfonated ***Snowtexpolystyrene*** revealed similar thermal stabilities for both membranes under acidic conditions.

Conclusion

Sol-gel nanoparticles that incorporate sulfonic acid groups were synthesized and characterized by IR, TGA and NMR spectroscopy. TEM and DLS showed that the particles had ~ 6 nm diameters, and titration indicates an acid content of 2.2 mmol/g. When embedded in polymer matrices, only membranes with 50 wt% particle contents were conductive. Agglomeration of the nanoparticles into micrometer-sized aggregates was observed by confocal microscopy. Membranes prepared with 50 wt% sol-gel particles were initially less conductive than comparable membranes prepared from snowtex particles, but after 100 hours of long term aging, the two membranes have nearly identical conductivities.

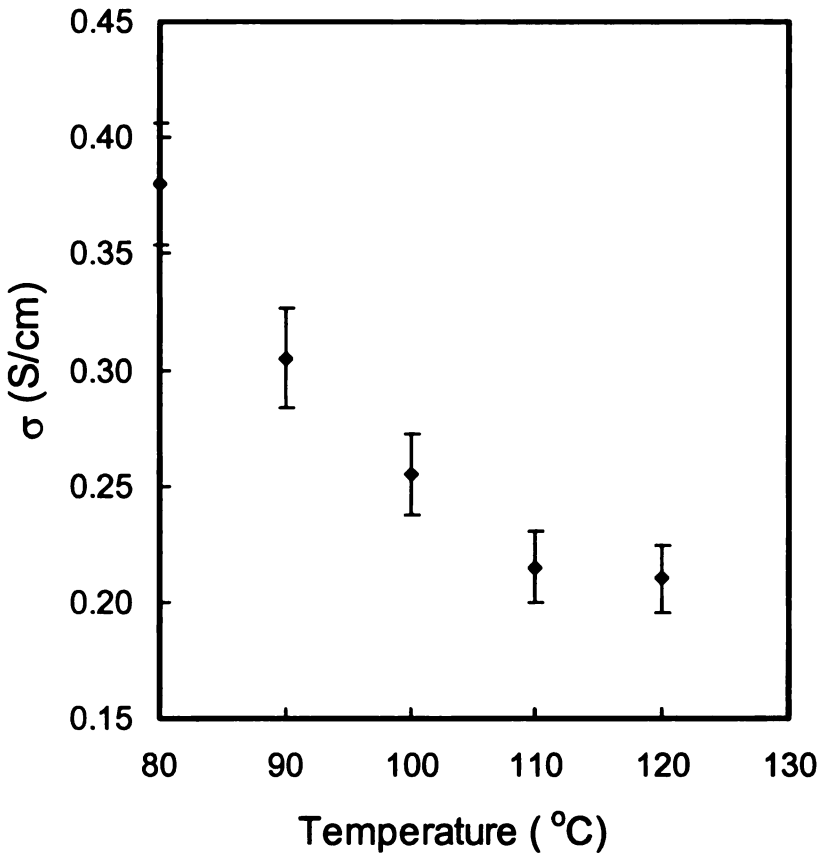

Figure 5.11. Temperature dependent proton conductivity of composite membranes with 50% particle contents. Membranes were soaked in 8M H_3PO_4 for 48 hrs at 50 °C before measurements. Measurements were taken at 0.3 atmosphere humidity. Each data point was average of two independent samples.

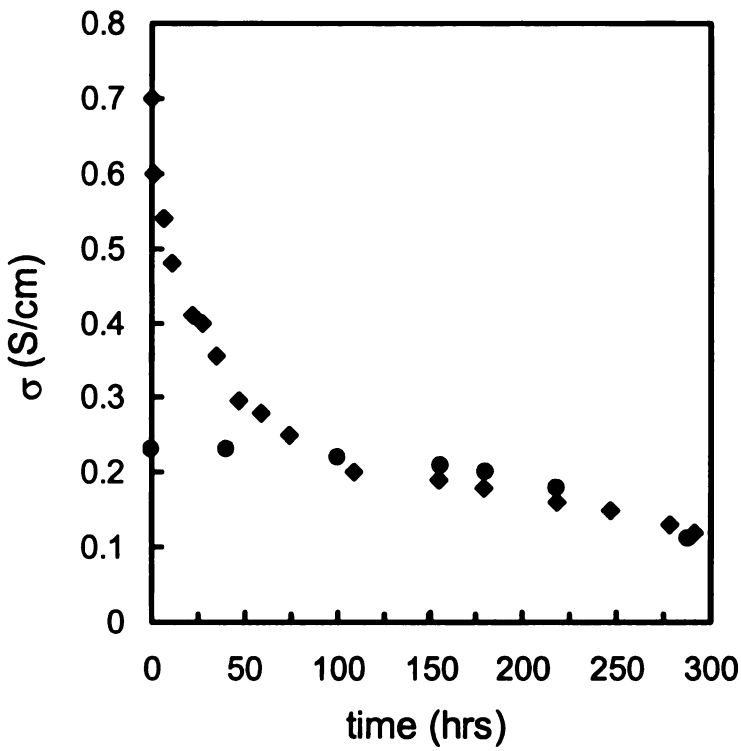

Figure 5.12. High temperature aging of composite membranes containing 50 wt% particles at 120 °C, 0.3 atmosphere humidity. •, sol-gelSO_3H; ▲, snowpolystyreneSO_3H. The membranes were soaked in 8M H_3PO_4 at 50 °C for 48 hours before the before the first measurement.

Experimental

Triton X-100, 1-hexanol (98%), tetraethyl orthosilicate (98%), cyclohexane (99%), (3-mercaptopropyl)trimethoxysilane (95%), H_2O_2 (30%), poly(vinylidene fluoride and (PVDF, M_w 534,000) were obtained from Aldrich and used as received. Cy3 fluorescent dye was obtained from Jackson ImmunoResearch Laborotary, Inc.

^{13}C solid state NMR spectra were obtained at 79.5 MHz on a Varian 400 spectrometer under ^{1}H cross-polarization, magic angle spinning conditions. Samples (~ 100 mg) were packed in a 7.0 mm zirconia rotor, and a spinning frequency of 4 KHz was used. Chemical shifts are reported in ppm and are referenced to adamantane. A Nicolet IR/42 spectrometer purged with dry nitrogen was used to obtain infrared spectra. Samples used were 1 cm^2 pressed pellets prepared from ~ 100 mg of various modified silica. All spectra reported were acquired by signal averaging 32 scans at a resolution of 4 cm^{-1}. DRIFT IR (diffuse reflectance infrared Fourier transform spectroscopy) spectra were collected from a computer-controlled Nicolet Protégé 460 equipped with a DRIFTS Auxiliary experiment module. All spectra reported were acquired by signal averaging 100 scans at a resolution of 4 cm^{-1}. Thermogravimetric analyses (TGA) were performed in dry air at a heating rate of 10 °C/min on a Perkin Elmer TGA 7 instrument. Samples were held at 110 °C for 30 min before the run.

AC impedance data were obtained from an HP 4192A LF Impedance Analyzer controlled by an in-house designed LabView application, scanning from 5 Hz to 13 MHz with an applied voltage of 10 mV. Rectangular membrane strips (~ 2.0 × 0.5 cm) were sandwiched between 2 Teflon blocks with two membrane ends in contact with platinum electrodes. The blocks and membrane were isolated in an oven which was

equipped with a gas inlet and outlet. Humidity control (0.3 atmosphere humidity) was obtained by bubbling dry N_2 into 75 °C deionized water at atmospheric pressure.

TEM images were acquired using a JEOX 100CX Transmission Electron Microscope. Membrane samples for TEM were prepared by cryosectioning using a PowerTome-XL by BAL-TEC RMC with a thickness control of ~80 nm. Dynamic Light Scattering (DLS) measurements were performed with a Protein Solutions Dyna Pro-MS/X system with temperature control. Samples were sonicated for 20 min, filtered and allowed to equilibrate in the instrument for 25 minutes at 25 °C before measurements. Confocal microscopy images were taken using LSM 5PASCAL using He-Ne laser light at an exciting wavelength of 543 nm.

Sol-gelSH nanoparticles Triton X-100 (10.6 mL), cyclohexane (25 mL), and 1-hexanol (10.8 mL) were added to a 100 mL round bottom flask and stirred until the mixture became clear (~ 5min). A mixture of deionized water (1.4 mL) and EtOH (0.6 mL) was syringed into the flask drop-wise, and then a premixed solution of tetraethyl orthosilicate (0.8 mL, 5.26 mmol) and (3-mercaptopropyl)trimethoxysilane (0.5 mL, 4.1 mmol) was syringed into to flask over 25 min. The solution was stirred under N_2 at room temperature for 5h. As NH_4OH (0.7 mL) was slowly injected into the flask, the solution became milky white, and the reaction was stirred for 24 hours. Acetone (30 mL) was added to the solution and the solid particles were isolated by centrifugation at 2000 rpm, washed with toluene (4 × 30 mL) and dried under vacuum at 80 °C for 12 h to yield 0.61 g of ***Sol-gelSH***.

Sol-gelSO_3H nanoparticles. ***Sol-gelSH*** (0.3 g), ground into a fine powder with a mortar and pestle, was transferred into a 50 mL round bottom flask. MeOH (10 mL)

and H_2O_2 (3 mL) were added into the flask and the suspension was stirred 48 h at room temperature in air. The solid particles were isolated by centrifuge at 2000 rpm, washed with H_2O (2 × 30 mL) followed by a final wash with 30 mL EtOH. The wet material was re-suspended in 0.5 M H_2SO_4. After 4h, the particles were isolated by centrifugation and washed with EtOH (4 × 30 mL) until the supernatant was neutral. The particles were dried under vacuum at 80 °C for 12 hours to yield 0.26 g of ***Sol-gelSO$_3$H*** (86% yield).

Measurement of the ion exchange capacity (IEC). ***Sol-gelSO$_3$H*** silica (0.10 g) was added to a 5 mL mixture of of 2M NaCl and 5 mL of 2-methoxyethyl ether with stirring. After soaking for 24 h, the silica was collected by filtration, washed 3 times with 5 mL of 1:1 (v/v) DMF and 2M NaCl. The solution was ultrasonicated for 1h, and allowed to soak overnight. The solids were collected by centrifugation and washed 3 times with 1:1 DMF (5 mL) and 2M NaCl. The combined liquid filtrate was titrated to the phenolphthalein end point with 0.010 M NaOH. Dried **Sol-gelSH** titrated under same conditions was used as a blank.

Membrane preparation PVDF (0.01g) and 0.4 mL DMF were added to a vial and stirred at room temperature until the PVDF dissolved. The desired amount of ***Sol-gelSO$_3$H*** particles, previously ground in a mortar and pestle, was weighed into a second vial with 0.2 mL DMF and stirred for 30 min until homogeneous. The two solutions were combined and stirred for 12 h, and then the membrane was cast by pouring the final solution onto a glass slide heated to ~ 50 °C on a hot plate. Round membranes ~1 cm in diameter were obtained after solvent evaporation and were further dried in a vacuum oven at 80 °C overnight to remove residual solvent.

Sol-gel membrane pretreatment. Membranes cast on glass plates were cut into ~ 2.0 × 0.5 cm rectangular strips with a razor blade and their size and thickness were measured with a micrometer. The cut membrane was released from its support by immersion in water, and was boiled in 8% HNO_3 for 30 min, rinsed with water, then boiled in deionized water for 30 min. The treated membranes were stored in deionized water at room temperature.

Absorption of phosphoric acid in sol-gel membranes. Pretreated membranes were blotted dry with filter paper and immersed in various concentrations of phosphoric acid for 2 days at 50 °C. The treated samples were stored in phosphoric acid at room temperature.

Membrane samples for confocal microscopy Rectangular strips of the membrane (~ 2.0 × 0.5 cm) were soaked in 0.1% aqueous solution of Cy3 for ~5 min, and then the membrane was removed from the solution, spread on a clean glass slide, and soft paper tissues were applied gently to absorb excess solution on both sides of the membrane. The membrane was sandwiched between a cover glass and glass slide, wrapped with aluminum foil and stored at 4 °C before measurements.

Conductivity measurements on Sol-gelSO_3H powder. Dry ***sol-gelSO_3H*** particles were tightly packed into a 1.5 × 6.0 × 25 mm cavity in a Teflon block. The packed powder was soaked with deionized water, and the top and bottom of the cell was sealed with two stainless steel discs. The cell was connected to platinum electrodes and the sample was characterized by AC impedance spectroscopy.

Chapter 6

Attempts to tether perfluorinated sulfonic acids to silica surfaces

The previous chapters described studies designed to optimize the ion exchange capacity and particle size in proton conducting composite membranes. Previously, we found that membranes with alkylsulfonic acid or aromatic sulfonic acid groups on silica surfaces had comparable thermal stabilities and behaved similarly under acidic conditions. In this chapter we describe efforts to attach perfluorinated sulfonic acids to silica surfaces. The higher acidity of these acids and their improved oxidative stability compared to alkyl and aryl systems make perfluorinated sulfonic acids attractive candidates for nanoparticulate solid acids. However, a limitation of perfluorinated polymers is that they are difficult to process, the diversity of fluoropolymer architectures is limited, and the monomers are expensive.

Anchoring methylsiloxane oligomers to nanoparticles and subsequent hydrosilylation reactions involving their Si-H bonds can be used to anchor vinyl-substituted groups to silica. A surface initiated polymerization of a cyclic hydrosiloxane monomer would be the logical route to the tethered oligomers since it may offer linear polymers with control over the molecular weight. The high sensitivity of Si-H bonds toward nucleophilic agents precludes anionic polymerization of cyclic hydrosiloxanes and therefore a cationic route must be employed.[154] The synthesis of poly(methylsiloxane) by cationic polymerization of 1,3,5,7-tetramethylcyclotetrasiloxane (D_4^H) was studied by Hemery et al.,[154] but attaching initiators to a silica surface and initiating a cationic ring opening polymerization of D_4^H has not been reported.[155-157]

Hydrosilylation refers to the catalyzed addition of a hydrosilane (Si-H) to a carbon-carbon double bond to form an alkylsilane. The reaction is widely utilized for the production of silicon related products. The accepted mechanism for hydrosilation using homogeneous monomeric platinum catalysts was proposed by Chalk and Harrod.[158] Lewis et al. proposed an alternative mechanism involving colloidal Pt as the active catalyst,[159-164] which accounts for an induction time, the formation of colored solutions and the presence of colloids. The literature suggests that the effectiveness of hydrosilylation on solid silica surfaces is very low, with the highest yield reported to date <40% for hydrosilylation from a single hydrosilane layer on 60 μm silica particles.[188] The Lewis mechanism may explain the difficulty of hydrosilylation from solid surfaces; the presence of two solid phase reactants in the system, i.e., the hydride groups on the silica surface and the platinum particles, may hinder the catalytic reaction.[165]

Scheme 6.1 shows the synthetic steps used to attach perfluorinated alkylsulfonic acids to the surface of A200 silica particles. We used a condensation approach to attach linear methylsiloxane oligomers to the silica surface.[166] In this scheme, dichloromethylsilane was hydrolyzed in the presence of A200, with the A200 acting as a terminating site for the silanol end groups of growing siloxane chains.[166-169] Because of the large number of reactive silanols on the surface of the nanoparticles the particles also could act as a cross-linking agent and cause particle agglomeration. Dynamic light scattering measurements support cross-linking since the particle diameter increased from 14 nm for pristine A200 to ~ 600 nm for the modified silica (**Figure 6.1**). The TEM images shown in (**Figure 6.2**) also indicated large scale agglomeration of particles.

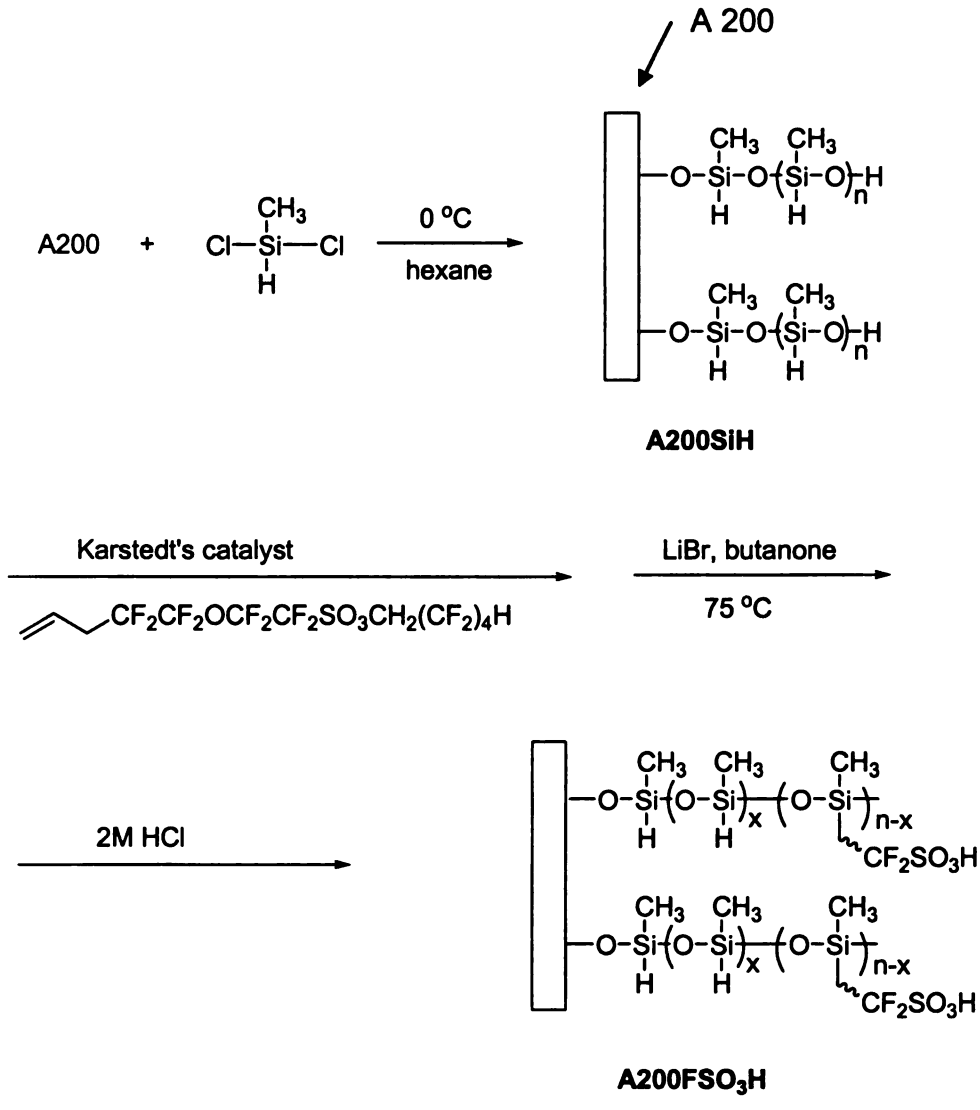

Scheme 6.1. Scheme used to tether perfluorinated sulfonic acids to silica surfaces.

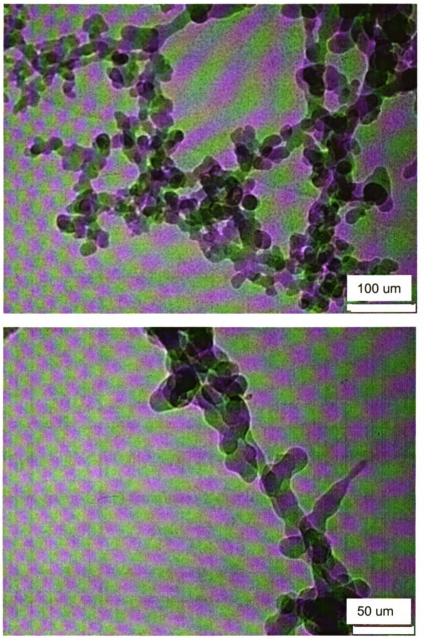

Figure 6.1. TEM images of A200SiH. Samples were prepared by deposition of a suspension of ***A200SiH*** in hexane onto lacey formvar/carbon coated on a 300 mesh copper grid.

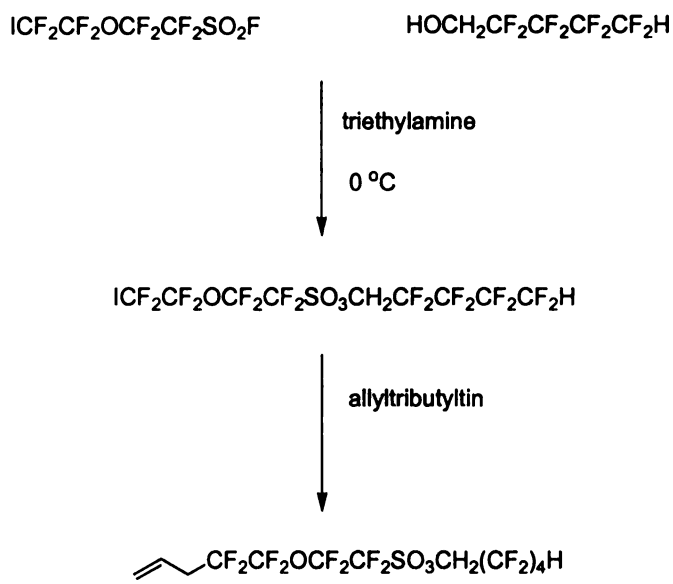

Scheme 6.2. Synthesis of the allyl substituted perfluorosulfonate ester 2,2,3,3,4,4,5,5-octafluoropentyl-4-(prop-1-ene)-tetrafluoro-2-(tetrafluoro-2-ethoxy)ethanesulfonate.

Since the perfluorinated alkylsulfonic acid is incompatible with the hydrosilylation conditions, we used an allyl-terminated perfluorinated sulfonate ester reported by Shriver et al.[170] as the substrate. Treatment with LiBr in 2-butanone converts the ester to the corresponding lithium sulfonate,[170] and the sulfonic acid is generated via ion exchange. The synthesis of the perfluorinated sulfonate ester is shown in **Scheme 6.2** and the ^{19}F NMR spectra of the fluorinated intermediates and products are shown in **Figure 6.2.**

Figure 6.3 shows transmission FTIR spectra of methylsiloxane oligomers tethered to A200 (***A200SiH***), and the particles after subsequent modification by hydrosilylation (***A200F ester***). Both spectra were normalized to the silica mass of each sample using TGA results. The most prominent bands in the IR of ***A200SiH*** are Si-H stretching at 2250 cm^{-1} and C-H stretching at ~2970 cm^{-1}. After hydrosilylation, the Si-H band decreased and we estimate a 30% yield based on the reduction of the band intensity. As a control, we replaced A200 silica with triethoxysilane and ran the hydrosilylation reaction under similar conditions. ^{1}H NMR showed complete disappearance of the terminal double bond in the homogeneous reaction. ^{1}H and ^{13}C NMR spectra of the products are shown in **Figures 6.4 and 6.5**, respectively.

TGA curves for A200SiH and A200 are shown **in Figure 6.4**. The weight loss trace for A200SiH showed a slight increase near 400 °C, and then gradually decreased for a total loss of ~2.3% at 700 °C. Seeing a weight gain in TGA experiments is uncommon, but occasionally seen for certain oxidation events. In the case of A200SiH, the weight increase is likely due to oxidation of Si-H to Si-OH followed by condensation of adjacent

Figure 6.2. ^{19}F NMR spectra of components for synthesis of allyl substituted perfluorosulfonate esters

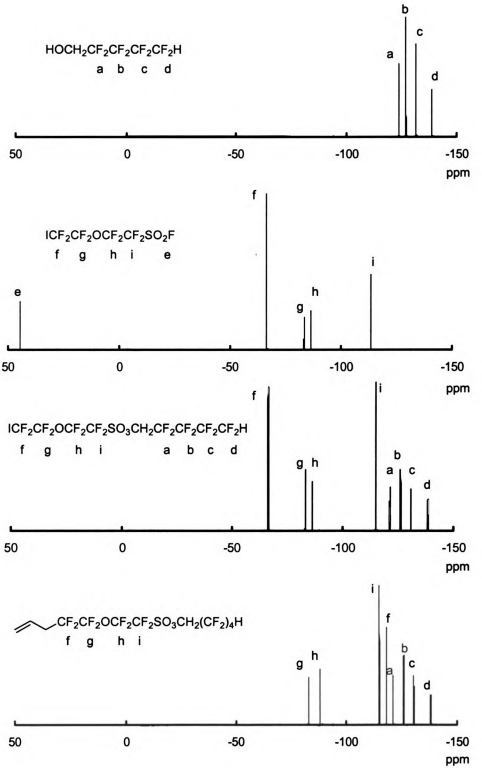

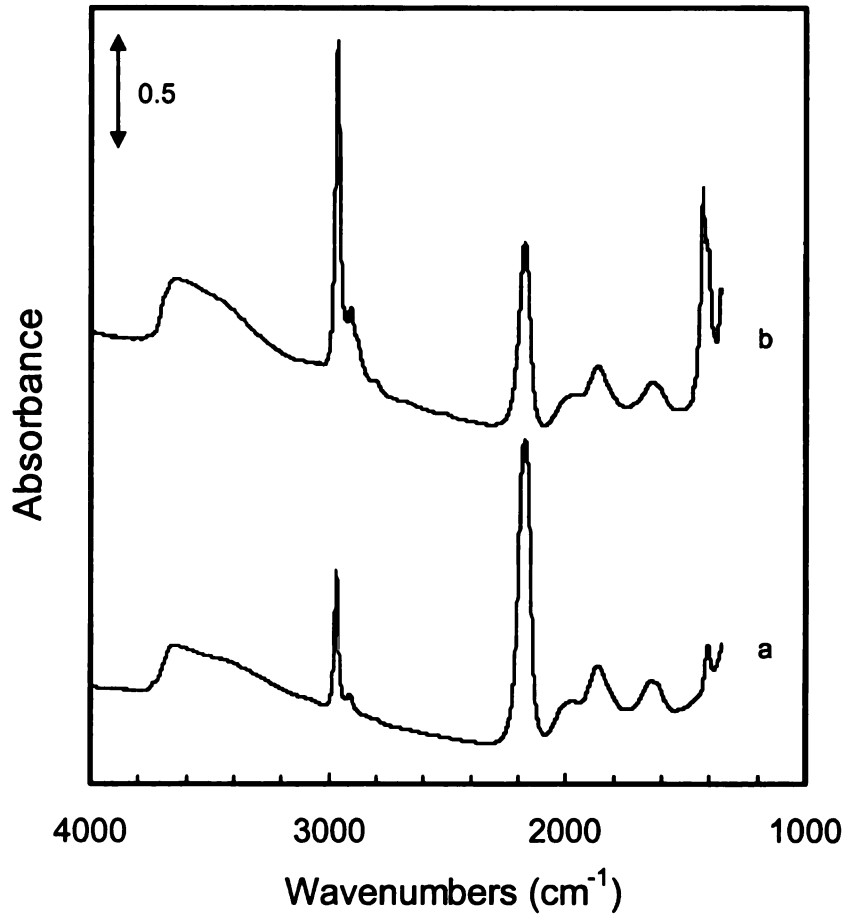

Figure 6.3. IR spectra of A200SiH before (**a**) and after hydrosilation (**b**) with the allyl substituted perfluorosulfonate ester 2,2,3,3,4,4,5,5-octafluoropentyl-4-(prop-1-ene)-tetrafluoro-2-(tetrafluoro-2-ethoxy)ethanesulfonate (A200SiF ester). TGA data were used to normalize the spectra to the same silica content.

Figure 6.4. ^{1}H NMR of the homogeneous hydrosilylation product 1,1,2,2,3,3,4,4-octafluorobutyl 1,1,2,2-tetrafluoro-2-(1,1,2,2-tetrafluoro-5-(triethoxysilyl)pentyloxy) ethanesulfonate.

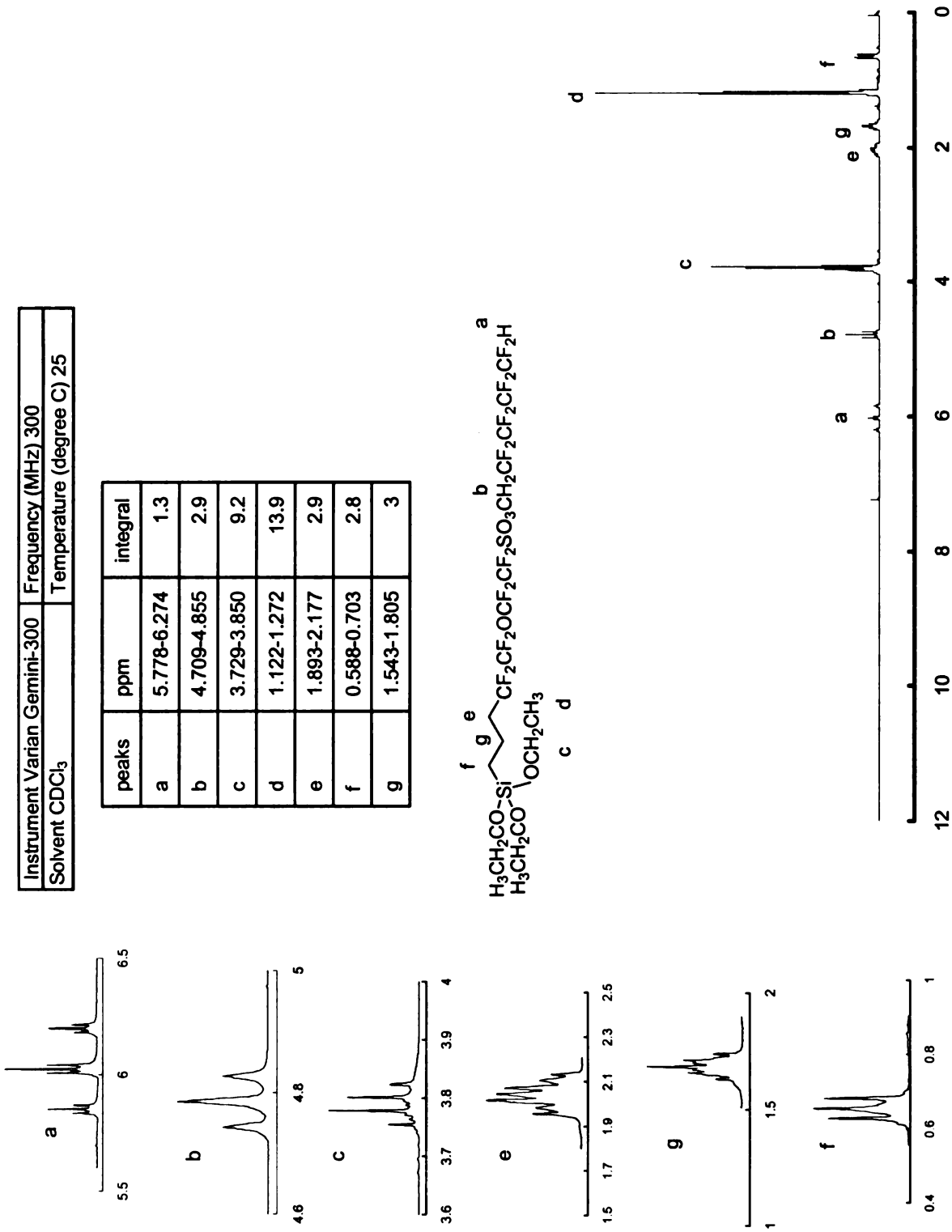

Figure 6.5. ^{13}C NMR of the homogeneous hydrosilylation product 1,1,2,2,3,3,4,4-octafluorobutyl 1,1,2,2-tetrafluoro-2-(1,1,2,2-tetrafluoro-5-(triethoxysilyl)pentyloxy) ethanesulfonate.

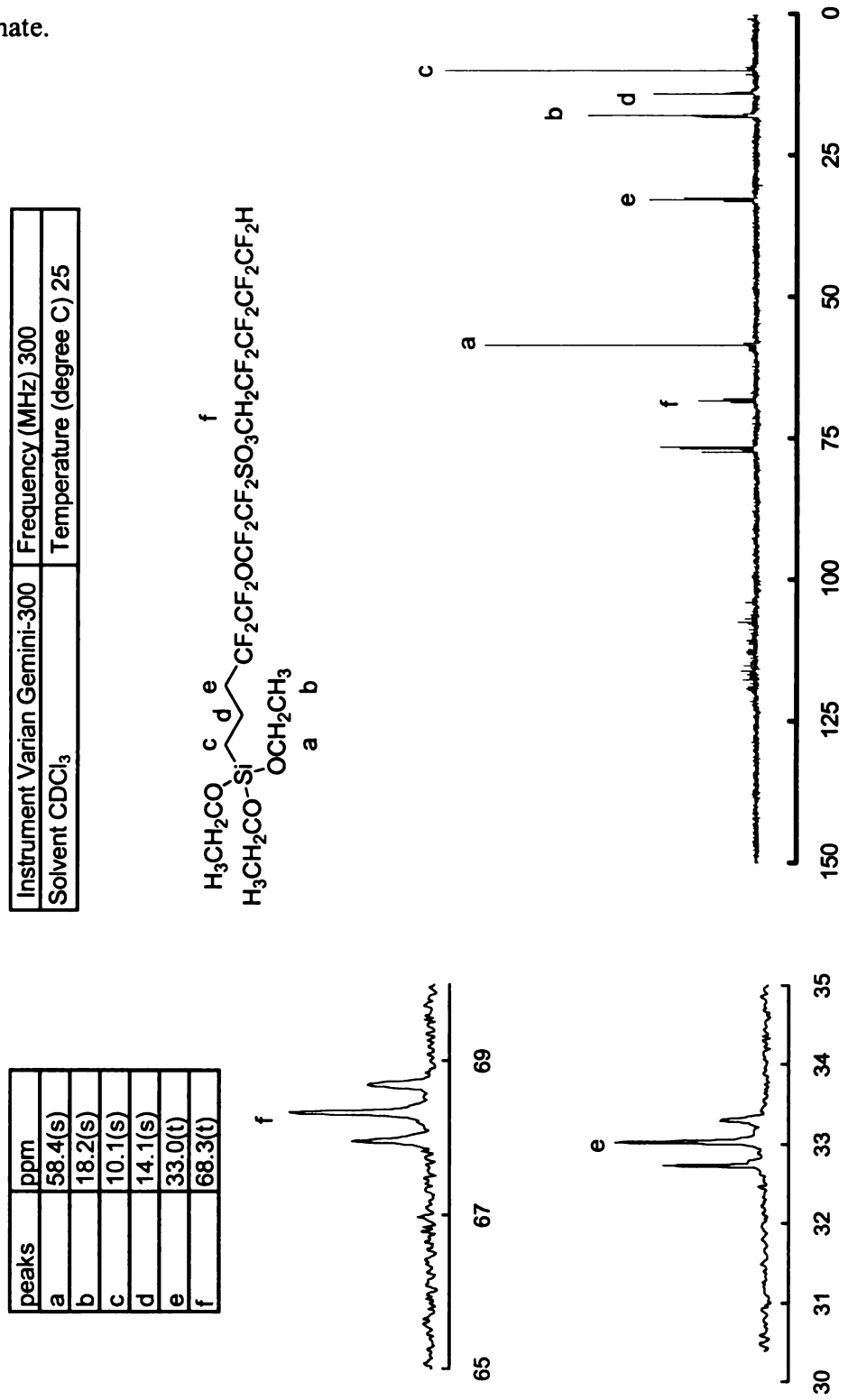

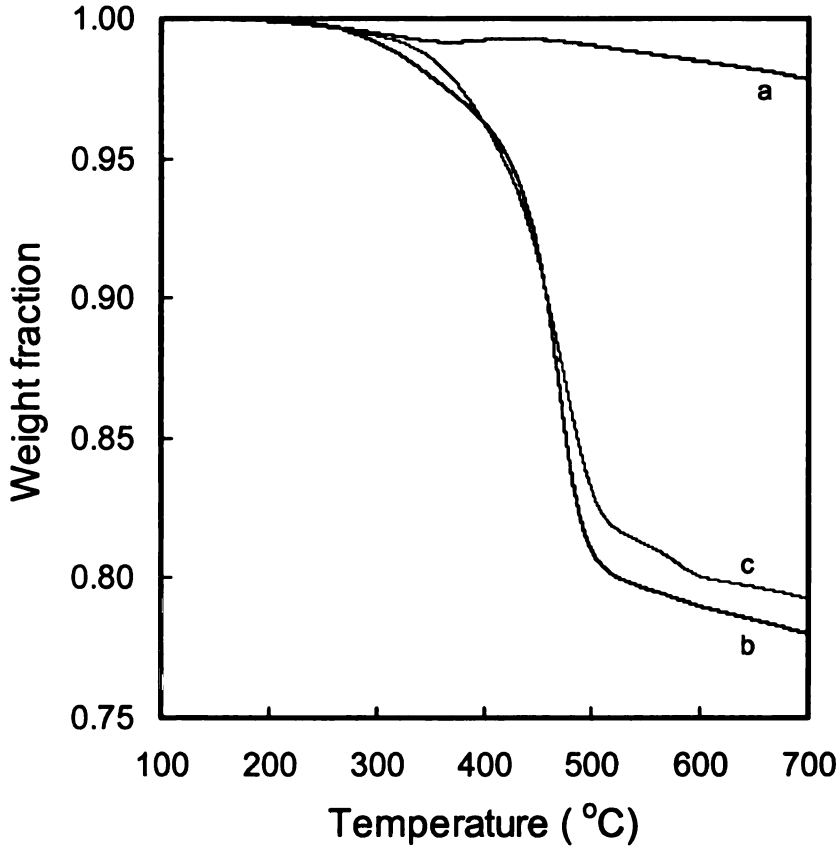

Figure 6.6. TGA data for A200SiH before (**a**) and after hydrosilylation (**b**) with the allyl substituted perfluorosulfonate ester 2,2,3,3,4,4,5,5-octafluoropentyl-4-(prop-1-ene)-tetrafluoro-2-(tetrafluoro-2-ethoxy)ethanesulfonate (A200SiF ester), and (**c**) after conversion of the ester to the Li salt.

silanols. A similar pattern was seen in TGA experiments with poly(methylsiloxane).[171] Titration of the Si-H groups with 40% aqueous KOH revealed 1.8 mmol of Si-H per gram of sample. After hydrosilylation (~2 wt% catalyst loading) the particle weight loss increased to ~23%. The increase in the TGA weight loss should correspond to the loss of the attached perfluorosulfonate ester which can be estimated from the TGA data to be ~ 0.6 mmol/g sample. The ***A200SiF*** ester particles were extracted overnight toluene under Sohxlet conditions and dried before TGA measurements.

Unfortunately, deprotection of the perfluorosulfonate ester to provide the corresponding lithium salt proved problematic. After deprotection, there was no significant change in the TGA profile with <1% difference in the weight loss at 700°. The use of longer reaction times, higher temperatures and excess LiBr failed to effect deprotection. ^{19}F NMR detected a trace of detached $BrCH_2CF_2CF_2CF_2CF_2H$ (4 F peaks) but the intensity of the signals was very low. Poor hydrosilylation yields and our inability to convert the perfluorosulfonate ester to the acid prompted us to suspend this study.

Conclusion

Allyl perfluorosulfonylesters, precursors to perfluorosulfonic acids, were hydrosilylated onto silica surfaces in ~30% yield. Under similar conditions the reaction of the perfluorosulfonylester with trimethoxysilane was complete. However, attempts to hydrolyze the ester to the acid failed.

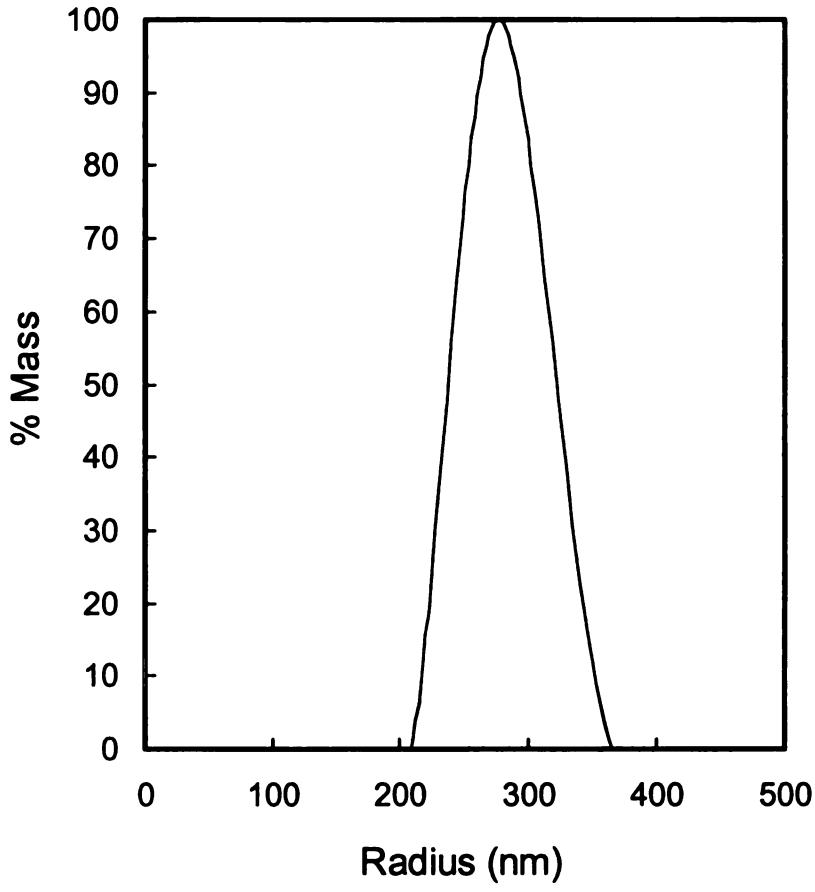

Figure 6.7. Dynamic light scattering measurements of A200 modified with perfluorinated esters in methanol at 25 °C. The 2 mg/mL solutions were sonicated for 20 min and passed through a 200 μm filter before measurement.

Experimental

2,2,3,3,4,4,5,5-Octafluoro-1-pentanol (98%), allyltributyltin (97%), tetrafluoro-2-(tetrafluoro-2-iodoethoxy)ethanesulfonylfluoride (97%), dichlorosilane (97%), Karstedt's catalyst, potassium fluoride dihydrate (AR), and 2,2'-azobisisobutyronitrile (AIBN) were purchased from Aldrich and used as received. Triethylamine were distilled from CaH_2.

^1H and ^{13}C NMR spectra were obtained at room temperature in $CDCl_3$ using a Varian Gemini-300 spectrometer, with the proton and carbon signals from the solvent used as chemical shift standards. ^{19}F NMR spectra were measured in $CDCl_3$ using a Varian Inova-300 spectrometer at 282.2 MHz. The chemical shifts are reported in ppm relative to α,α,α-trifluoromethylbenzene. A Nicolet IR/42 spectrometer purged with dry nitrogen was used to obtain infrared spectra. Samples used were 1 cm^2 pressed pellets prepared from ~ 100 mg of various modified silica. All spectra reported were acquired by signal averaging 32 scans at a resolution of 4 cm^{-1}. Thermogravimetric analyses (TGA) were performed in dry air at heating rate of 10 °C/min on a Perkin Elmer TGA 7 instrument. Samples were held at 110 °C for 30 min before the run was started.

2,2,3,3,4,4,5,5-Octafluoropentyl tetrafluoro-2-(tetrafluoro-2-iodoethoxy) ethanesulfonate (1) Triethylamine (40 mL, distilled from CaH_2) and 0.1 mol of 2,2,3,3,4,4,5,5-octafluoro-1-pentanol (98%) were syringed into a flame-dried round bottom flask under N_2 atmosphere with stirring. The reaction solution was chilled in an ice bath, and then tetrafluoro-2-(tetrafluoro-2-iodoethoxy) ethanesulfonyl fluoride (21.3 g, 0.05 mol) was added dropwise. The reaction mixture was stirred for 8 hours

at 0 °C, slowly warmed to room temperature, and then stirred until the ^{19}F NMR peak at δ 45 (sulfonyl fluoride) disappeared (24-48 h). The reaction mixture was quenched with 100 mL of deionized water, and HCl (1M) was added until the aqueous phase became acidic. The aqueous layer was extracted with hexane (5 × 40 mL), and the combined organic layers were washed with deionized water until the aqueous phase was neutral. The organic phase was dried over $MgSO_4$, filtered, and the solvent was removed by purging with a stream of N_2 at room temperature. Vacuum distillation of the residue gave 21.0 of **1** as a clear liquid (65.7%, yield). ^{19}F NMR δ -65.9 (t, 2), -82.8 (t, 2), -85.9 (s, 2), -114.3 (s, 2), -120.6 (q, 2), -125.3 (s, 2), -130.0 (m, 2), -137.7 (d, 2)

2,2,3,3,4,4,5,5-Octafluoropentyl-4-(prop-1-ene)-tetrafluoro-2-(tetrafluoro-2-ethoxy)ethanesulfonate **(2)** 2,2'-Azobisisobutyronitrile (AIBN 0.0005 mol) and 60 mL of hexane were transferred to a flame dried three neck round bottom flask. After de-gassing via 3 freeze-pump-thaw-cycles, the flask was backfilled with N_2 and allyltributyltin (6.62 g, 0.02 mol) and **1** (6.38 g, 0.01 mol) were syringed into the flask. The flask was partially evacuated with a syringe, transferred to an oil bath, and stirred for 8 hours at a 60 °C. After the reaction was complete (indicated by a shift in ^{19}F NMR peak from δ-66 (I-CF_2) to δ-118 (allyl-CF_2)), the flask was cooled to room temperature and the hexanes were removed by rotary evaporation. The crude product was added to a plastic bottle containing 20 mL of a 0.015 M solution of aqueous potassium fluoride dihydrate and thoroughly agitated to convert $ISnBu_3$ to $FSnBu_3$. Acetone (20 mL) was added to the resulting emulsion, and then a white precipitate was removed by filtration. The organic solution was diluted with diethyl ether (75

mL), and then washed with deionized water (3 × 100 mL). The organic layer was dried over $MgSO_4$. Ether was removed by purging with a stream of N_2 at room temperature, resulting in 2 immiscible phases. The two components were separated and the bottom phase was purified using dry flash chromatography. The silica column was eluted with hexanes until ^1H NMR indicated complete removal of the allyltributyltin. The elutent was then changed to 10 % ether in hexanes (v/v). The fractions containing product were combined, dried over $MgSO_4$ and filtered. The solvent was removed by purging with a stream of N_2 at room temperature to yield 3.2 g of **2** as a clear, colorless liquid (58% yield). The product was stored over activated 4-Å molecular sieves under N_2. ^{19}F NMR d -82.7 (t, 2), -87.7 (s, 2), -114.4 (s, 2), -117.6 (s, 2), -120.5 (q, 2, -125.3 (s, 2), -129.9 (m, 2), -137.6 (m, 2)

A200SiH. Hexane (150 mL) and DMF (30 mL) were added to a 500 mL three neck round bottom flask containing 3 g of dried A200 at room temperature. The mixture was stirred under N_2 for 1 hour, and then cooled to 0 °C and exposed to air. A mechanical stirrer was installed, and under strong stirring, ice was added until the flask was almost full. The suspension was stirred at 0 °C for 4 hours, and then was gradually warmed to room temperature and stirring was continued for another 20 h. The solids were isolated by centrifugation, and washed with 1:1 acetone/DMF (4 × 50 mL) until the supernatant was neutral. The solids were dried under vacuum at 80 °C overnight to yield 2.95 g of ***A200SiH*** (98% yield). IR: Si-H strong peaks at 2180 cm^{-1}; Si-H titration gave 1.6 mmol/g sample.

A200F ester. Toluene (60 mL) was added to a 100 mL round bottom flask containing dry A200SiH (0.8 g). 2,2,3,3,4,4,5,5-Octafluoropentyl-4-(prop-1-ene)-

tetrafluoro-2-(tetrafluoro-2-ethoxy)ethanesulfonate (**2**) (1.65g, 2.9 mmol) and Karstedt's catalyst (0.02 g) were syringed into the flask and stirring was continued for 20 min.. The solution was purged with dry air for 15 min and then was stirred at 80 °C for 72 hours. The solids were isolated by centrifugation, washed with toluene (4 × 30 mL) and dried under vacuum at 80 °C overnight to yield 0.76 g of ***A200F ester*** (95% yield).

Hydrosilylation of 2,2,3,3,4,4,5,5-octafluoropentyl-4-(prop-1-ene)-tetra fluoro-2-(tetrafluoro-2-ethoxy)ethanesulfonate with triethoxysilane. Triethoxysilane (0.37 mL, 2.0 mmol), Karstedt's catalyst (0.01 g) and triethoxysilane (1.18 g, 2.0 mmol) were added to a 100 mL round bottom flask containing 30 mL toluene. The mixture was stirred for 20 min and purged with dry air for 15 min. The flask was sealed with a rubber septum and the solution was continuously stirred at 80 °C for 24 hours. Completion of the reaction was verified by disappearance of resonance from the vinylic hydrogen at δ 5.2-5.3 ppm in ^{1}H NMR. The reaction mixture was cooled to room temperature and passed through a carbon black column. The clear liquid was collected and was dried over $MgSO_4$. Vacuum distillation (110 °C, 40 mtorr) gave 0.028 g (20% yield) of the hydrosilation product as a clear liquid. ^{1}H NMR ($CDCl_3$, ppm) δ 0.588-0.703 (t, 2H), δ 1.122-1.272 (t, 9H), δ 1.543-1.805 (m, 2H), δ 1.893-2.177 (m. 2H), δ 3.729-3.850 (q, 6H), δ 4.709-4.805 (t, 2H), δ 5.778-2.674 (m, 1H). ^{13}C NMR ($CDCl_3$, ppm) δ 10.1 (s), δ 14.1 (s), δ 18.2 (s), δ 33.0 (t), δ 58.4 (s), δ 68.3 (t).

Si-H functional group quantification A 100 mL three neck round bottom flask was charged with 1.0 g of dry **A200SiH.** One neck was connected to a gas

volumeter and the other 2 necks were sealed with rubber stoppers. Aqueous KOH (6.0 mL of a 40% solution) was injected into the flask. The Si-H content was calculated from volume of hydrogen gas evolved using the ideal gas law.

Chapter 7

Summary and Recommendations for Future Work

This research explored the design of composite proton exchange membranes as alternatives to single component membranes such as Nafion. The driving hypothesis was that adopting a two component approach simplifies membrane design by decoupling the problems of optimizing the physical and conductive properties of proton exchange membranes. Other advantages of a composite approach include simplification of membrane synthesis, rapid prototyping, and reduced cost. The conductivity of some membranes were comparable to Nafion, and had better high temperature performance.

The composite membranes studied used inorganic particles chemically functionalized to have acid groups on their surface. The chemistry for anchoring the acids to the surface used standard methodology. While this work focused on silica particles, any inert particle, in principal, could be compatible with the two-phase composite membrane approach. Various sized particles were examined, ranging from macroscopic A200 fumed silica to nanoparticles such as Snowtex. The higher surface to volume ratio of nanoparticles allows higher loadings of acid groups in composite membranes. Another benefit of using nanoparticles was improved water retention at high temperatures, presumably due to more effective capillarity in aggregates of nanoparticles.

The proton conductivity depends on the number of charge carriers (protons) and their mobility (related to electrolyte structure). We found that immobilizing a single layer of acid groups on the surface of A200 fumed silica provided too few carriers to support conductivity. We solved this problem in two ways. First, we increased the concentration of acids groups on the surface by growing polystyrene from initiators anchored to the

surface, and then sulfonated the polymers. Tethering acids to the polymers dramatically increases the number of available acid groups (2~3 mmol/g) and membranes prepared by embedding these particles in PVDF had conductivities of ~0.08 S/cm. A second approach was the sol-gel synthesis of nanoparticles containing alkyl thiols as a component of their structure. Oxidizing the thiols provided sulfonic acids tethered to the surface. Composites prepared from these particles also exhibited high conductivities.

The proton mobility in a composite membrane depends on the existence of conductive paths through the membrane. These paths are defined by the arrangement of the particles in the membrane, and preferably, continuous paths form at low volume fractions of particles. We observed percolation thresholds when measuring the proton conductivity of membranes, with the conductivity increasing several orders of magnitude when the particle content approached 30 wt%. Examination of membranes using TEM and confocal microscopy showed that particles in poorly conductive membranes aggregated in non-continuous domains, but at higher particle contents, the domains were connected providing continuous conductive paths and high conductivity.

The physical properties of the membranes depend on the matrix polymer, PVDF in this research, and the particle content. Composite films are flexible and resilient when the particle contents are <40 wt%, but become increasingly brittle at higher levels. Since useful conductivities occur at ~40 wt%, control over the arrangement of particles in membranes is needed to optimize both the conductive and physical properties. One approach to lowering the percolation threshold is to align the particles within the membrane structure. As noted in the introduction, application of a strong AC field (1-100 kV/cm) can align conductive particles,[100] and if applied during the membrane casting

process, the particles may align along the applied field. Similarly, magnetic fields may be used to align ferretic particles.

Improvements in the acid groups tethered to the particles are possible. The long term stability of polystyrene tethers used in our work is questionable since radical attack at tertiary carbons along the polymer backbone can cause chain degradation.[172] While our initial attempts to anchor fluorinated sulfonic acids to particles were unsuccessful, this approach remains attractive due to their high acidity and chemical stability of fluorinated compounds. The hydrosilation efficiency on silica surface (currently < 40%) must be improved, and a suitable synthesis strategy for tethering perfluorinated chains to silica surfaces must be identified.[173,174]

References

1. Hoogers, G. Ed, *Fuel Cell Technology Handbook*, 2003, CRC Press. p. 3.

2. Hirschenhofer, J. H.; Stauffer, D. B.; Engleman, R. R.; Klett, M. G, *Fuel Cell Handbook*, Fourth Edition, November 1998.

3. Barbir, F. *PEM Fuel Cells: Theory and Practice*, 2005, Elsevier Academic Press. p. 23.

5. Vielstich, W.; Lamm, A.; Gasteiger, H. A. Eds, *Handbook of Fuel Cells: Fundamentals Technology and Applications*. John Wiley & Sons Ltd, Chichester, U. K.

6. Hickner, M. A.; Ghassemi, H.; Kim. Y. S.; Einsla, B. R.; McGrath, J. E. *Chem. Rev.* **2004**, *104*, 4587-4612.

7. Li, Q.; He, R.; Jensen, J. O.; Bjerrum, N. J. *Chem. Mater.* **2003**, *15*, 4896-4915.

8. Rikukawa, W.; Sanui, K.; *Prog. Polym. Sci.* **2000**, *25*, 1463-1502.

9. Laria, D.; Marti, J.; Guardia, E. *J. Am. Chem. Soc.* **2004**, *126*, 2125-2134.

10. Marx, D.; Tuckerman, M. E.; Hutter, J.; Parrinello, M. *Nature* **1999**, *397*, 601-604.

11. Vuilleumier, R. *J. Chem. Phys.* **1999**, *111*, 4251-4265.

12. von Grotthuss, C. J. D. *Ann. Chim.* **1806**, 58, 54.

13. Agmon, N. *Chem. Phys. Lett.* **1995**, *244*, 456-462.

14. Kornyshev, A. A.; Kuznetsov, A. M.; Spohr, E.; Ulstrup, J. *J. Phys. Chem.* **2003**, *107*, 3351-3366.

15. Schmitt. U.; Voth, G. A. *J. Chem. Phys.* **1999**, *111*, 9361-9381.

16. Day, T. J. F.; Schmitt, U. W.; Voth, G. A. *J. Am. Chem. Soc.* **2000**, *122*, 12027-1028.

17. Walbran. S., Kornyshev. A. A., *J. Chem. Phys.* **2001**, *114*, 10039-10048.

18. Zundel, G.; Metzger, H. Z. *Phys. Chem.* **1968**, *58*, 225.

19. Zundel, G.; Fritsh, J. *Spectroscopy of Solvation*, in *The Chemical Physics of Solvation, part b*, Dogonadze, R. R.; Kalman, E.; Kornyshev, A. A.; Ulstrup, J. Eds, 1986, Elsevier: Amsterdam. p. 21.

20. Kreuer, K. D.; Rabenau, A.; Wepper, W. *Angew. Chem. Int. Ed.* **1982**, *3*, 208-209.

21. Gillespie, R. J.; Robinson, E. A. in *Non Aquous Solvent System*, Waddington, T. C .Ed. 1965, Academic Press,

22. Li, Q.; He, R.; Jenson, J. O.; Bjerrum, N. J. *Fuel Cells* **2004**, *4*, 147-159.

23. Ma, Y. L.; Wainright, J. S.; Litt, M. H.; Savinell, R. F. *J. Electrochem. Soc.* **2004**, *151*, A8-A16.

24. Dippel, T.; Kreuer, K. D. *Solid State Ionics* **1991**, *46*, 3.

25. Mauritz, K. A.; Moore, R. B. *Chem. Rev.* **2004**, *104*, 4535-4585.

26. Hsu, W. Y.; Gierke, T. D. *J. Membrane. Sci.* **1983**, *13*, 307.

27. Brian, C. H.; Steele, G.; Heinzel, A. *Nature* **2001**. *414*, 345-352.

28. Zawodzinski, T. A.; Springer, T. E.; Uribe, F.; Gottesfeld, S. *Solid State Ionics* **1993**, *60*, 199-211.

29. Berg, P.; Promislow, K.; Pierre, J. S.; Stumper, J.; Wetton, B. *J. Electrochem. Soc.* **2004**, *151*, A341-A353.

30. Hickner, M. A.; Pivovar, B. S. *Fuel Cells* **2005**, *5*, 213-229.

31. Mishra, V.; Yang, F.; Pitchomani, R. *J. Power Sources* **2005**, *141*, 47-64.

32. Carrette, L.; Friedrich, K. A.; Stimming, U. *CHEMPHYSCHEM* **2000**, *1*, 162-193.

33. Prakash, G. K. S.; Smart, M. C.; Wang, Q.; Atti, A.; Pleynet, V.; Chun, W.; Valdez, T.; Surampudi, S. *J. Fluorine Chem.* **2004**, *125*, 1217-1230.

34. Kerres, D.; Cui, W.; Reichle, S. *J. Polym. Sci. Part A* **1996**, *34*, 2421.

35. Hickner, M. A.; Ghassemi, H.; Kim, Y. S.; Einsla, B. R.; McGrath, J. E. *Chem. Rev.* **2004**, *104*, 4587-4612.

36. Wang, F.; Hickner, M.; Kim, Y. S.; Zawodzinski, T. A.; McGrath, J. E. *Macromol. Symp.* **2001**, *175*, 387.

37. Harrison, W. L.; Hickner, M. A.; Kim, Y. S.; MacGrath, J. E. *Fuel Cells* **2005**, *5*, 201.

38. Genies. C.; Mercier, R.; Sillion, B.; Cornet, N.; Gebel, G.; Pineri, M. *Polymer* **2001**, *42*, 359.

39. Fang, J.; Guo, X.; Harada, S.; Watari, T.; Tanaka, K.; Kita, H.; Okamoto, K. *Macromolecules* **2002**, *35*, 9022.

40. Guo, X.; Fang, J.; Watari, T.; Tanaka, K.; Kita, H.; Okamoto, K. *Macromolecules* **2002**, *35*, 6707.

41. Miyatake, K.; Zhou, H.; Uchida, H.; Watanabe, M. *Chem. Commun.* **2003**, 368.

42. Asano, N.; Miyatake, K.; Watanabe, M. *Chem. Mater.* **2004**, *16*, 2841.

44. Yang, S. J.; Jang, W.; Lee, C.; Shul, Y. G.; Han, H. *J. Polym. Sci: Part B: Polym.Phys.* **2005**, *43*, 1455.

45. Allcock, H. R.; Klingenberg, E. H.; Welker, M. F. *Macromolecules* **1993**, *26*, 5512.

46. Graves, R.; Pintauro, P. N. *J. Appl. Polym Sci.* **1998**, *68*, 827.

47. Wycisk, R.; Lee, J. K.; Pintauro, P. N. *J. Electrochem. Soc.* **2005**, *152*, A892.

48. Allcock, H. R.; Hofman, M. A.; Ambler, C. M.; Morford, R. V. *Macromolecules* **2002**, *35*, 3484.

49. Hofman, M. A.; Ambler, C. M.; Maher, A. E.; Chalkova, E.; Zhou, X. Y.; Lvov, S. N.; Allcock, H. R. *Macromolecules* **2002**, *35*, 6490.

50. Tang, H.; Pintauro, P. N. *J. Appl. Polym. Sci.* **2001**, *79*, 49.

51. Andrianov, A. K.; Marin, A.; Chen, J.; Sargent, J.; Corbett, N. *Macromolecules* **2004**, *37*, 4075.

52. Miyatake, K.; Hay, A. S. *J. Poly. Sci., Part A: Polym. Chem.* **2001**, *39*, 3211.

53. Alberti, G.; Casciola, M.; Palombari, R. *J. Membr. Sci.* **2000**, *172*, 233.

54. Boysen, D. A.; Uda, T.; Chisholm, C. R. I.; Haile, S, M. *Science* **2004**, *2*, 68.

55. Stefanithis. K. A.; Mauritz. I. D.; Davis. S. V.; Scheetz. R. W.; Pop. R. K.; Wilkes. G. L.; Huang. H. H. *J. Appl. Polym. Sci., Part B: Polym. Phys.* **1995**, *55*, 181.

56. Gummaraju. R. V.; Moore. R. B.; Mauritz. K. A. *J. Polym. Sci., Part B: Polym. Phys.* **1996**, *34*, 2383.

57. Apichatachuapan, W.; Moore, R. B.; Mauritz, K. A. *J. Appl. Polym. Sci.* **1996**, *62*, 417.

58. Shao, O. L.; Mauritz, K. A.; Moore, R. B. *Chem. Mater.* **1995**, *7*, 192.

59. Shao, Z.; Joghee, P.; Hsing, I. S. *J. Memb. Sci.* **2004**, *229*, 43.

60. Miyake, N.; Wainright, J. S.; Savinell, R. F. *J. Electrochem. Soc.* **2001**, *148*, A905.

61. Klein, L. C.; Daiko, Y.; Aparicio, M.; Damay, F. *Polymer* **2005**, *46*, 4504.

62. Prado, L. A. S. D.; Wittich, H.; Schulte, K, Nunes, S. P. *J. Poly. Sci., Part B: Poly. Phys.* **2003**, *42*, 567.

63. Young, S. K.; Mauritz, K. A. *J. Poly. Sci. Part B: Poly. Phys.* **2002**, *40*, 2237.

64. Chalkova, E.; Pague, M. B.; Fedkin, M. V.; Wesolowski, D. J.; Lvov, S. N. *J. Electrochem. Soc.* **2005**, *152*, A1035-A1040.

65. Wang, Y.; Wang, X.; Li, J.; Mo, Z.; Zhao, X.; Jing, X.; Wang, F. *Adv. Mater.* **2001**, *13*, 1582.

66. Adjemian, K. T.; Lee, S. J.; Srinivasan, S.; Benziger, J.; Bocarsly, A. *J. Electrochem. Soc.* **2002**, *149*, A256-A261.

68. Mauritz, K. A.; Stefanithis, I. D.; Davis, S. V.; Scheetz, R. W.; Pope, R. K.; Wilkes, G. L. *J. Appl. Polym. Sci.* **1995**, *55*, 181.

69. Chalkova, E.; Pague, M. B.; Fedkin, M. V.; Wesolowski, D. J.; Lvov, S. N. *J. Electrochem. Soc.* **2005**, *152*, A1035-A1040.

70. Adjemain, K. T.; Dominey, R.; Krishnan, L.; Ota, H.; Majsztrik, P.; Zhang, T.; Mann, J.; Kirby, B.; Gatto, L.; Simpson, M. V.; Leahy, J.; Srinivasan, S.; Benziger, J. B.; Bocarsly, A. B. *Chem. Mater.* **2006**, *18*, 2238.

71. Prashantha, K.; Park, S. G. *J. Appl. Poly. Sci.* **2005**, *98*, 1875.

72. Rhee, C. H.; Kim, H. K.; Chang, H.; Lee, J. S. *Chem. Mater.* **2005**, *17,* 1691-1697.

73. Si, Y.; Kunz, R.; Fenton, J. M. *J. Electrochem. Soc.* **2004**, *A623-A631.*

74. Ramani, V.; Kunz, H. R.; Fenton, J. M. *J. Membr. Sci.* **2004**, *232*, 31.

75. Aparico, M.; Klein, L. C. *J. Elcctrochem. Soc.* **2005**, *152*, A493.

76. Sweikart, M. A.; Herring, A. M.; Turner, J. A.; Williamson, D. L.; McCloskey, B. D.; Boonrueng, S. R.; Sanchez, M. *J. Elctrochem. Soc.* **2005**, *152*, A98.

77. Zaidi, S. M.; Mikhailenko, S. D.; Robertson, G. P.; Guiver, M. D.; Kaliaguine, S. *J. Membr. Sci.* **2000**, *173*, 17.

78. Chen, S.; Krishnam, L.; Srinivasan, S.; Benziger, J.; Bocarsly, A. B. *J. Membr. Sci.* **2004**, *243*, 327.

79. Malhotra, S.; Datta, R. *J. Electrochem. Soc.* **1997**, *144*, L23-26.

80. Tazi, B.; Savadogo, O. *Electrochim. Acta.* **2000**, *45*, 4329-4339.

81. Mecheri, B.; Epifanio, A. D.; Vona, M. L. D.; Traversa, E.; Licoccia, S.; Miyayama, M. *J. Electrochem. Soc.* **2006**, *153*, A463.

82. Rhee, C. H.; Kim, H. K.; Chang, H.; Lee, J. S. *Chem. Mater.* **2005**, *17*, 1691.

83. Gasa, J. V.; Boob, S.; Weiss, R. A.; Shaw, M. T. *J. Mem. Sci.* **2006**, *269*, 177.

84. Si, Y.; Kunz, R.; Fenton, J. M. *J. Electrochem. Soc.* **2004**, *A623-A631.*

85. Hong, L.; Chen, N. *J.Poly. Sci. Part B: Poly. Phys.* **2002**, *38*, 1530.

86. Kanamura, K.; Mitsui, T.; Munakata, H. *Chem. Mater.* **2005**, *17*, 4845.

87. Chen, S. Li.; Krishnan, L.; Srinivasan, S.; Benziger, J.; Bocarsly, A. B. *J. Membr. Sci.* **2004**, *243*, 327-333.

88. Nakajima, H.; Nomura, S.; Sugimoto, T.; Nishikawa. S.; Honma, I. *J. Electrochem. Soc.* **2002**, *149*, A953-A959.

89. Honma, I.; Nishikawa, O.; Sugimoto, T.; Nomura, S.; Nakajima, H. *Fuel Cells* **2002**, *2*, 52-58.

90. Honma, I.; Nakajima, H.; Nishikawa, O.; Sugimoto, T.; Nomura, S. *J. Electrochem. Soc.* **2002**, *149*, A1389-A1392.

91. Boysen, D. A.; Chisholm, C. R. I.; Haile, S. M.; Narayanan, S. R. *J. Electrochem. Soc.* **2000**, 147, 3610-3613.

92. Linares, A.; Acosta, J. L. *Polym. Int.* **2005**, *54*, 972-979

93. Smitha, B.; Sridhar, S.; Khan, A. A. *J. Polym. Sci. Part B: Polym. Phys.* **2005**, *43*, 1538-1547.

94. Alberti, G.; Casciola, M.; Pica, M.; Tarpanelli, T.; Sganappa, M. *Fuel Cells* **2005**, *5*, 366-374.

95. Yamazaki, Y.; Jang, M. Y.; Taniyama, T. *Sci. Tech. Adv. Mater.* **2004**, *5*, 455.

96. Lin, C. W.; Thangamuthu, R.; Yang, C. J. *J. Mem. Sci.* **2005**, *253*, 23.

97. Honma, T.; Kim, J. D. *J. Electrochem. Soc.* **2004**, *151*, A1396.

98. Feng, F.; Yang, Z.; Coutinho, D. H.; Ferraris, J. P.; Kenneth, J.; Balkus, Jr. *Micropor. Mesopor. Mater.* **2005**, *81*, 217.

99. Binsu, V. V.; Nagarale, R. K.; Shahi, V. K. *J. Mater. Chem.* **2005**, *15*, 4823.

100. Oren, Y.; Freger, V.; Lindar, C. *J. Membrane. Sci.* **2004**, *239*, 17.

101. Brijmohan, S. B.; Shaw, M. T. *Polymer* **2006**, *47*, 2856.

102. Prakash, G. K. S.; Smart, M. C.; Wang, Q.; Atti, A.; Pleynet, V.; Yang, B.; McGrath, K.; Olah, A.; Narayanan, S. R.; Chun, W.; Valdez, T.; Surampudi, S. *J. Fluorine Chem.* **2004**, *125*, 1217.

103. Chen, N.; Hong, L. *Polymer* **2004**, *45*, 2403.

104. Savinell, R.; Yeager, E.; Tryk, D.; Landau, U.; Wainright, J.; Weng, D.; Lux, K.; Litt, M.; Rogers, C. *J. Electrochem. Soc.* **1994**, *141*, L46-L48.

105. Ma, Y. L.; Wainright, J. S.; Litt, M. H.; Savinell, R. F. *J. Electrochem. Soc.* **2004**, *151*, A8-A16.

106. Khan, A. S.; Baker, G. L.; Colson, S. *Chem. Mater.* **1994**, *6*, 2359-2363.

107. Coleou, C.; Xu, K.; Lesaffre, B.; Brzoska, J. B; *Hydrological Process* **1999**, *13*, 1721-1732.

108. Ivanov, D.; Petrova, H. *Teaching Physics* **2000**, *35*, 262-266.

109. Tortet, L.; Gavarri, J. R.; Musso, J.; Nihoul, G.; Sarychev, A. K. *J. Solid State Chem.* **1998**, *141*, 392-403.

110. Lux, F.; *J. Mater. Sci.* **1993**, *28*, 285-301.

111. Chen, X. B.; Devaux, J.; Issi, J. P.; Billaud, D. *Polym. Eng. Sci.* **1995**, *35*, 637-641.

112. Mamunya, E. P.; Davidenko, V. V.; Lebedev, E. V. *Polymer Composites* **1995**, *16*, 319-324

113. Pinto, G.; Maaroufi, A. K. *J. Appl. Polym. Sci.* **2005**, *96*, 2011.

114. Bouckary, L. T.; Jones, D. J.; Roziere, J. *Fuel Cells* **2002**, *2*, 40-45.

115. Yamagushi, T.; Miyata, F.; Nakao, S. *Adv. Mater.* 2003, 15, 1198-1201.

116. Li, H.; Nogami, M. *Adv. Mater.* **2002**, *14*, 912-914.

117. Kwak, S. H.; Peck, D. H.; Chun, Y. G.; Kim, C. S.; Yoon, K. H. *J. New Mater. Electrochem. Sys.* **2001**, *4*, 25-29.

118. Liu, F.; Yi, B.; Xing, D.; Yu, J.; Hou, Z.; Fu, Y. *J. Power Sources* **2003**, *124*, 81-89.

119. Xing, D. M.; Yi, B. L.; Liu, F. Q.; Fu, Y. Z.; Zhang, H. M. *Fuel Cells* **2005**, *5*, 406-411.

120. Michael, G.; Ferch, H. *Technical Bulletin Pigments*, Degussa AG, 1993.

121. Mathias, J.; Wannemmacher, G. *J. Coll. Interface Sci.* **1988**, *125*, 61.

122. Hou, J. Ph D Thesis, 1997, Michigan State University

123. Vansant, E. F.; Voort, P. V. D.; Vrancken, K. C. *Characterization and Chemical Modification of the Silica Surface*, Elsevier, 1995.

124. Benedict, R. C.; Stedman, R. L. *Analyst* **1970**, *95*, 296.

125. Edmondson, S.; Osborne, V. L.; Huck, T. S. *Chem. Soc. Rev.* **2004**, *33*, 14-22.

126. Ebata, K.; Furukawa, K.; Matsumoto, N. *J. Am. Chem. Soc.* **1998**, *120*, 7367-7368.

127. Mansky, P.; Liu, Y.; Huang, E.; Russell, T. P.; Hawker, C. *Science* **1997**, *275*, 1458.

128. Tsubokawa, N.; Hosoya, M.; Yanadori, K.; Sone, Y. *J. Macromol. Sci. Chem.* **1990**, *A27*, 445-457.

129. Matyjaszewski, K. Ed, *Controlled Radical Polymerization*, American Chemical Society, Washington, DC, 1998, p. 685.

130. Matyjaszewski, K, Ed, *Controlled / Living Radical Polymerization: Progress in ATRP, NMP, and RAFT*, American Chemical Society: Washington, DC, 2000, p. 768

131. Pyun, J.; Kowalewski, T.; Matyjaszewski, K. *Macromol. Rapid. Commun.* **2003**, *24*, 1043-1059.

132. Zhao, B.; Brittain, W. J. *J. Am. Chem. Soc.* **1999**, *121*, 3557-3558.

133. Bontempo, D.; Tirelli, N.; Feldman, K.; Masci, G.; Crescenzi, V.; Hubbell, J. A. *Adv. Mater.* **2002**, *14*, 1239-12411.

134. Nakagawa, Y.; Miller, P. J.; Matyjaszewski, K. *Polymer* **1998**, *39*, 5163-5170.

135. Pyun, J.; Matyjaszewski, K., Kowalewski, T.; Savin, D.; Patterson, G.; Kickelbick, G.; Huesing, N. *J. Am. Chem. Soc.* **2001**, *123*, 9445-9446.

136. Werne, T.; Patten, T. E. *J. Am. Chem. Soc.* **1999**, *121*, 7409-7410.

137. Nakagawa, Y.; Miller, P. J.; Matyjaszewski, K. *Polymer* **1998**, *39*, 5163.

138. Han, S.; Hyeon, T. *Chem. Commun.* **1999**, 1955.

139. Li, S.; Liu, M. *Elctrochim. Acta.* **2003**, *48*, 4271.

140. Walcarius, A.; Mandler, D.; Cox, J. A.; Collinson, M.; Lev, O. *J. Mater. Chem.* **2005**, *15*, 3663.

141. Badley, R. D.; Ford, W. T. *J. Org. Chem.* **1998**, *54*, 5437.